UNCERTAINTY QUANTIFICATION IN ENGINEERING OPTIMIZATION APPLICATIONS

LI GUILIN

NATIONAL UNIVERSITY OF SINGAPORE

2017

UNCERTAINTY QUANTIFICATION IN ENGINEERING OPTIMIZATION APPLICATIONS

LI GUILIN

(B.Sc., Nankai University, 2012)

A THESIS SUBMITTED

FOR THE DEGREE OF DOCTOR OF PHILOSOPHY

DEPARTMENT OF INDUSTRIAL & SYSTEMS ENGINEERING

NATIONAL UNIVERISITY OF SINGAPORE

2017

Supervisor:

Associate Professor Ng Szu Hui

Examiners:

Dr Chen Nan

Professor Goh Thong Ngee

Associate Professor Rong Pan, Arizona State University

Declaration

I hereby declare that this thesis is my original work and it has been written by me in its entirety. I have duly acknowledged all the sources of information wich have been used in the thesis.

This thesis has also not been submitted for any degree in any university previously.

Li Guilin

March, 2017

Acknowledgments

I wish to express my sincere gratitude to my supervisor Associate Professor Ng Szu Hui. She has shown me how good research is done and how to be a good researcher. I appreciate all her contributions of time, patience, ideas, and resources to make my Ph.D. experience inspiring and productive.

There were many sources of support during this process. I am grateful to both Associate Professor Chua and Royston Tan. Thanks for them providing valuable physics and engineering expert knowledge during our collaboration on the manufacturing case study. Dr. Chen, Dr. Tan and Dr. Ye provided inspiring lectures and great guidelines for how to be a good researcher. I also acknowledge National University of Singapore for supporting me with the research scholarship for the first four years of my research.

Finally, I would like to thank my parents and my husband Matthias Tan that are always present for supporting me during all the good and the difficult moments of my research life. This thesis would not be possible without them.

CONTENTS

LIST OF TABLES

LIST OF FIGURES

Summary

This dissertation reports three distinct pieces of work for uncertainty quantification in engineering optimization applications using statistical methods. The purpose of engineering optimization is to choose a set of settings for the design factors of the system such that the system performance is optimized. To analyze and optimize an engineering system, a mathematical model is typically constructed based on technical knowledge of how the engineering system operates and some available data. However, the presence of various types of uncertainty in the engineering optimization process has brought many challenges in making a reliable decision. These uncertainties include the inherent randomness in physical observations, modeling uncertainty (discrepancy between the mathematical model and actual system), or parameter uncertainty arising from lack of information or the ambiguity in the definition of certain parameters. In this dissertation, only the modeling of the inherent randomness, the modeling uncertainty and the parameter uncertainty in the system performance function was covered.

The third chapter of this thesis is motivated by modeling data from a semiconductor manufacturing experiment. The objective is to correlate the wafer defects with the design factors and to identify the optimum design setting. Since the experiment is conducted on a high-quality manufacturing line, 96 percent of the observations are zeros. It is known that zero-inflated data are very non-informative because they provide little information on the system randomness. Other than the zero-inflation, three different types of variations are also identified from this data. In this chapter, a multilevel zero-inflated model and its inference method are proposed for modeling the inherent randomness arising in the near zero-defect manufacturing process.

In engineering optimization problems, the estimation of the optimum setting is the ultimate goal. For a process with various variations, the main concern is that the obtained optimum setting may suffer from large estimation uncertainty.

And an efficient experiment should collect data informative about reducing the estimation uncertainty of the optimum setting instead of the whole regression model. Hence, in the fourth chapter, a Bayesian optimal design framework is developed for the efficient estimation of the optimum setting. The developed framework employs a Shannon information utility measure to quantify the reduction in the uncertainty of the optimum setting from an experiment.

The fifth chapter looks into the parameter uncertainty problem in the objective function of computer model-based engineering optimization problem. When using stochastic computer models for engineering optimization, a frequently encountered but ignored problem is that the objective function may contain some uncertain parameters. In this work, we leverage on the flexible and efficient radial basis function metamodel and a novel experimental design approach to model the objective function as a function of both the design factors and the uncertain objective function parameters. In this way, the system can be easily optimized under different choices of the uncertain parameters. This facilitates the modeling and reduction of the parameter uncertainty in the objective function.

These three developed methodologies together contribute to the modeling of uncertainty in engineering optimization process.

Keywords: engineering optimization, process variation, parameter uncertainty, multilevel zero-inflated model, Bayesian optimal design, Shannon information, objective function uncertainty

CHAPTER 1

INTRODUCTION

1.1 Uncertainties in engineering optimization

The purpose of engineering optimization is to choose a set of settings for the design factors of the system such that the system performance is optimized. To analyze and optimize an engineering system, a mathematical model is typically constructed based on technical knowledge of how the engineering system operates and some available data. However, the presence of various types of uncertainty in the engineering system has brought many challenges in building an accurate model for predicting and optimizing the system performance. The proper modeling of the uncertainty in the investigated engineering system is essential for reliable and robust design decision making.

In engineering optimization applications, there are two broad types of uncertainty: namely, the aleatory uncertainty and the epistemic uncertainty.

Aleatory uncertainty is the uncertainty associated with the natural randomness in a process. For example, flipping a coin and predicting either head or tail is aleatory uncertainty. This type of uncertainty is inherent to the problem and cannot be reduced. This uncertainty type is characterized by a probability distribution and is typically addressed by collecting a large number of observations. To describe the probability distribution uniquely, the parameters indexing the

distributions need to be estimated based on the collected observations. Using these parameter estimates, the uncertainty in the model predictions can then be evaluated through statistical inference methods such as bootstrapping. Hence, the estimation of the distribution parameters is itself a major component of the uncertainty analysis. However, the number of observations one can collect is often restricted by the limited resources. Hence, efficient collection of data using techniques such as optimal design will provide more accurate information about the distribution parameters and can lead to high confidence in choosing the optimum setting for engineering optimization.

Epistemic uncertainty is the uncertainty arises from insufficient knowledge about the processes which could be reduced with more time and resources. A lack of knowledge about the underlying processes means that we must adopt models that reflect our best understanding but which are actually inaccurate. For example, when using finite element analysis for structural design, many idealized assumptions about the material and geometry are made, leading to a discrepancy between a computer model prediction and the actual system behavior. To reduce the uncertainty arises from inaccurate modeling of the system, one possibility is that a large set of functional bases could be assumed to be adequate for describing the functional relationship between the design factors and the process responses. For this type, model selection techniques or Bayesian model averaging can be used to reduce the modeling uncertainties.

Moreover, epistemic uncertainty also arise from model parameters which may be unknown, unmeasurable or only indirectly observed. This parameters uncertainty comes in two classes. One is the uncertain parameters that are inputs to the mathematical model but whose exact values are unknown. For example, when using stochastic simulation to evaluate the performance of complex stochastic systems, the inputs that are used to drive the simulation are often estimated from real-world data. The estimation error of these inputs brings epistemic uncertainty to the model predictions. To propagate the uncertainty in model inputs to model outputs, many numerical methods were proposed, including Bayesian

model average (Chick (2001)), bootstrap (Barton and Schruben (2001)), simulation confidence intervals (Barton et al. (2013)), etc. The other type of parameter uncertainty is the uncertain parameters in the system's performance function/ objective function. In many areas of applications, the system performance function may contain some uncertain parameters, such as uncertain preference parameters for conflicting goals or difficult-to-evaluate parameters. For example, when designing a nuclear power plant building, the cost incurred by varying rates of leakage of radioactive material can be hard to quantify. When the objective function contains some fuzzy part or difficult-to-evaluate parameters, a rational procedure is to conduct *sensitivity analysis* (post-optimality analysis) (Wallace (2000)). The results of *sensitivity analysis* provide information on how sensitive the optimal solution is to changes in the uncertain parameters and establish the upper and lower bounds for the uncertain parameters within which they can vary without causing violent changes in the current optimal solution. Due to the complexity of the engineering optimization problems, capturing this type of uncertainty is in an early developmental stage due to the lack of computationally efficient tools.

In this thesis, the developed three pieces of work tackle the quantification of the process variation (aleatory uncertainty), modeling uncertainty and parameter uncertainty in the objective function. The parameter uncertainty of system inputs are beyond the scope of this thesis. The parameter uncertainty of system inputs are beyond the scope of this thesis.

1.2 Data collection for the modeling of uncertainty

In the design and optimization of engineering systems, the system behavior is predicted based on information from technical knowledge and available data. A large number of data are important to accurately model the uncertainties in the system. And these data can be collected from two different methods: (1) physical experiment or observations; (2) computer experiment.

When physical experiments or observations are used to collect data for sys-

tem prediction and uncertainty quantification, the following stages are typically used: (1) selection of design factors with major effects on the system through preliminary screening experiments or engineering knowledge, and the delimitation of the design region based on the objective of the study; (2) the planning and conducting of the physical experimental design; (3) the statistical modeling of the experiment result; (4) the evaluation of the modeling uncertainty and model fitness; (5) the verification of the necessity to perform follow-up experiment to reduce the uncertainty. The third chapter of this thesis focuses on the modeling of uncertainty with statistical models built from physical experiment data. The fourth chapter focuses on efficient physical experiment data collection for reducing the uncertainty associated with optimum setting estimation.

Computer experiments are another method for collecting data for system prediction and uncertainty quantification. To conduct a computer experiment, a computer model is constructed first to simulate the behavior of an engineering system based on knowledge of how the system operates. These computer experiments are useful in cases where the physical experiment of the engineering system is very expensive to run, or the system under investigation is hypothetical (to be built) such that one cannot conduct the physical experiment. The fifth chapter of this thesis focuses on capturing the parameter uncertainty in the objective function of computer models.

To build a computer model and conduct a computer experiment, Law and McComas (2001) provided the following steps:

- Problem formation: define the objectives and criteria of the study; define the performance measure of the computer model.

- Parameter specification: collect data to specify computer model parameters and the distributions of the system random variables.

- Model development: develop a mathematical model; translate the mathematical model to computer code; verify that the computer code executes correctively.

- Experiment: select the experiment design points and conduct the computer experiments by running the computer code

- Model validation: validate the computer model by comparing the output of the built computer model with the real system performance; update the computer model if necessary.

The steps of data collection for the modeling of uncertainty are often highly iterative–parts of the steps often need to be repeated many times before making the final decision. For example, when the initial understanding of a system, a process, or a new product is poor, a preliminary experiment is usually conducted first to collect data about the uncertainties of the system. Based on the initial data, analysis tools such as plausible reasoning, hypothesis test or model selection can be used to identify the sources/characteristics of the uncertainties and determine the shape of the response surface. Often, however, as the preliminary experiments are conducted on a small scale, the uncertainties can be inadequately described or can be too large. Hence, additional budgets for conducting follow-up experiments can be allocated to collect data to better describe or reduce the uncertainties. These steps are repeated until some satisfactory results are obtained.

1.3 Objective and significance

Uncertainty quantification in engineering optimization appears in many areas of application and brings many challenges in both concept and computation. Motivated by several engineering optimization applications, we summarizes some of the current research gaps for the modeling of uncertainty in engineering optimization problems. The summary focuses on the process variation(aleatory uncertainty), modeling uncertainty and parameter uncertainty in the objective function. The parameter uncertainty in inputs of mathematical models are beyond the scope of this thesis.

- One type of engineering optimization problems is to optimize the high-quality manufacturing process. For example, wafers are generally manufactured in a near zero-defect manufacturing line. Yet, further reduction of the defect rate through optimizing the process would make the product more competitive and bring enormous economic benefits. In such processes, the experimental measurements are characterized by zero-inflation. It is known that zero-inflated count data are very non-informative because they provide little information on the inherent randomness. In such processes, the parameter estimation can be highly biased and unstable. Besides the excessive zeros, the manufacturing processes are often characterized by various types of process variations. As a result, the estimated optimum setting would suffer from large prediction error if these variations/uncertainties are not modeled properly. However, there are currently no statistical procedures that can model both the zero-inflation and the various types of process variations together effectively. In addition, in the current study of data modeling for engineering optimization applications, very few works investigate the mechanism causing the randomness to arise and attempt to develop a probability distribution of the random variable based on engineering knowledge. Compared to simply assigning some typical distributions based on statistical testing, concurrently analyze the data and the underlying process would facilitate a model more loyal to the true process and reduce the modeling uncertainty.

- In many engineering optimization problems, the determination of the optimum setting yielding best system performance is the ultimate goal. Therefore, the data collection step should serve to reduce the estimation uncertainty of the optimum setting instead of the overall predictive model. Currently, most of the research on experimental design has been focused on collecting information on reducing the uncertainty of the overall predictive model. For example, the well-known D-optimality criterion (Chaloner and Verdinelli (1995); Dror and Steinberg (2008); Gotwalt et al. (2009);

Russell et al. (2009)) assigns equal degree of importance to all elements of the model parameters, regardless of their influence on the optimum setting. However, the optimal designs for a globally well estimated model may not be the 'best' with regards to reducing the uncertainty of the optimum point. Although many published articles are available on finding the optimum point in a sequential experiment (Box and Wilson (1951); Chatterjee and Mandal (1981); Liyana-Pathirana and Shahidi (2005)), little work has been published on batch experiment design in which all design points need to be chosen before conducting the experiment. On the other hand, research on batch experimental design for this topic has been limited to assuming the optimum point being a stationary point (see Chaloner (1989); Mandal and Heiligers (1992); Pronzato and Walter (1993); Fedorov and Müller (1997)). However, in many practical instances, the design region and hence the optimum point is limited within a constrained region of interest. In such cases, the optimum point can be located at the boundaries when the stationary point is a saddle point or be located outside the region of interest. Therefore, a more general treatment which relaxes the restrictive stationary point assumption on the optimum point is desired.

- In the design of complex engineering systems, a frequently encountered but often ignored problem is that the objective function representing system performance may contain some uncertain parameters, such as uncertain trade-offs (weights) among conflicting goals or difficult-to-evaluate parameters. In the optimization literature, an ideal procedure for a multi-objective problem is the *posteriori approach* (Burke and Kendall (2013)), in which a set of different trade-off optimal solutions is first obtained and then a multiple-criterion decision-making technique (such as using high-level information) (Deb and Sundar (2006)) is used to analyze the solutions to choose a most preferred solution. Likewise, when the objective function contains some difficult-to-evaluate parameters, a rational procedure is to conduct *sensitivity analysis* (post-optimality analysis) (Wallace (2000)).

As pointed by Burke and Kendall (2013), the classical methods use a different philosophy such that the objective function uncertainty is artificially forced out of sight, mainly due to a lack of suitable optimization tools to obtain many optimal solutions efficiently. Development of computationally efficient solution to capture this objective parameter uncertainty is hence of great importance to facilitate robust decisions in engineering optimization problems.

Motivated by several engineering optimization applications, this thesis intends to solve three aspects of the quantification of uncertainty in engineering optimization. To be specific, the following problems are to be solved:

- The development of a multilevel zero-inflated model that provides a data analysis tool for zero-inflate defect data collected from a high-quality manufacturing line with multilevel process variations. This model should be able to describe the characteristics of various types of variations in a near zero-defect manufacturing process. Model inferential procedures such as parameter estimation methods and parameter uncertainty quantification tools should be provided.

- The development of a Bayesian optimal designs framework for the efficient estimation of the optimum setting of an engineering system. The developed framework should collect data that is informative for reducing the uncertainty of the estimation of the optimum setting. The efficient evaluation method of the proposed design criterion should also be developed to facilitate the implementation of the developed framework in practical applications.

- To properly capture the parameter uncertainty in the system performance function, the most straightforward method should be to optimize the system many times with various settings of the uncertain parameters. However, for a time-consuming stochastic computer model, this would usually incur extensive computational burden. A computationally efficient tool

should be developed to obtain many optimal solutions efficiently for different choice of the uncertain parameter in the system performance function.

The results of this thesis may provide more efficient tools for capturing and reducing the uncertainties in engineering optimization problems. More specifically, the tools developed in this thesis may help in improving

- The modeling of the uncertainties in multilevel high-quality manufacturing process.
- The reduction of the uncertainty in estimating the optimum settings of a system through efficient experimental design.
- The determination of an optimal system setting that is robust to parameter uncertainty in system performance function through computationally efficient tools.

1.4 Organization

This thesis contains 6 chapters. In Chapter 2, a literature review is provided for regression models for system defects data analysis, experimental design method for reducing the uncertainties in engineering optimization, and parameter uncertainty in system performance function.

In Chapter 3, we built a multilevel zero-inflated model motivated by solving a real engineering optimization problem from a local semiconductor company. Specifically, we extend the zero-inflated model, which assumes the system randomly shifts between a zero state and a count state, to a multilevel model to capture the low failure observation and multilevel variations in a high-quality manufacturing line. To develop this multilevel model, we first analyzed the mechanism causing the uncertainty in the state shift to determine at which level the state shift occurs. Then, the distribution describing the uncertainties in the count state is derived based on the underlying mechanism of the engineering problem. And finally, flexible distributions of random effects are incorporated

into the model to account for the non-normal variations. An approximate Adaptive Gaussian Quadrature EM algorithm is then proposed to estimate the parameters of the model. The formulas for calculating the uncertainty in estimating the parameters are also derived. Our analysis of the process and development of the model enables reducing of the modeling uncertainty and accurate modeling of the aleatory uncertainty.

In Chapter 4, we focus on the development of Bayesian optimal designs for the efficient estimation of the optimum setting of an engineering system. The developed framework employs a Shannon information utility measure to quantify the reduction in the uncertainty of the optimum setting from an experiment. To evaluate the developed utility measure, we provide an efficient approximation method based on decomposing the criterion into the utility measure for D-optimal criterion and a 'missing information' term which can be estimated using Monte Carlo without a nested structure. This approximation greatly reduces the computational burden of a pure MCMC algorithm and makes searching for the optimal design feasible. We motivate, develop, and illustrate this framework with an example from semiconductor manufacturing, where the design objective is to optimize the etching step to reduce the surface defects on the wafers.

In Chapter 5, we look into metamodel-based optimization of stochastic computer models where there are uncertain parameters in the objective function. These uncertain parameters may come from difficult-to-evaluate parameters in the cost function or the subjective trade-off parameters between conflicting goals such as the scale parameters in desirability function. We employ a flexible and efficient radial basis function metamodel to model the objective function as a function of both the design factors and the uncertain objective function parameters. We propose the use of a design that is a Cartesian product of a design for the design factors and a design for the uncertain parameters. This allows us to derive a fast fitting algorithm to construct the RBF metamodel. To illustrate the effectiveness of the developed tools in solving practical problems, they are applied to optimize a drug delivery system with conflicting goals.

Finally, Chapter 6 summarizes these studies for capturing the uncertainties in engineering optimization and provides some directions for future work.

CHAPTER 2

LITERATURE REVIEW

In this thesis, the first work focuses on the modeling of zero-inflated count data with multilevel variations. The second work focuses on efficient data collection for reducing the uncertainty associated with optimum setting estimation, and the third work builds a solution to capture the parameter uncertainty in objective function of computer models. These problems account for several important research gaps in uncertainty modeling in engineering optimization problems. In this chapter, we review the previous works on these topics.

2.1 Review of regression analysis for modeling process variations in count data

The first work of this thesis is motivated by modeling the physical experiment data for improving the integrated circuits design. The experiment collects wafer defect data for different settings of the design factors. A preliminary analysis of the data identified two characteristics of the collected defective count: excessive zeros and multilevel variations. It is known that zero-inflated data are very non-informative because they provide little information on the randomness and make the modeling of the uncertainties extremely difficult. These two character-

istics are common in high-quality manufacturing lines that are subjected to multi sources of inherent uncertainty. Typically, the defective counts are modeled by the generalized linear models (GLMs) such as the Poisson regression model. In high-quality manufacturing processes, however, standard GLMs can considerably overestimate the probability of zeros. The zero-inflated family of models were proposed by Mullahy (1986), Lambert (1992) and Greene (1994) to handle this extra uncertainty induced by excessive zeros. Zero-inflated (ZI) models (Lambert (1992)) assume the distribution of the response is a mixture of a point mass at zero and a count distribution. Lambert (1992) examined zero-inflated defects in manufacturing, noting that one interpretation for the excessive zeros is that changes of unobserved factors may cause the process to shift randomly between a zero state in which defects are nonexistent and a count state in which defects can occur according to a Poisson distribution. Hurdle models (Mullahy (1986)) take a slightly different approach: they combine a zero component with a truncated count distribution.

In the presence of multilevel process variations and underlying heterogeneity , extensions of the ZI models to the multilevel modeling are desired. Hall (2000) extended Lambert (1992)'s ZI model to a mixed effect model by incorporating a normally distributed random effects into the log-linear parts of the ZI model to capture the block level uncertainty. They were motivated by an example from horticulture, where count data with excess zeros were collected in an experiment with blocks. Although directly incorporating normally distributed random effects in the ZI models is convenient, it can, however, cause problems in certain situations. Furthermore, for engineering optimization problems where the optimum setting is of interest , a wrong assumption on the random effects can lead to a poor estimation of the optimum setting, as this optimum point is functionally dependent on the mean of the random effects in the ZI model. Currently, however, there are no straightforward approaches to incorporate a more flexible distribution to capture various types of variations in manufacturing line.

2.2 Review of Bayesian experimental design for efficient estimation of optimum point

As computational power has evolved over the decades, the development of Bayesian experimental design is facilitating more complex design problems to be solved. The Bayesian framework provides a unified approach for incorporating prior information regarding the statistical model, with a utility function describing the experimental objectives.

One of the most commonly used formation of utility function for Bayesian design criteria is the mutual information (Lindley et al. (1972)). From a Bayesian point of view, Lindley et al. (1972) suggested that an efficient way of experimental design is to specify a utility function reflecting the value of the experiment, regard the design choice as a decision problem, and select a design that maximizes the utility.

Specifically, the Bayesian optimal design $\boldsymbol{e}^*$, maximizes the expected utility function $U(\boldsymbol{e})$ over the experimental design space $\mathcal{X}^E$ with respect to the future observations $\boldsymbol{y_e} \in \mathcal{Y}$ and model parameter $\boldsymbol{\theta} \in \mathcal{R}^p$:

$$\begin{aligned} \boldsymbol{e}^* &= argmax_{\boldsymbol{e}\in\mathcal{X}^E} E\{U(\boldsymbol{e}, \boldsymbol{\theta}, \boldsymbol{y_e})\} \\ &= argmax_{\boldsymbol{e}\in\mathcal{X}^E} \int_{\mathcal{Y}} \int_{\mathcal{R}^p} U(\boldsymbol{e}, \boldsymbol{\theta}, \boldsymbol{y_e}) p(\boldsymbol{\theta}|\boldsymbol{e}, \boldsymbol{y_e}) p(\boldsymbol{y_e}|\boldsymbol{e}) d\boldsymbol{y_e} d\boldsymbol{\theta} \end{aligned} \tag{2.1}$$

For example, the well-known Bayesian D-optimality criterion (Chaloner and Verdinelli (1995); Dror and Steinberg (2008); Cook et al. (2008); Lewi et al. (2009); Drovandi et al. (2013); Huan and Marzouk (2013); Ryan et al. (2014)) seeks to maximize the mutual information between the observations and the parameter vector. This criterion puts equal attention to all elements of the parameter vector, regardless of their influence on the potential measurement of interest. However, it is of great importance that the utility function incorporates the specific experimental objectives and is specific to the application of interest. For example, the utility function for efficient estimation of parameter may not perform well when the design objective is to reduce the prediction uncertainty.

Therefore, other utility functions such as utilities for model discrimination (Box and Hill (1967); Ng and Chick (2004); Cavagnaro et al. (2010); McGree et al. (2012)) and utilities for prediction of future observations (Zidek et al. (2000); Solonen et al. (2012); Liepe et al. (2013) have been proposed to incorporate specific design objectives.

Nevertheless, the literature on Bayesian optimal designs for estimating optimum points is scarce despite the fact that many engineering problems have estimation of optimum settings as their ultimate goal.

Although many published articles are available on finding the optimum point in a sequential experiment (Box and Wilson (1951); Chatterjee and Mandal (1981); Liyana-Pathirana and Shahidi (2005)), these algorithms can not be used when the experiment is not sequential in nature, as dictated by practical constraints. Box and Wilson (1951) initiated the research on sequentially attaining optimum point by estimating the first derivatives of the response surface and moving toward the optimum with the path of steepest ascent defined by previous estimates. However, this sequential search method would not be applicable to many manufacturing and clinical experiments where measurements are carried out simultaneously in a batch (for example, see Millette et al. (1995); Ruiz et al. (2013)). In such cases, all the design points have to be chosen without feedback information. On the other hand, research on batch experimental design for this topic has been limited to assuming the optimum point being a stationary point (Chaloner (1989); Mandal and Heiligers (1992); Pronzato and Walter (1993); Fedorov and Müller (1997)). For example, Chaloner (1989); Mandal and Heiligers (1992) studied the problem with linear regression models, and assumed that the optimum point was a stationary point and can be written as a closed form function of the model parameters. However, in many practical instances, the design region and hence the optimum point is limited within a constrained region of interest. In such cases, the optimum point can be located at the boundaries when the stationary point is a saddle point or be located outside the region of interest. Currently there are no design criteria that relax the restrictive stationary point

assumption on the optimum point.

The reason that Bayesian optimal design has been limited to simple utility functions mainly because of the computational burden to perform the integration and maximization of equation 4.1. To evaluate the Bayesian utility function, one must estimate the posterior distribution $p(\boldsymbol{\theta}|\boldsymbol{e}, \boldsymbol{y_e})$. Generally, thousands of these posterior distributions must be calculated for each potential future experimental observations $\boldsymbol{y_e}$, which is drawn from the prior predictive distribution $p(\boldsymbol{y_e}|\boldsymbol{e}, \boldsymbol{\theta})p(\boldsymbol{\theta})$. To evaluate these posterior distributions, many computational strategies have been proposed. These include Laplace approximation Chaloner and Verdinelli (1995); Long et al. (2013); smoothing of Monte Carlo simulations (Müller (2005)), Markov Chain Monte Carlo (MCMC) (Ryan (2003); Müller (2005)); and sequential Monte Carlo methods (Amzal et al. (2006)).

In the case where the utility function represents the information gain on the optimum point, the posterior distributions of the optimum point are required to be calculated. And the conditions for normal approximation are no longer satisfied, the Chaloner and Verdinelli (1995)'s method can not be directly followed. On the other hand, it can be too computationally intensive to perform Monte Carlo to estimate the posterior distribution of optimum point for each of the thousands of iterations required in the optimal search algorithms.

To broaden the applicability of Bayesian optimal design by making it more accessible to practitioners, efficient evaluation of the utility function is desirable.

2.3 Review of the objective function uncertainty problem of stochastic computer models

With the constantly upgraded computing power, stochastic computer models are becoming important tools for understanding and optimizing engineering systems that are analytically intractable and subject to random fluctuations. These tools have been recently successfully applied to many engineering optimization applications including the integrated photonic filters design in electrical

engineering (Weng et al. (2017)), aerospike nozzle design in aerospace engineering(Stevens and Branam (2015)), continuous stirred-tank (CSTR) reactor design in chemical engineering (Ding et al. (2010)), etc.

An ideal case would be such that the design engineer or the investigator has complete knowledge for determining the objective functions for optimizing the system performance. However, this may not always be true especially when analyzing complex engineering systems. In many areas of applications, there are multiple objectives or difficult-to-evaluate parameters in the objective functions (for example Ristow et al. (2005); Pant et al. (2011); Bozsak et al. (2015)). When multiple objectives need to be optimized simultaneously, the most popular method is to form a composite objective function through weighted sum (Marler and Arora (2010)) or desirability functions (Wu (2004); Park and Kim (2005)), where a weight or scale parameter proportional to the user preference is assigned to a particular objective. However, the determination of these preference parameters is usually highly subjective and not straightforward. It requires an investigation of the qualitative and experience-driven information to determine the quantitative preference parameter values. Without the possible trade-off optimal solutions in hand, this is an even more challenging task. Besides these uncertain preference parameters, the uncertainty in an objective function may also come from the difficult-to-evaluate parameters. For example, when designing a nuclear power plant building, the cost incurred by varying rates of leakage of radioactive material can be hard to quantify (Korsakissok et al. (2013)). And a change in the potential cost will possibly result in a totally different optimal solution. This objective function uncertainty problem appears in various areas of application and brings many challenges in both concept and computation.

When dealing with this uncertainty problem, the current development of stochastic computer models mainly focuses on replacing the uncertain parameters by some estimates and assuming the objective function is precisely determined, for example, see Humphrey and Wilson (2000); Cao et al. (2004); Ristow et al. (2005); Kleijnen (2014); Weng et al. (2017). By such a choice, the uncer-

tainty is pushed out of sight through approximating the uncertain parameters by some particular estimates, such as decision maker's preference information, expert judgment, historical records, or a sample mean. Meanwhile, the inferential procedure for other choices of the uncertain parameters is simply ignored. However, unless a reliable preference or accurate estimate is available, the optimal solution obtained by such methods would be highly subjective to the specific investigator or largely sensitive to the choice of the estimates(Wurl and Albin (1999)).

In the optimization literature, an ideal procedure for a multi-objective problem is the *posteriori approach* (Burke and Kendall (2013)), in which a set of different trade-off optimal solutions is first obtained and then a multiple-criterion decision-making technique (such as using high-level information) (Deb and Sundar (2006)) is used to analyze the solutions to choose a most preferred solution. This is because any two different optimal solutions (such as Pareto-points) represent different trade-offs among the objectives, and the decision maker would be in a better position to balance risk when such choices are presented. Likewise, when the objective function contains some difficult-to-evaluate parameters, a rational procedure is to conduct *sensitivity analysis* (post-optimality analysis) (Wallace (2000)). For example, when the cost of failure is uncertain, it is important for the investigator to know how profit would be affected by a change in the potential failure cost. The results of *sensitivity analysis* provide how sensitive the optimal solution is to the change in the uncertain parameters and establish the upper and lower bounds for the uncertain parameters within which they can vary without causing violent changes in the current optimal solution.

As pointed by Burke and Kendall (2013), the classical methods use a different philosophy such that the objective function uncertainty is artificially forced out of sight, mainly due to a lack of suitable optimization tools to obtain many optimal solutions efficiently. To properly capture this uncertainty, the most straightforward method should be to optimize the system many times with various settings of the uncertain parameters. However, for a time-consuming stochastic com-

puter model, this would usually incur extensive computational burden. In the context of multi-objective optimization, an alternative solution is the *interactive approach* (Deb et al. (2010); Boyle and Shin (1996)), in which the decision maker's responses to specific questions were used iteratively to guide the solution towards the preferred part of the Pareto-optimal region. Although this method reduces the computational burden of optimizing the system repeatedly for many different uncertain parameter choices, it requires a lot of cognitive efforts of the decision maker. Moreover, when the modeler and the decision maker is not the same person, this method can be infeasible or very inefficient.

CHAPTER 3

A MULTILEVEL ZERO-INFLATED MODEL FOR INTEGRATED CIRCUITS DESIGN

In this chapter, we focus on the development of regression and inferential analysis methods for zero-inflated manufacturing processes. This work is motivated by modeling the results of a large-scale semiconductor experiment, for improving the integrated circuits design.

3.1 Introduction

One type of engineering optimization problems is to optimize the high-quality manufacturing process. For example, wafers are generally manufactured in a near zero-defect manufacturing line. Yet, further reduction of the defect rate through optimizing the process would make the product more competitive and bring enormous economic benefits. In such processes, the experimental measurements are characterized by zero-inflation. It is known that zero-inflated count data are very non-informative because they provide little information on the inherent randomness. In such processes, the parameter estimation can be highly biased and unstable. Besides the excessive zeros, the manufacturing processes are often characterized by various types of process variations. As a result, the estimated optimum setting would suffer from large prediction error if these vari-

ations/uncertainties are not modeled properly. These two characteristics are common in high-quality manufacturing lines that are subjected to multi sources of variability/uncertainty. However, there are currently no statistical procedures that can handle both these complex characteristics together effectively.

In this work, motivated by modeling the results of a large-scale semiconductor experiment, we develop a multilevel zero-inflated model for modeling observations from zero-inflated manufacturing processes. The objective of the motivating experiment is to correlate the integrated circuits defective count with several design factors and find the optimum setting yielding minimum defects.

Typically, when defective count data is encountered, the counts are modeled by generalized linear model (GLM) which assumes the counts distributed as Poisson or Negative binomial distribution. Hamada and Nelder (1997) provides comprehensive guidelines on the use of GLMs for a range of applications in quality-improvement experiments. In high quality manufacturing processes, however, there are often many more zeros than the count distributions can predict. The zero-inflated family of models were proposed by Mullahy (1986), Lambert (1992) and Greene (1994). Lambert (1992) examines defects in manufacturing, noting that one interpretation for the excessive zeros is that changes of unobserved environment factors may cause the process to shift randomly between a zero state in which defects are non existent and a count state in which defects can occur according to a Poisson distribution.

In semiconductor manufacturing, it has also been widely reported that there are multi-sources of variability. For example, Stapper (1985) modeled the wafer to wafer variation with a compound distribution that assumes the mean number of defects per wafer behaves like another random variable with its own probability distribution $P\{N = k\}$, where $k = 0, 1, 2, \ldots$. Albin and Friedman (1989) applied a Neyman distribution to model wafer defect data that exhibits clustering. In our motivating problem, we observed that there are variations in the layer, wafer and lot levels. In this work, the multilevel variations are handled in three different ways. Variation among the four metal layers is modeled by a hi-

erarchical/nested model structure. For the wafer-to-wafer variation, through investigating the observations and decomposing the distribution based on a hillock height variable and a hillocks number variable, we conclude that it is most likely caused by small variations in the mean number of hillocks for different wafers. Hence, we treat the mean number of hillocks for different wafers in the same lot as a random variable instead of a fixed parameter. This is similar to the observations and treatment of Stapper (1985). Finally, the lot-to-lot variation is the dominant source of variation, and it was generally modeled as a normally distributed random factor Robinson et al. (2006). However, in the current case, the lot random effect displays multi-modal and skewed distribution features. To account for this, we treat it as a random factor and adopt the semi-nonparametric (SNP) representation proposed by Gallant and Nychka (1987) to model its distribution. This SNP density is flexible, enabling skewed, multi-modal and tailed features to be modeled, and includes the normal as a special case.

The remainder of this chapter is organized as follows: Section 1.2 describes the details of our motivating experiment. Section 1.3 reviews the current work on modeling zero-inflated data. In Section 1.4, some preliminary analyses are done to identify the key characteristics of the data, and several assumptions are made for further model development. In Section 1.5, we link the characteristics identified for the observations back to the underlying process, and derive the response distribution based on the mechanism giving rise to the data. Then a multilevel ZI model is proposed and an approximate Adaptive Gaussian Quadrature EM (approximate AGQ-EM) algorithm is proposed to estimate the model parameters, and the estimation procedure of the standard error is provided. The algorithm's performance is then evaluated through simulation. Finally, Section 1.6 provide a detailed analysis of the motivating problem using the proposed model and recommendations for design.

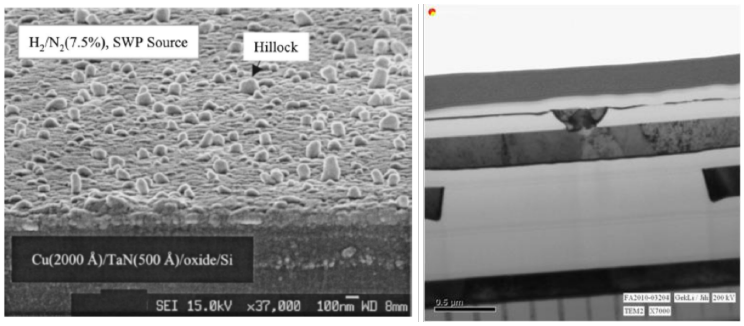

Figure 3.1: (a) shows a single layer of hillocks growing up from a Cu layer below (Kang and Chou (2004)); (b) shows a Cu hillock growing from the bottom metal line across the insulator to top metal line causing a short; (c) a magnified picture of (b), showing the connection formed between the two layers by the copper hillock

3.2 Motivating example

In this section, we describe the large-scale experiment in detail.

In most modern Integrated circuits (ICs) today, the back end interconnects are made of layers of copper lines. As ICs are rapidly shrinking in size, copper hillocks growing vertically from the copper lines may cause inter-layer metallic shorts and reliability issues. Growth of hillocks (Figure 3.1) is an inherent part of the manufacturing process, but these hillocks are harmless unless they grow high enough to connect the layers. A better understanding of copper hillocks growth is required in order to minimize shorts through wisely designing the copper metal dimensions. In our collaborating lab, a large-scale manufacturing experiment was conducted to explore the design factors' effect on the formation of hillocks through measuring the metallic shorts. By analyzing the experiment observations and properly capturing the system uncertainties , we hope to be able to infer how the hillocks growth process is influenced by the process conditions and design factors, and recommend to designers Design For Manufacturing (DFM) rules to ensure robust and reliable manufacturing.

From the literature, it is known that the growth of hillocks are governed by factors such as deposition stress, heating cycling and ICs design parameters (Herley et al. (2001); Jakkaraju and Greer (2002)). However, in a typical semiconductor fab, the process factors are usually fixed and little tuning can be done

without adversely affecting the other parts of the complex process and the reliability performance of the ICs. Thus, in this experiment, the width and length of the metal layer in ICs are identified as key controllable design factors that can be optimized to reduce copper hillocks growth. Figure 3.1b show a magnified picture of a hillock found on a production wafer. In order to physically identify this individual hillock, great effort has been expended by the failure analysis team to slice through the wafer and carefully examine the cross sections under a transmission electron microscope. Therefore, it would not be feasible to physically detect and measure each hillock in the experiment. Given the difficulty to measure hillocks directly, an indirect method is applied, i.e. measuring the shorts they cause.

For that purpose, an electrical test (E-Test) structure was designed. E-test structures are purposefully designed structures that are placed along scribe lines that lie between the ICs produced on a wafer. These structures are separate from the ICs and do not affect their function in any way. To detect the shorts from the structures, two layers with interlacing structures that are electrically separate were designed. In the non-defective case where no hillocks are higher than the the layer spacing, the two structures are separate and no current should be detected across them. In the defective case, at least one hillock growing higher than the layer spacing would cause a short (A detailed explanation of the E-test structure is provided in the supplementary material).

Limited space available in the scribe lines and competition for space dictated the number of designs the engineers could study. Due to this limitation, it was decided to cover at least length and width design factors separately. Six combinations of width and length settings were identified by the designers and designed in the E-test structures. These coincide with the typical design settings and range requested by customers. These structures are placed on 11 selected sites on each wafer across the four layers: Metal1-Metal2 (Layer 1), Metal2-Metal3 (Layer 2), Metal3-Metal4 (Layer 3) and Metal4-Metal5 (Layer 4) (see Figure 3.2). As the metal layers are stacked one on top of another, earlier metal

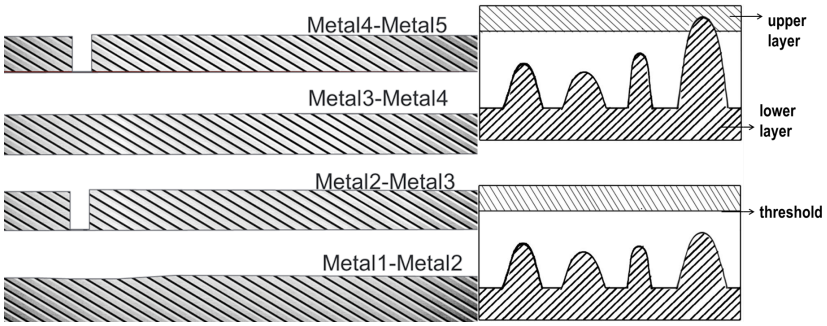

Figure 3.2: Left panel: ICs Layers; Right panel: Hillocks growing between layers

layers undergo more heat treatment and stress as more layers are capped and processed above it. Hence, the metal layers can have an effect on the hillock growth, and the six design settings are nested in the four metal layers in the experiment. The design settings in the four layers are summarized in Table 3.1 below.

The experiment was conducted on 70 lots with 25 pieces of wafer in each lot.

Design	Layer1		Layer2	
	Width	Length	Width	Length
1	-1.48	0.68	-1.48	0.68
2	-1.00	0.68	-1.00	0.68
3	-0.35	0.68	-0.35	0.68
4	0.94	0.68	0.94	0.68
5	0.94	-0.89	0.94	-0.89
6	0.94	-1.83	0.94	-1.83
Design	Layer3		Layer4	
	Width	Length	Width	Length
1	-1.48	0.68	-1.48	0.68
2	-1.00	0.68	-1.00	0.68
3	-0.35	0.68	-0.35	0.68
4	0.94	0.68	0.94	0.68
5	0.94	-0.89	0.94	-0.89
6	0.94	-1.83	0.94	-1.83

Table 3.1: Experiment design: six width and length settings nested in four layers. For confidentiality reasons, the values of width and length have been centered by their means and scaled by their standard deviations.

From each E-test structure, an independent binary observation for binary variable y_{ilwsd}, of design d, site s, wafer w, layer l, and lot i was obtained. Figure 3.3 shows the multilevel structure of the wafer manufacturing line. In this multilevel

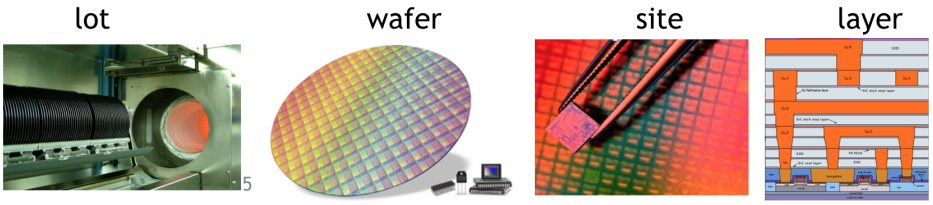

Figure 3.3: multilevel structure of wafer manufacturing line

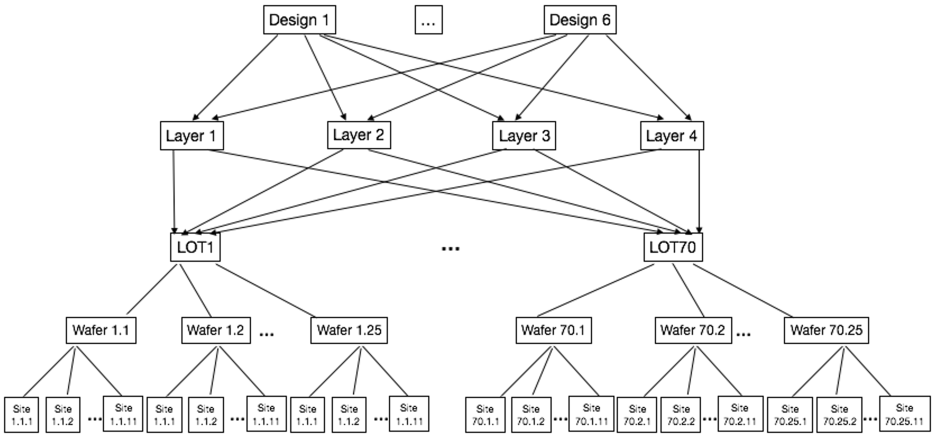

Figure 3.4: hierarchy structure of wafer manufacturing experiment

experiment, the 6 design settings are crossed in four layers and these four layers are crossed in 70 lots. Meanwhile, 11 sites are nested in each wafer and 25 wafers are nested in each of the 70 lots. Graph 3.4 plots this hierarchical structure and Table 3.2 details the index and observation numbers for the experiment.

One major consideration in the experiment is the multiple sources of varia-

	lot	layer	wafer	site	design	observations
Index	i	l	w	s	d	y_{ilwsd}
Number	I=70	L=4	W=25	S=11	D=6	n=462000

Table 3.2: Experiment observations

tions. To get a practical and accurate analysis result, these variations should be either controlled or modeled appropriately. Typical ICs are produced through a series of processes, including lithography, etch, deposition, polishing and cleaning. Each of these processes can add process variability to the final product. Steps like in-line control are taken to reduce variation and ensure stability of the production line. Listed below are four types of variability identified in our

experiment:

1. Site level variability: In the experiment, 11 sites on the wafers are measured, including the sites in the center and on the edges. Potential site level variability can be caused by the occasional uneven circular patterns from the center of the wafer.

2. Layer level variability: As stated, the layer level variability is caused by the earlier metal layers undergoing more heat treatment and stress. This level of variability is identified as a nested effect.

3. Wafer level variability: Wafers are typically processed in lots of 25, and wafers in the same lot tend to go through the same manufacturing tools (although sometimes through different chambers), and have the same amount wait time between processing. However, due to the possible different chambers used, there can be some wafer-to-wafer variation in terms of thickness deposited, thickness removed etc.

4. Lot level variability: Wafers in the fab are grouped into lots of 25 and are processed together. Hence they are relatively uniform across a lot. The lots however tend to vary from one to another due to their processing on different tools and conditions. This type of process variation is potentially the largest among the variations. Hence adequately capturing and modeling it is important for identifying the key features of the process.

3.3 Review of literature

Typically, when defective counts data are observed, generalized linear models (GLMs) such as Poisson regression model are adopted to fit the data. Hamada and Nelder (1997) provided comprehensive guidelines on the use of GLMs for a range of applications in quality-improvement experiments. However, in high-quality manufacturing processes, the observed defective counts would often contain excessive zeros. When the number of zeros is greater than it can be predicted

from a standard count distribution such as the Poisson or the Negative Binomial distribution, the data are said to be zero-inflated. In this situation, the commonly used models such as Poisson regression can underestimate the probability of zero and hence make it difficult to identify significant control factors' effects and lead to poor prediction. Zero-inflated (ZI) model and hurdle model for fitting zero-inflated count data were proposed by Mullahy (1986), Lambert (1992) and Greene (1994).

In this section, we first describe these two models in detail and explain the suitability of the ZI model for modeling the ICs experiment observations in hand. Then we reviewed ZI/hurdle model with random effects. Following that, estimation methods for ZI/hurdle model with random effect were reviewed.

3.3.1 Zero-inflated regression model

Lambert (1992) examined defects in manufacturing, noting that one interpretation for the excessive zeros is that changes of unobserved environment factors may cause the process to shift randomly between a zero state in which defects are nonexistent and a count state in which defects can occur according to a Poisson distribution. In the current problem, the formation of shorts are caused by hillocks growing higher than the threshold between layers, see Figure 3.1. Specifically, copper hillocks shorter than the spacing between upper and lower layer (threshold height) are harmless as they do not cause shorts, and only hillocks grown higher than the threshold cause a current short. Hence, if the height density of the hillocks grown has a maximum height of less than the threshold height, regardless of the number of hillocks grown, the process will be in a perfect zero defect state (no short). If however, the height density has a maximum height larger than the threshold, then the process can be viewed as in a non-perfect (defect) count state, with hillocks potentially causing shorts. Lambert's ZI model was used to model zero-inflated data in many applications (Böhning et al., 1999; Cheung, 2002; Hasan and Sneddon, 2009).

The ZI model assumes that data are from a mixture of a point mass at zero

distribution and a regular count distribution, such as the Poisson distribution or the Negative Binomial distribution, etc. These two states are also called zero state and count state. In this model, there are two sources of zeros: zeros from the point mass at zero, and zeros resulting from the count distribution. To model which state the independent observations $y_i (i = 1, \cdots, n)$ comes from, a state indicator variable m_i is used:

$$m_i = \begin{cases} 0 & y_i \text{ is from the zero state} \\ 1 & y_i \text{ is from the count state} \end{cases} \tag{3.1}$$

When the count state is modeled by a count distribution $g(\cdot|\mu_i)$ with mean μ_i,

$$\begin{cases} P(y_i = 0) = 1 - p_i + g(0|\mu_i) & 0 \leqslant p_i \leqslant 1 \\ P(y_i = k) = p_i g(k|\mu_i) & k = 1, 2, \ldots \end{cases} \tag{3.2}$$

With linear predictors Z'_{i1} and Z'_{i2} , p_i and μ_i are typically modeled by

$$\text{logit } (p_i) = Z'_{i1}\boldsymbol{\beta} \quad \text{and} \quad \log (\mu) = Z'_{i2}\boldsymbol{\alpha} \tag{3.3}$$

where $\boldsymbol{\beta}$ and $\boldsymbol{\alpha}$ are coefficients corresponding to the logit and log components of the model respectively, and the predictors Z'_{i1} and Z'_{i2} are not necessarily the same.

The likelihood function is

$$L(\boldsymbol{\beta}, \boldsymbol{\alpha}) = \prod_{i=1}^{n} [1 - p_i(\boldsymbol{\beta})]^{1-m_i} [p_i(\boldsymbol{\beta}) g(y_i; \mu_i(\boldsymbol{\alpha}))]^{m_i} \tag{3.4}$$

To obtain the estimates, an EM algorithm was derived by Lambert (1992).

3.3.2 Hurdle models

The hurdle model, proposed by Arulampalam and Booth (1997) and Mullahy (1986) uses a two-stage modeling strategy. The first stage models the binary outcome of whether the response has a zero or a positive realization. If the realiza-

tion is positive, the 'hurdle' is crossed. The second stage uses a truncated-at-zero distribution to model the randomness in the positive observations. Applications include a Mexico health care utilization study used a zero-truncated NB hurdle model for predicting health care demand (Brown et al. (2005)).

For independent observations $y_i (i = 1, \cdots, n)$, suppose the probability of y_i being positive is ϕ_i, and the positives $y_i | y_i > 0$ follows a truncated-at-zero count distribution, such as a truncated Poisson or truncated NB. For truncated Poisson hurdle model, the distribution is:

$$\begin{cases} P(y_i = 0) = 1 - \phi_i & 0 \leqslant \phi_i \leqslant 1 \\ P(y_i = k) = \phi_i \frac{e^{-\lambda_i} \lambda_i^k / k!}{1 - e^{-\lambda_i}} & k = 1, 2, \ldots \end{cases} \tag{3.5}$$

Similar with ZI model, regression structure is also built into the model through:

$$\text{logit } (\phi_i) = Z'_{i1} \boldsymbol{\beta} \quad \text{and} \quad \log (\lambda_i) = Z'_{i2} \boldsymbol{\alpha} \tag{3.6}$$

where the covariates Z'_{1i} and Z'_{2i} appearing in the logistic and log components are not necessarily the same.

The likelihood function is

$$L(\boldsymbol{\beta}, \boldsymbol{\alpha}) = \prod_{i=1}^{n} [1 - \phi_i(\boldsymbol{\beta})]^{I(y_i = 0)} [\phi_i(\boldsymbol{\beta}) \frac{e^{-\lambda_i(\boldsymbol{\alpha})} \lambda_i(\boldsymbol{\alpha})^{y_i} / y_i!}{1 - e^{-\lambda_i(\boldsymbol{\alpha})}}]^{1 - I(y_i = 0)} \tag{3.7}$$

where $I(\cdot)$ is the indicator function.

The log-likelihood can be write into two terms,

$$l(\boldsymbol{\beta}, \boldsymbol{\alpha}) = l_1(\boldsymbol{\beta}) + l_2(\boldsymbol{\alpha}) \tag{3.8}$$

where,

$$l_1(\boldsymbol{\beta}) = \sum_{y_i = 0} [\log (1 - \phi_i(\boldsymbol{\beta})] + \sum_{y_i > 0} [\log \phi_i(\boldsymbol{\beta})] \tag{3.9}$$

is the log likelihood function for the binary part, and

$$l_2(\boldsymbol{\alpha}) = \sum_{y_i>0} [-\lambda_i(\boldsymbol{\alpha}) + y_i \log(\lambda_i(\boldsymbol{\alpha})) - \log(y_i!) - \log(1 - e^{-\lambda_i(\boldsymbol{\alpha})})] \quad (3.10)$$

is the log-likelihood function for the truncated model part.

For this hurdle mode, one can obtain maximum likelihood (ML) estimates by separately maximizing these two parts. Compared with the ZI models, hurdle models are easier to fit, as the two model components can be fitted separately.

3.3.3 ZI model with random effects

In semiconductor manufacturing, it has also been widely reported that there are multi-sources of variability. For example, Stapper (1985) modeled the wafer to wafer variation with a compound distribution that assumes the mean number of defects per wafer behaves like another random variable with its probability distribution $P\{N = k\}$, where $k = 0, 1, 2, \ldots$. Albin and Friedman (1989) applied a Neyman distribution to model wafer defect data that exhibits clustering. In our problem, we also observed that there are variations in the layer, wafer and lot levels.

Another method to accommodate heterogeneity is incorporating random effect to the regression model. In the split-plot experiment, the block factor levels are chosen at random from a larger population of possible levels, and there are wishes to draw conclusions about the entire population of block levels, not just those that have been collected. In this situation, the block factor is said to be a random factor. In our experiment, the lot is the random factor because the population of lot factor levels could be seen as infinite size because in the manufacturing line, there would be large enough lots been processed.

Hall (2000) extended Lambert (1992)'s ZI model to a mixed effect model by incorporating a normally distributed random effects into the log-linear parts of the ZI model. They were motivated by an example from horticulture, where count data with excess zeros were collected in an experiment with blocks. Simi-

larly, hurdle model with random effects has also been developed in the context of modeling the clustered observations occurs with longitudinal data, where the different subjects are the source of random effects. Min and Agresti (2005) extend the hurdle model to include random effects by incorporating random effects into both the logistic and the log-linear parts of the hurdle model, and assume the random effects are multivariate normally distributed.

The ZI model with random effects can be described as follows: let y_{ij} be observation $j(j = 1, \ldots, n_i)$ for block $i(i = 1, \ldots, m)$. To account for this block/lot level variation, the random effects term $\boldsymbol{b}_i = (b_{1i}, b_{2i})$ is incorporated into the linear predictors of the fixed effect ZI model Equation (3.3) as latent variables.

$$\begin{aligned} \text{logit } (p_{ij}|\boldsymbol{b}_i) &= Z'_{1i}\boldsymbol{\beta} + b_{1i} \\ \log (\mu_{ij}|\boldsymbol{b}_i) &= Z'_{2i}\boldsymbol{\alpha} + b_{2i} \end{aligned} \tag{3.11}$$

Generalizations to multivariate random effects for the two components are straightforward.

Let $\boldsymbol{\psi}$ represent the unknown parameters, the marginal log likelihood for the ZI random effect model is:

$$l(\boldsymbol{\psi}) = \sum_{i=1}^{m} \log L_i(\boldsymbol{\psi}) \tag{3.12}$$

where

$$L_i(\boldsymbol{\psi}) = \int \left[\prod_{j=1}^{n_i} (1 - p_{ij})^{1-m_{ij}} [p_{ij} g(y_{ij})]^{m_{ij}} \right] \varphi(\boldsymbol{b}_i) d\boldsymbol{b}_i \tag{3.13}$$

and φ denotes the joint density function for the random effects.

Since $\boldsymbol{b}_i$ is hidden variable and hence difficult to detect the distribution of it. Generally φ is assumed to be multivariate normal distribution. However, in the current case, the lot random effect displays multi-modal and skewed distribution features. We would relax the normality distribution in this thesis.

To estimate $\boldsymbol{\psi}$, the MLEs can be obtained by maximizing Equation (3.13). This is similar with the parameter estimation of the generalized linear mixed

models (GLMMs). The fundamental difficulty in using GLMMs is that $\boldsymbol{b}_i$ is hidden variable and no closed analytical expression for the likelihood is available. Newton-Raphson (NR)-type methods and EM are widely used to evaluate such problems. Although the NR-type methods have faster convergence rates than the EM method, these benefits are at the expense of numerical stability (i.e. these algorithms may not converge unless the model provides a reasonable good fit to the data and good initial values are used) (Dempster et al. (1977)). The EM algorithm, on the other hand, is very stable albeit being slow. In this problem, we would adopt the EM algorithm to ensure more stable estimations.

Meanwhile, no matter Newton-Raphson (NR)-type methods or EM is adopted to maximizing Equation (3.13), one first need to obtain the marginal likelihood by integrating out the random effects. These integrals are analytically intractable, and hence numerical or approximation methods must be applied. A variety of approaches have been proposed to circumvent this difficulty in fitting GLMMs, including approximate likelihood approaches, such as penalized quasi-likelihood (PQL) (Breslow and Clayton (1993)), numerical approaches, such as Laplace approximations and Gauss-Hermite quadrature (GHQ), and approaches based on the use of Monte Carlo methods, such as Markov Chain Monte Carlo (MCMC) techniques (McCulloch (1994)). In the ZI or hurdle model literature, both Hall (2000) and Min and Agresti (2005) adopted the GHQ method to approximate the integrals.

In current work, we would propose to represent the distribution of random effect variable by a more flexible distribution than the normal distribution. Hence more efficient approximation method to integrate the random effect distribution would be proposed.

3.4 Preliminary analysis

In this section, we first explain the generating process of the excessive zeros by a random state shift process, then identify the state shift level in the multilevel structure. Following that, we adopt the ZI model with normal random effects

by Hall (2000) to fit the data and show the deficiency of this model.

To facilitate the analyses, we define the aggregated variables on wafer and lot level as $y_{ilwd} = \sum_{s=1}^{S} y_{ilwsd}$ and $y_{ild} = \sum_{w=1}^{W} \sum_{s=1}^{S} y_{ilwsd}$.

3.4.1 Zero inflated observations

The most distinct characteristic of the experiment observations y_{ilwsd} is that approximately 96 percent of them are zeros. Additionally, when we examine the lot level count variable y_{ild}, large jumps are observed among counts across the design factors' different settings d. For example, at a fixed length, when width settings vary from -1.48, -1, -0.35, 0.94, we observe counts of 0, 56, 0, 178 for a fixed lot and layer. This implies that the expectation of y_{ild} is likely correlated with the design factors through a jump function $E(y_{ild}) = J_{il}(d)$, instead of a continuous one. Traditional count models, like the Poisson regression model, however, fail to capture these large jumps. One interpretation for these jumps was that slight, unobserved changes in the environment caused the process to shift randomly between a state in which defects are impossible and a state in which defects are possible but not inevitable. To capture this shift, the zero-inflated (ZI) model (Lambert (1992)) is the natural model to be adopted.

3.4.2 Multilevel structure and random shift level

Besides zero inflation, the observations are also characterized by a multilevel structure due to the nature of the IC manufacturing process. In the literature, ZI model practitioners generally directly treat the count in hand as randomly shifting from the two states for different designs d (for example, Moghimbeigi et al. (2008)). However, in multi-level structure cases like the problem studied here, the system state may be the same within the lower level (site or wafer level) while independently shifting between the zero state and the count state at the higher level (lot level). Hence, to build a practical multi-level ZI model, an important step is to decide at which level the random shift happens. For instance,

if it happens at the wafer level, the state indicator variable m has independent realization for each wafer w in a lot while the values within one wafer for the S sites are the same; if however, the random shift happens at the lot level, then the realizations of m for the W wafers in a lot take on the same values. To determine the random state shift level, we first examine the site, wafer and lot level observations to draw insights.

In the experiment, for each wafer, the test structures are placed on 11 separate sites and hence, the observations obtained at each site s, $s = 1, ..., 11$ are independent binary observations, with $y_{ilwsd} \sim Bernoulli(e_{ilwsd})$, where e_{ilwsd} is the probability of a short for design d at site s on wafer w in layer l of lot i. To determine if these short observations are identical across sites on the same wafer, a Kolmogorov-Smirnov approximation test was conducted.

The common Bernoulli success probability test cannot be directly employed here because there is only one observation from each site and 96 percent of them are zeros. Instead, we adopt the aggregated count of site location s over all designs, layers, wafers, and lots (every site summed over the same conditions), as the test statistic. This statistic is defined as $y_s = \sum_{i=1}^{I} \sum_{l=1}^{L} \sum_{w=1}^{W} \sum_{d=1}^{D} y_{ilwsd}, s = 1, \cdots, S$. These $y_s, s = 1, \cdots, S$ are from the same distribution because the experiment has a balanced design, where there are $N_s = I * L * W * D$ observations y_{ilwsd} for each site s.

According to Chen and Liu (1997), when N_s is large and all e_{ilwsd} are small but not necessarily equal (in our case, e_{ilwsd} are different due the lot, layer, and wafer level variations), the distribution of y_s can be approximated by a Poisson distribution with mean

$$\lambda_s = \sum_{i=1}^{I} \sum_{l=1}^{L} \sum_{w=1}^{W} \sum_{d=1}^{D} e_{ilwsd} \tag{3.14}$$

For these sites to be identical, within the same lot i, layer l, wafer w, and design d, the site-level probability e_{ilwsd}, for $s = 1, \cdots, S$, should be equal. As the design is balanced at all sites, this would imply that λ_s are also equal to each other. Hence $y_s, s = 1, \cdots, S$ should come from the same Poisson distribution.

We perform the following Kolmogorov-Smirnov test for every site s:

$$H_0 : y_s \sim Possion(\lambda_0), s = 1, \cdots, S, \quad \text{where} \quad \lambda_0 = \frac{\sum_{s=1}^{S} y_s}{S} \tag{3.15}$$

The results indicate that all the hypotheses cannot be rejected at a 0.01 level of significance, suggesting that the y_s at all S sites follow a Poisson distribution with the same mean λ_0.

The results indicate that they are identically distributed with $e_{ilw1d} = \cdots = e_{ilwSd}$. We hereby drop the site index s and denote this probability as e_{ilwd}. Hence, for all $S = 11$ sites on the same wafer, if $e_{ilwd} = 0$, then $y_{ilwsd} = 0$ indicating that the system is in the zero state; and if $e_{ilwd} > 0$, then $y_{ilwsd} \overset{iid}{\sim} Bernoulli(e_{ilwd})$, resulting in $y_{ilwd} \sim Binomial(S, e_{ilwd})$. This also leads us to conclude that the random shift in the ZI model does not occur at the site level. Following the $i.i.d$ observations at the site level, further examination of the data shows that, for fixed lot i, layer l and design d, observations y_{ilwd} for wafer $w = 1, \cdots, W$ are either all zeros or all positives. This suggests that the short probability e_{ilwd}, for wafer $w = 1, \cdots, W$ are either all zeros or all larger than zero, indicating that the state indicator variable m_{ilwd} are not independent among different wafers in the same lot, but instead, they share the same value for all wafers in the same lot. Hence this leads to a conclusion that the random shift in ZI model does not happen at the wafer level. Finally, at the lot level, as described in the subsection 3.4.1, we observe large jumps in y_{ild}, hence the random shift occurs at the lot level.

To model this shift and at the same time ensure that the indicator variable m_{ilwd} has the same realization within a lot for the W different wafers, we treat the lot level shorts count y_{ild} as the response variable. In the zero state, $e_{ilwd} = 0$ and $y_{ilwd} = 0, w = 1, \cdots, W$, hence y_{ild} has a point mass at zero distribution; in the count state, $e_{ilwd} > 0, w = 1, \cdots, W$ and hence y_{ild} follows a count distribution $g(\cdot|\mu)$.

Although there is no wafer variation on $m_{ilwd}, w = 1, \cdots, W$, conditioned on $m_{ilwd} > 0$, we allow for the probabilities $e_{ilwd}, w = 1, \cdots, W$ within the same

lot to be different, as we observed that the counts from different wafers (for the same design and layer) can be quite different. This is similar to observations by Stapper (1985) who noted that very seldom do all wafers have the same mean number of defects on them due to the nature of ICs manufacturing lines, and this should be properly accounted for in the model. We explain how to address this in the model development section.

3.4.3 Initial model fit

In our split-plot experiment, lot is a block factor and should be modeled as a random effect. Hall (2000) extended Lambert (1992)'s ZI model to a mixed effect model by incorporating normally distributed random effects into the ZI model. They were motivated by an example from horticulture, where count data with excess zeros were collected in an experiment with blocks. Here, we initially consider this model to describe the data in hand. Additionally, since in our problem the design parameters are nested within four ICs layers, we would allow the coefficients to vary among these layers. Speacially, let y_{ild} be observation $d(d = 1, \ldots, D)$ for layer $l = 1, 2, 3, 4$ and lot $i(i = 1, \ldots, I)$. To account for this lot level variation, the random effects term $\boldsymbol{b}_i = (b_{1i}, b_{2i})$ is incorporated into the linear predictors as latent variables:

$$\begin{aligned} &\text{logit } (p_{ild}|\boldsymbol{b}_i) = Z'_{1ild}\boldsymbol{\beta}_l + b_{1i} \\ &\log (\mu_{ild}|\boldsymbol{b}_i) = Z'_{2ild}\boldsymbol{\alpha}_l + b_{2i}, \qquad l = 1, 2, 3, 4 \end{aligned} \tag{3.16}$$

Since b_{1i} and b_{2i} are hidden variables and it is difficult to detect their distributions, we adopt the normality assumption as Hall (2000), and assume $b_{1i} \sim N(M_1, \sigma_1^2), b_{2i} \sim N(M_2, \sigma_2^2)$.

To fit this model, Hall (2000) provided an EM algorithm with Gaussian quadrature to approximate the E-step. We adopt this algorithm and fit the ZI models with $g(\cdot|\mu_{ild})$ being Binomial, Poisson and Negative Binomial (NB) dis-

tribution respectively. Based on BIC criteria, ZI_NB model is preferred.

After fitting this model, we check the deviation between the fitted model and the observations. Table 3.3 presents the observed and fitted frequencies for y_{ild} from the ZI_Nb model with normal random effects. We can see that this model overestimate the frequency of zeros by more than 20 percent, meanwhile, underestimate the frequency of large count ($y_{ild} > 150$) by 68 percent. This significant deviation of the observed frequencies from those fitted frequencies reflects the lack of fit of the current model.

This lot variation is often treated as a random factor in manufacturing pro-

Table 3.3: Observed and fitted frequencies for ZINB with normal random effects

y_{ild}	0	1	2	3	4	5	6	> 6
Observed	1090	59	37	30	24	19	16	405
ZINB(norm)	1328.6	50.9	29.1	22.1	17.9	14.5	12.7	275.3

cesses, and is generally assumed to be normally distributed (Shang et al. (2013)). This is typically for convenience as the random factor is a hidden variable and is inherently difficult to detect the true distribution of it. As there are two sources of zeros in the ZI model, the zero state and the count state, both M_{ild} and $\boldsymbol{y_x}|M_{ild} = 1$ are hidden values. To informally check the distribution shape of the lot effect, we use the observable variable $\overline{M}_{ild} = I(\boldsymbol{y_x} > 0)$ as a substitute of M_{ild}. Then a simple logistic regression model is fitted: logit $(\overline{p_{ild}}) = a_0 + \boldsymbol{a} \cdot LOT$, where $P(\overline{M}_{ild} = 1) = \overline{p_{ild}}$. The lots are included into the regression model as dummy variables and $\boldsymbol{a}$ are the corresponding coefficients. As the experiment design is balanced within each lot, the design and layer effects are roughly summarized in the parameter a_0, and hence, the estimated $\hat{\boldsymbol{a}}$ would reflect the relative lot effects. The kernel density estimate of the lot coefficients $\hat{\boldsymbol{a}}$ is shown in Figure 3.5. The multi-modality and right skewed characteristics of this lot effect for $\overline{M}_{ild}$ clearly indicates non-normality. Next, to informally check the normality assumption on random effects, we plot the kernel densities for the empirical estimates $\hat{b_{1i}}$ and $\hat{b_{2i}}, i = 1, \cdots, I$ from the fitted model. Suppose the normality assumption is valid, these densities should shape similar with normal

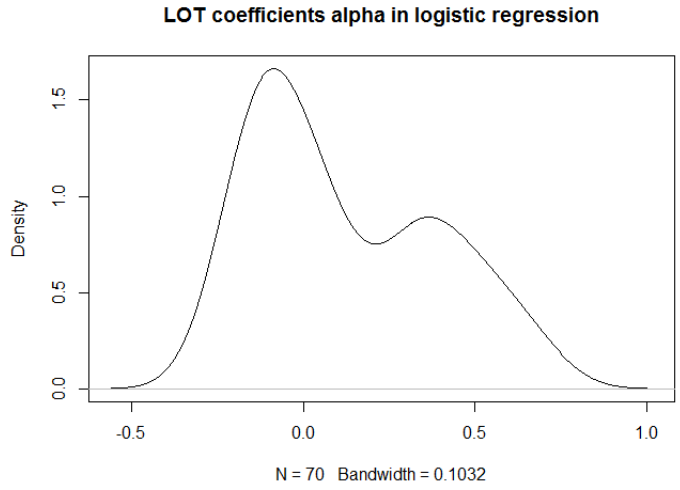

Figure 3.5: Kernel density estimates for lot coefficients

distribution. However, from the plots in Figure 3.6, we can clearly see the bi-modal shape. This indicate that the observed discrepancy is potentially due to the improper of normal distribution for describing the random effects.

Then we check how non-normality of random effects could influence the

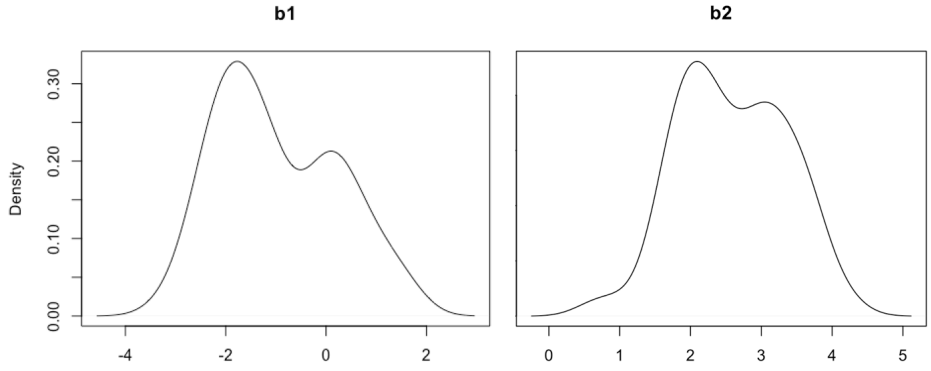

Figure 3.6: Estimated posterior modes of lot random effects

inference. One of our key modeling objectives is to calculate the optimum ICs design setting which minimizes the predicted response:

$$\hat{y}_{ld} = \hat{p}_{ld} * \hat{\mu}_{ld} = \frac{\exp(Z'_{1ld}\hat{\boldsymbol{\beta}}_l + \hat{M}_1 + Z'_{2ld}\hat{\boldsymbol{\alpha}}_l + \hat{M}_2)}{\exp(Z'_{1ld}\hat{\boldsymbol{\beta}}_l + \hat{M}_1) + 1} \quad l = 1, 2, 3, 4 \qquad (3.17)$$

From this nonlinear prediction formula, we can see that in ZI random effects model, the optimum point would be determined by both the fixed effects coef-

ficients ($\hat{\boldsymbol{\beta}}_l, \hat{\boldsymbol{\alpha}}_l$), and the random effects mean ($\hat{M}_1$, $\hat{M}_2$). Hence it is natural to concern about the efficiency of inference on the optimum point to non-normality of random effects. Thus, for ZI random effects model, relaxing the normality assumption may provide the opportunity to reduce the deviation in prediction and provide a better estimation of the optimum point.

3.5 Model development

In this section, through analyzing the features observed from the data, we make inference about the underlying hillocks formation process and handle the multilevel variations in three different ways. Variation among the four metal layers is modeled by varying the coefficients, and wafer-to-wafer variation is handled by assuming the mean number of hillocks per wafer behaves as a random variable. As the lot-to-lot variation is observed to be the largest with bimodal distribution features, we propose to model it as a random factor with a semi-nonparametric (SNP) distribution. In the ZI model with SNP random effects setting, the inference is complicated by the unbalanced data (excessive zeros) and the need for integration over the SNP density. Explicit formulas and computational algorithms are hence provided to estimate and evaluate the model parameters.

3.5.1 Multilevel zero-inflated model

We now go backward to the mechanism how the hillock-induced shorts happen and derive the count state distribution $g(\mu)$. This derivation allows us to capture the wafer-to-wafer variation based on the underlying hillocks growth process and provides us the opportunity to gain more insights on the impact of design factors on the formation of copper hillocks.

State shift and hillocks height

To understand the hidden factor causing the state shift in ZI model, we first analyze how hillocks can cause shorts. As previously described, the growth of hillocks is an inherent part of the manufacturing process, but these hillocks are harmless unless their heights are higher than the separation distance T (threshold) between layers (see Figure 3.2). In a testing site, if at least one hillock grows higher than T, a short would be detected. Hence, factors affecting the number of shorts are the hillock heights and the hillock numbers. As the number of hillocks grown in the process is quite large (from physical knowledge of the process), it can be assumed that the numbers are generated from a single non-zero process. It is then believed that the shift from the zero state to the count state can be largely explained instead by the existence of two different height densities for the hillocks growth heights in the zero state and the count state. Specifically, for the zero state height density, the maximum height of the density is always lower than T (dotted line density function in Figure 3.7), and hence, the hillocks with height from this density will never cause a short. For the count state height density, the maximum height is higher than the threshold (solid line density in Figure 3.7), and hillocks grown with height coming from this density can grow higher than T (with probability ρ), which then causes a short. The random shift between the two hillocks height densities for each design is caused by the uncontrollable combination effect of environmental factors in the process. This shift model is also supported by experimental results from Puttlitz et al. (1989) where they conclude that with the same metal line dimensions of 0.75μm thickness, hillock heights $\leqslant 1.3\mu$m were observed for 325° C in the nitride deposition cycle, while the hillock heights of $\leqslant 0.5\mu$m were observed for temperature 275°C.

Based on the previous observation that the state does not shift at the wafer level, the hillock height densities for hillocks grown in the same lot across W wafers (for fixed design and layer) can be reasonably assumed to be identical. Hence, in the zero state, the height density for each hillock on any wafer within

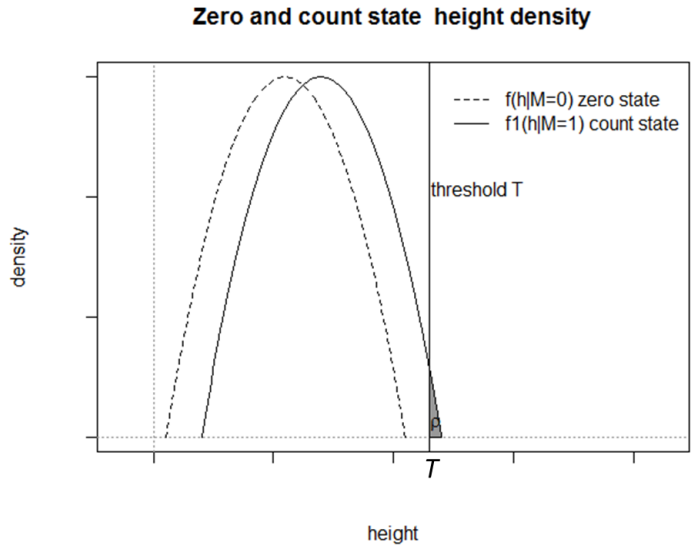

Figure 3.7: Zero and count state hillocks height density

lot i for layer l and design d can be described as:

$$f_{ild}(h|M_{ild}=0), h \in (0,T), \tag{3.18}$$

and in the count state,

$$f_{ild}(h|M_{ild}=1), h \in (0,\overline{T}], \overline{T} \geqslant T \tag{3.19}$$

where h is the height of each individual hillock, and $T \leqslant \overline{T} < \infty$ (based on the physical limits of the metal lines). Defining ρ_{ild} to be the probability of an individual hillock crossing the threshold T (see the shaded area in Figure 3.7), it can be expressed as

$$\rho_{ild} = \int_{T}^{\overline{T}} f_{ild}(h|M_{ild}=1)dh \tag{3.20}$$

Derivation of the count state distribution function $g(\mu)$

To simplify notations, we denote the conditional count state variable $y|m=1$ as y^c: y^c_{ilwsd}, y^c_{ilwd} and y^c_{ild}. Following, we first derive the site level short probability e_{ilwd} ($e_{ilwd} = P[y^c_{ilwsd}=1], e_{ilwd} > 0$) based on the fundamental distributions

of the number hillocks grown at a site and the hillocks growth heights, and analyze the origins of the wafer-to-wafer variation on e_{ilwd}. Following that, with the wafer level variation accounted for, we derive the distribution of wafer level count variable y^c_{ilwd}. This is finally followed by the derivation of the distribution for the lot level count variable y^c_{ild}.

1. Decomposition of site level short probability e_{ilwd}:

In the count state, to observe a short at a site indicates that there is at least one hillock at that site that has grown higher than T. We write the number of hillocks with height $h > T$ at site s as the random variable Z_{ilwsd}. Conditioned on the total number of hillocks grown at a site, N_{ilwsd}, $Z_{ilwsd}|N_{ilwsd} \sim Binomial(N_{ilwsd}, \rho_{ild})$, with probability ρ_{ild} given by Equation (3.20). Since N_{ilwsd} is an integer random variable, it is reasonable to assume it to be Poisson distributed. Hence, based on the site level $i.i.d$ observation, we assume $N_{ilwsd} \sim Poisson(\vartheta_{ilwd})$ on the same wafer for all S sites. After integrating out N_{ilwsd}, the unconditional distribution of Z_{ilwsd} remains a Poisson distribution, with mean $\xi_{ilwd} = \rho_{ild} * \vartheta_{ilwd}$. Combine with the fact that observing $y^c_{ilwsd} = 1$ is equivalent to observing $z_{ilwsd} \geqslant 1$, the short probability e_{ilwsd} can then be represented with parameters associated with hillocks height and number by:

$$e_{ilwd} = P(y^c_{ilwsd} = 1) = 1 - P(z_{ilwsd} = 0) = 1 - e^{-\xi_{ilwd}} \approx \xi_{ilwd} = \rho_{ild} \cdot \vartheta_{ilwd} \quad (3.21)$$

The approximation holds for the zero-inflated case, as ξ_{ilwd} is very small (Taylor expansion near zero).

From the analysis in Section 3.4.2, we know that e_{ilwd} varies among wafers in the same lot. From Equation (3.21), we can see that the parameter ρ_{ild} associated with hillocks height does not vary among wafers, hence the source of the wafer variation on e_{ilwd} is the mean number of hillocks grown at a site, ϑ_{ilwd}. In the ICs manufacturing process, the sources of wafer variation on hillocks height and number include thermal stresses and the pressure of the upper layers resulting in intrinsic stresses in the film. These stresses could be either compressive or tensile in nature depending on the growth process conditions. In this work,

the growth processes were consistent due to lot processes. Both these two environmental factors have relatively small variations among wafers: during the thermal processes, 25 wafers within the same lot are loaded into a single column together for processing; and the pressure of the upper layers depends on the thickness of the layers involved. As the thickness variation among wafers is also well controlled in the process, it is believed that the small variations in the environmental conditions do not cause a variation in hillocks height density but instead lead only to a variation in the number of hillocks grown. This indicates that the factor conditions initiating the growth of hillocks are more sensitive to environmental changes. As such, from the manufacturing perspective, as long as hillocks start to grow, it is important to ensure these hillocks do not reach the threshold height.

2. The distribution of wafer level counts variable y^c_{ilwd}:

Recall that $y^c_{ilwd} \sim Binomial(S, e_{ilwd})$ and since less than 4 percent of the site observations are ones, e_{ilwd} here is a very small value. According to Chen and Liu (1997), a Poisson approximate to the distribution of y^c_{ilwd} can be made as:

$$y^c_{ilwd} \sim Poisson(\lambda_{ilwd}), \quad \lambda_{ilwd} = S \cdot e_{ilwd} \approx S \cdot \rho_{ild} \cdot \vartheta_{ilwd} \tag{3.22}$$

As ϑ_{ilwd} varies among wafers, we model it as a random variable with a Gamma distribution.This is similar to the approach taken by Stapper (1985). Formally, we denote $\vartheta_{ilwd} \sim \text{Gamma}(r, \theta_{ild})$, then $\lambda_{ilwd} = S \cdot \rho_{ild} \cdot \vartheta_{ilwd}$ would also be Gamma distributed with $\lambda_{ilwd} \sim \text{Gamma}(r, S \cdot \rho_{ild} \cdot \theta_{ild})$. Integrating out λ_{ilwd} in Equation (3.22), the unconditional distribution of y^c_{ilwd} is then a Negative binomial distribution (NB) with mean $\bar{\mu}_{ild} = r \cdot S \cdot \rho_{ild} \cdot \theta_{ild}$ and dispersion parameter r.

3. The distribution for the lot level count variable y^c_{ild}

Since the lot level count is the sum of the counts on the individual wafers, $y^c_{ild} = \sum_{w=1}^{W} y^c_{ilwd}$, it will still follow a NB distribution with the same dispersion parameter r and mean $\mu_{ild} = W \cdot \bar{\mu}_{ild} = W \cdot S \cdot \rho_{ild} \cdot \theta_{ild}$, with the distribution

function:

$$P(y^c_{ild} = y_{ild}) = \frac{\Gamma(y_{ild} + r)}{\Gamma(r)\Gamma(y_{ild} + 1)} \left(\frac{\mu_{ild}}{\mu_{ild} + r}\right)^{y_{ild}} \left(\frac{r}{\mu_{ild} + r}\right)^{r} \tag{3.23}$$

Through a detailed breakdown of how shorts are observed on the wafers, we derive the count distribution $g(\mu)$ of the ZI model in Equation (3.2) with both hillocks height parameter ρ_{ild} and hillock number parameter θ_{ild}. The wafer to wafer variation in the count state is also explained by the difference on the mean number of hillocks grown on different wafers.

Multilevel ZI model with semi-nonparametric lot random effect

As observed from the data, the lot variation is dominant due to the processing on different tools and conditions for different lots. To account for this lot level variation, the random effects term $\boldsymbol{b}_i = (b_{1i}, b_{2i})$ are incorporated into the linear predictors of the ZI model as latent variables.

$$\begin{aligned} &\text{logit } (p_{ild}|\boldsymbol{b}_i) = Z'_{1ild}\boldsymbol{\beta}_l + b_{1i} \\ &\log (\mu_{ild}|\boldsymbol{b}_i) = Z'_{2ild}\boldsymbol{\alpha}_l + b_{2i}, l = 1, 2, 3, 4 \end{aligned} \tag{3.24}$$

The random effect ZI distribution is then written as

$$Y|\boldsymbol{b}_i \sim \begin{cases} 0 & \text{with probability } 1 - p_{ild} \\ g(\mu_{ild}) & \text{with probability } p_{ild} \end{cases} \tag{3.25}$$

where the distribution of $g(\mu_{ild})$ is the NB distribution with dispersion parameter r given by Equation (3.23).

From the previous section we see that the distribution of lot random effects $\boldsymbol{b}_i$ is likely non-normal and as hidden variables, it is difficult to detect their distribution. Here, we relax the normality assumption for $\boldsymbol{b}_i$, and assume only that they come from a smooth class of densities, and represent it with the semi-

nonparametric (SNP) representation proposed by Gallant and Nychka (1987). This representation encompasses a wider class of densities, enabling skewed, multi-modal and fat or thin-tailed densities and also the normal density to be captured. It has been previously used to model random effects in linear and generalized linear mixed models (Zhang and Davidian (2001); Chen et al. (2002)). We adopt this representation as it enables a general and adaptive class of random effects to be incorporated into the ZI model. Detailed studies on the performance of SNP estimators can be found in Fenton and Gallant (1996).

To facilitate further development, we rescale the random effects $\boldsymbol{b}_i$ by

$$\boldsymbol{b}_i = R\boldsymbol{z}_i + \boldsymbol{\tau} \tag{3.26}$$

where $\boldsymbol{\tau} \in \mathbb{R}^q$ location-transformation parameter and $R \in \mathbb{R}^{q\times q}$ is a scale-transformation lower triangular matrix. $\boldsymbol{z}_i$ is a $(q \times 1)$ random vector, and we assume it follows the SNP density:

$$h_K(\boldsymbol{z};\boldsymbol{\phi}) \sim P_K^2(\boldsymbol{z};\boldsymbol{\phi})\Phi_q(\boldsymbol{z}) = \left\{ \sum_{|k|=0}^{K} a_k \boldsymbol{z}^k \right\}^2 \Phi_q(\boldsymbol{z}) \tag{3.27}$$

for some fixed value K, where $\Phi_q(\cdot)$ is the standard q-variate normal distribution $N_q(0, I_q)$. Here, $P_K(\boldsymbol{z};\boldsymbol{\phi})$ is a multivariate polynomial of order K and $\boldsymbol{\phi}$ represent parameters in this form. For example, when $q = 2$ and $K = 2$, $\boldsymbol{z} = (z_1, z_2)^T (q = 2)$ and $P_K(\boldsymbol{z};\boldsymbol{\phi}) = a_{00} + a_{10}z_1 + a_{20}z_1^2 + a_{11}z_1z_2 + a_{02}z_2^2$. The proportionality constant is given by $1/\int P_K^2(x;\boldsymbol{\phi})\Phi_q(x)dx$, to ensure $h_K(\boldsymbol{z})$ integrates to 1. With $K = 0$, $P_K^2(\boldsymbol{z};\boldsymbol{\phi}) \equiv 1$, and $h_K(\boldsymbol{z})$ reduces to the standard normal density. The order K acts as a tuning parameter controlling the degree of flexibility of shape of the resulting density $h_K(\boldsymbol{z};\boldsymbol{\phi})$.

In the fitting of the density, it has been suggested to treat K as a tuning parameter, and to fit models for several values of K and then selecting K based on an information criteria, like the BIC (Zhang and Davidian (2001); Chen et al. (2002)). The numerical studies in these works also concluded that $K \leqslant 2$ is sufficient to capture many complicated density forms.

Combining transformation in Equation (3.26) and the SNP representation in Equation (3.27), the density of the ZI random effect $\boldsymbol{b}_i$ can be rewritten as

$$\varphi_K(\boldsymbol{b}_i;\boldsymbol{\delta}) = P_K[R^{-1}\boldsymbol{b}_i - \boldsymbol{\tau};\boldsymbol{\phi}] \cdot \Phi_q[R^{-1}\boldsymbol{b}_i - \boldsymbol{\tau}]/|\det(R)| \tag{3.28}$$

where $\boldsymbol{\delta}$ represent the parameters of random effects density, $\boldsymbol{\delta} = (\boldsymbol{\phi}, \boldsymbol{\tau}, R)$. Detailed studies on the performance of SNP estimators can be found in Fenton and Gallant (1996).

3.5.2 Model estimation

Likelihood

In the multilevel structure, we have $\boldsymbol{y} = (\boldsymbol{y}'_{\boldsymbol{1.}}, \cdots, \boldsymbol{y}'_{\boldsymbol{I.}})'$, with $\boldsymbol{y_{i.}} = [(y_{i11}, \cdots, y_{i1D})', \cdots, (y_{iL1}, \cdots, y_{iLD})']', i = 1 \cdots, I$. Hence, we have $f(\boldsymbol{y_{i.}}|\boldsymbol{b}_i;\boldsymbol{\theta}) = \prod_{l=1}^{L}\prod_{d=1}^{D} f(y_{ild}|\boldsymbol{b}_i;\boldsymbol{\theta}_l)$, where $\boldsymbol{\theta}_l = (\boldsymbol{\beta}_l, \boldsymbol{\alpha}_l)$ and $\boldsymbol{\theta} = (\boldsymbol{\theta}_1^T, \boldsymbol{\theta}_2^T, \boldsymbol{\theta}_3^T, \boldsymbol{\theta}_4^T)^T$. With the model developed in Equation (3.11) , (3.25) and (3.28), the marginal log likelihood function of the parameters $\boldsymbol{\psi} = (\boldsymbol{\theta}^T, \boldsymbol{\delta}^T)^T$ for a given K is then:

$$l(\boldsymbol{\psi}|\boldsymbol{y}) = \sum_{i=1}^{I} \log \int f(\boldsymbol{y_{i.}}|\boldsymbol{b}_i;\boldsymbol{\theta})\varphi_K(\boldsymbol{b}_i;\boldsymbol{\delta})d\boldsymbol{b}_i \tag{3.29}$$

where the integration is taken over the space for the random effects $\boldsymbol{b}_i = (b_{1i}, b_{2i})$.

To estimate $\boldsymbol{\psi}$, the MLEs can be obtained by maximizing Equation (3.29). However, as the integral and the first derivative of $l(\boldsymbol{\psi}|\boldsymbol{y})$ is intractable, numerical methods have to be applied. Newton-Raphson (NR)-type methods and EM are widely used to evaluate such problems. Although the NR-type methods have faster convergence rates than the EM method, these benefits are at the expense of numerical stability (i.e. these algorithms may not converge unless the model provides a reasonable good fit to the data and good initial values are used) (Dempster et al. (1977)). The EM algorithm, on the other hand is very stable albeit being generally slow. In this problem, we adopt the EM algorithm to ensure more stable estimations. In the next subsection, we first propose a general EM algorithm to estimate $\boldsymbol{\psi}$ and then develop an approximation algorithm

to reduce the computational expense for the quadrature evaluation procedure within the EM algorithm.

Computational details of the EM algorithm

The EM algorithm is generally well-suited for problems where there is incomplete data, and especially when it is difficult to maximize the observed log likelihood function directly, but much easier to maximize the loglikelihood function based on the complete data. In this ZI random effects model, the unobserved random effects, $\boldsymbol{b}$ can be treated as missing data, with complete data given as $(\boldsymbol{y}, \boldsymbol{b})$, The EM algorithm can then be adopted to fit this multilevel ZI random effects models.

As an iterative method, the EM algorithm estimates the parameters $\boldsymbol{\psi}$ in Equation (3.29) by iterating between the E-step and the M-step. Let $\boldsymbol{\psi}^t = (\boldsymbol{\theta}^t, \boldsymbol{\delta}^t)$ denote the estimated maximizer at iteration t for $t = 0, 1, \ldots$. The two steps in the EM algorithm are:

E-step: Given the current value $\boldsymbol{\psi}^t$, calculate the following Q function

$$Q(\boldsymbol{\psi}|\boldsymbol{\psi}^t) = \sum_{i=1}^{I} \int \log\, f(\boldsymbol{y_{i\cdot}}, \boldsymbol{b}_i; \boldsymbol{\psi}) f(\boldsymbol{b}_i|\boldsymbol{y_{i\cdot}}; \boldsymbol{\psi}^t) d\boldsymbol{b}_i \tag{3.30}$$

M-step: Maximize the computed Q function in Equation (3.30) with respect to $\boldsymbol{\psi}$ and set the optimal values to $\boldsymbol{\psi}^{t+1}$.

Return to the E step unless the stopping criterion is met. Here we adopt the *absolute convergence criterion* to mandate stopping when $|\boldsymbol{\psi}^{t+1} - \boldsymbol{\psi}^t| < 0.001$. Details about choosing stopping criteria for optimization problems like the EM can be found in Givens and Hoeting (2012).

In iteration t of the EM algorithm, function Q in Equation (3.30) can be expanded as

$$Q(\boldsymbol{\psi}|\boldsymbol{\psi}^t) = \sum_{i=1}^{I} \frac{\int \log\, \{f(\boldsymbol{y_{i\cdot}}|\boldsymbol{b}_i; \boldsymbol{\theta}) \varphi_K(\boldsymbol{b}_i; \boldsymbol{\delta})\} f(\boldsymbol{y_{i\cdot}}|\boldsymbol{b}_i; \boldsymbol{\theta}^t) \varphi_K(\boldsymbol{b}_i; \boldsymbol{\delta}^t) d\boldsymbol{b}_i}{\int f(\boldsymbol{y_{i\cdot}}|\boldsymbol{b}_i; \boldsymbol{\theta}^t) \varphi_K(\boldsymbol{b}_i; \boldsymbol{\delta}^t) d\boldsymbol{b}_i} \tag{3.31}$$

where

$$f(\boldsymbol{y_{i\cdot}}|\boldsymbol{b}_i;\boldsymbol{\theta}^t)=\prod_{l=1}^{L}\{\prod_{y_{ild}=0}[1-p_{ild}+p_{ild}\cdot g(y_{ild}=0)]\cdot\prod_{y_{ild}>0}[p_{ild}\cdot g(y_{ild})]\} \quad (3.32)$$

Integration of Equation (3.31) is analytically intractable, and hence numerical or approximation methods must be applied. However, in the case of the ZI model with random effects, traditional methods are either too computational intensive or inefficient. For example, with Monte Carlo methods, efficient sampling from the conditional distribution $f(\boldsymbol{b_i}|\boldsymbol{y_{i\cdot}},\boldsymbol{\psi}^t)$ are needed. Although Chen et al. (2002) proposed a 'double' rejection sampling method to generate a random sample for the conditional SNP density, for the zero-inflated type distributions the sampling would be inefficient due to the overwhelmingly high rejection rate. Additionally, in the case of SNP density, as the standard symmetry does not hold, the effectiveness of Laplace approximation methods would be poor. Similarly, a large amount of quadrature points would be needed for the Gaussian quadrature method.

To reduce the amount of quadrature points needed for a multi-modal density, we adopt the method proposed by Pinheiro and Bates (1995), where the quadrature points are centered at the mode of the integrand and scaled by inverse of the negative Hessian matrix. Specifically, to get the quadrature points at iteration t , we first obtain the empirical Bayes estimate of $\boldsymbol{b}_i$ as $\boldsymbol{b}_{i,t}$ and its covariance matrix $H_{i,t}=\text{cov}(\boldsymbol{b}_{i,t})$, given $\boldsymbol{\psi}^t=(\boldsymbol{\theta}^t,\boldsymbol{\delta}^t)$:

$$\boldsymbol{b}_{i,t}=\arg\max_{\boldsymbol{b}_i}(\sum_{l=1}^{L}\sum_{d=1}^{D}\log f(y_{ild}|\boldsymbol{b}_i;\boldsymbol{\theta}^t)+\log\varphi_K(\boldsymbol{b}_i;\boldsymbol{\delta}^t)) \quad (3.33)$$

$$=\arg\max_{\boldsymbol{b}_i}\{\sum_{l=1}^{L}\sum_{d=1}^{D}\log f(y_{ild}|\boldsymbol{b}_i;\boldsymbol{\theta}^t) \quad (3.34)$$

$$+\log\Phi_q[(R^t)^{-1}\boldsymbol{b}_i-\boldsymbol{\tau}^t]+\log P_K[(R^t)^{-1}\boldsymbol{b}_i-\boldsymbol{\tau}^t;\boldsymbol{\phi}^t]\} \quad (3.35)$$

Then in terms of mass points ζ_g with corresponding masses π_g, the G quadrature points $\boldsymbol{b}_{i,t}^Q = (\boldsymbol{b}_{i1,t}^Q, \ldots, \boldsymbol{b}_{iG,t}^Q)$ can be obtained from

$$\boldsymbol{b}_{ig,t}^Q = \boldsymbol{b}_{i,t} + H_{i,t}\zeta_g \text{ , for } g = 1, \ldots, G \tag{3.36}$$

After getting the quadrature points, we can use them to approximate the Q function in Equation (3.31) in iteration $t+1$. For the denominator of Equation (3.31), we have

$$f(\boldsymbol{y_{i\cdot}}.; \boldsymbol{\psi}) = \int f(\boldsymbol{y_{i\cdot}}|\boldsymbol{b}_i; \boldsymbol{\theta})\varphi_K(\boldsymbol{b}_i; \boldsymbol{\delta})d\boldsymbol{b}_i \tag{3.37}$$

$$\approx \sum_{g=1}^{G} |H_{i,t}^{\frac{1}{2}}|\pi_g f(\boldsymbol{y_{i\cdot}}|\boldsymbol{b}_{ig,t}^Q; \boldsymbol{\theta})\varphi_K(\boldsymbol{b}_{ig,t}^Q; \boldsymbol{\delta})\Phi(\zeta_g)^{-1} \tag{3.38}$$

$$=: f_G(\boldsymbol{y_{i\cdot}}.; \boldsymbol{\psi}) \tag{3.39}$$

then the Q function in Equation (3.31) is

$$\begin{aligned} Q_G(\boldsymbol{\psi}|\boldsymbol{\psi}^t) &= \sum_{i=1}^{I}\sum_{g=1}^{G} w_{ig}^t \log \{|H_{i,t}^{\frac{1}{2}}|\pi_g f(\boldsymbol{y_{i\cdot}}|\boldsymbol{b}_{ig,t}^Q; \boldsymbol{\theta})\varphi_K(\boldsymbol{b}_{ig,t}^Q; \boldsymbol{\delta})\Phi(\zeta_g)^{-1}\} \\ &= \sum_{i=1}^{I}\sum_{g=1}^{G} w_{ig}^t \log f(\boldsymbol{y_{i\cdot}}|\boldsymbol{b}_{ig,t}^Q; \boldsymbol{\theta}) \\ &\qquad + \sum_{i=1}^{I}\sum_{g=1}^{G} w_{ig}^t \log \{|H_{i,t}^{\frac{1}{2}}|\pi_g \varphi_K(\boldsymbol{b}_{ig,t}^Q; \boldsymbol{\delta})\Phi(\zeta_g)^{-1}\} \end{aligned} \tag{3.40}$$

where $w_{ig}^t = |H_{i,t}^{\frac{1}{2}}|\pi_g f(\boldsymbol{y_{i\cdot}}|\boldsymbol{b}_{ig,t}^Q; \boldsymbol{\theta}^t)\varphi_K(\boldsymbol{b}_{ig,t}^Q; \boldsymbol{\delta}^t)/f_G(\boldsymbol{y_{i\cdot}}.; \boldsymbol{\psi}^t)$.

In Equation (3.40), the parameters $\boldsymbol{\theta}$ and $\boldsymbol{\delta}$ are separated; thus maximization of Equation (3.40) at the M-step can be carried out in two steps, by optimizing the first and then the second term in Equation (3.40) respectively. Note that maximizing the second term in Equation (3.40), is a maximization of the SNP density parameters, and this can be carried out using fast estimation methods similar to those proposed in Zhang and Davidian (2001); Chen et al. (2002).

Computational approximation to the algorithm: estimating quadrature points

In the EM algorithm described, one would iterate between approximating the Q function using the quadrature points (Equation (3.31) and Equation (3.36)) and optimizing the Q function until stopping criteria is met, and then updating $\boldsymbol{\theta}$ and $\boldsymbol{\delta}$. However, for complex random effect densities like the SNP, the optimization to get Bayes estimates (Equation (3.35)) can be unstable and time consuming. For example, in the optimization of $\log P_K[(R^t)^{-1}\boldsymbol{b}_i - \boldsymbol{\tau}^t; \boldsymbol{\phi}^t]$, different starting points can result in significantly different local optimal points. Heuristically, we would like to circumvent this problem by centering the quadrature points close enough to the empirical estimates of $\boldsymbol{b}_i$. From the second line of Equation (3.35), we see that when number of observations within each lot and the number of lots are large (here in our case L and D), the sum of the first term has $n_i = L \cdot D$ terms which grows with these sample sizes. Moreover, the last two terms of Equation (3.35) are $O(1)$ (Wasserman (2013)), and hence, this first sum will dominate. We can then approximate Equation (3.35) asymptotically by this sum (and hence estimate $\boldsymbol{b}_{i,t}$ by its MLE), but since the second term does not pose a computational burden, we include it, and propose to approximate $\boldsymbol{b}_{i,t}$ in the iteration t by

$$\begin{aligned} \boldsymbol{b}_{i,t}^0 &= \arg\max_{\boldsymbol{b}_i}\{\sum_{l=1}^{L}\sum_{d=1}^{D} \log\, f(y_{ild}|\boldsymbol{b}_i;\boldsymbol{\theta}^t) + \log\, \Phi_q[(R^t)^{-1}\boldsymbol{b}_i - \boldsymbol{\tau}^t]\} \\ H_{i,t}^0 &= \mathrm{cov}(\boldsymbol{b}_{i,t}^0) \end{aligned} \tag{3.41}$$

Simulation studies in the next section also show that the approximation performs well in practice.

Then the G quadrature points $\boldsymbol{b}_{i,t}^Q = (\boldsymbol{b}_{i1,t}^Q, \ldots, \boldsymbol{b}_{iG,t}^Q)$ can be obtained by

$$\boldsymbol{b}_{ig,t}^Q = \boldsymbol{b}_{i,t}^0 + H_{i,t}^0\zeta_g, for g = 1, \ldots, G. \tag{3.42}$$

Proposed approximate adaptive Gaussian Quadrature EM (approximate AGQ-EM) algorithm

Overall, the proposed EM algorithm can be summarized as

1. **Starting values:** set values for K and starting values $\boldsymbol{\psi}^0$. Let $t = 0$.
2. **Quadrature points:** at iteration $(t+1)$, compute quadrature points $\boldsymbol{b}_{i,t}^Q$ from Equations (3.41) and (3.42).
3. **E-step**: approximate the Q function using $\boldsymbol{b}_{i,t}^Q$ and Equations (3.39) and (3.40).
4. **M-step**: obtain $\boldsymbol{\psi}^{t+1}$ by maximizing the Q function.
5. **Iterate**: Return to 2 and set $t = t + 1$ until the stopping criterion has been meet.

Good starting values of $\boldsymbol{\theta}_0$ can be obtained similarly with Lambert (1992); Hall (2000). In the ZI model, the zeros come from both the zero state and the count state (while we do not know which are from the zero state). Pretending all zeros are from the zero state and all positives are from the count state will allow us to fit the logistic and log regression in Equation (3.11) separately. Specially, we first fit the logistic regression with normal random effects (K=0) using $\overline{m_{ild}} = I(y_{ild} > 0)$ as the response variable. Then we fit the Poisson/NB regression with normal random effects using $y_{ild}|y_{ild} > 0$ as the response variable. These two regressions can be fitted separately using existing R package ("glmmML"). We use the estimated coefficients as initial values $\boldsymbol{\theta}^0 = (\boldsymbol{\beta}_0, \boldsymbol{\alpha}_0)$. Then we treat the estimated empirical estimates b_{1i0}, and $b_{2i0}, i = 1, \cdots, I$ as samples from the underlying SNP random effects distributions and obtain the initial value for random effects parameters $\boldsymbol{\delta}^0$. This $\boldsymbol{\delta}^0$ is a good starting value because a similar argument with Equation (3.41), from which we know that the empirical estimates of $\boldsymbol{b}_i$ from assuming $K = 0$ (normal) and $K = 1, 2 \cdots$ would be different but not far from each other. The proposed EM algorithm converges after around 20 iterations for the current problem with these initial values.

Convergence of the EM algorithm for ZI model also follows from arguments similar to those given by Lambert (1992); Hall (2000). Hall (2000) used Gaussian quadrature for approximating the E step, instead we use approximate AGQ which focuses on improving the approximation procedure. Intuitively, the Gaussian quadrature rule can be viewed as a deterministic version of Monte Carlo integration with samples ζ_g and weights π_g fixed beforehand (Pinheiro and Bates (1995)), while AGQ can be comparable to importance sampling, which increases the number of samples on the area of interest (AGQ places a larger weight on the mode of the integrand). In the random effects model, when the distribution of random effects has a complicated form such as the SNP, we cannot easily estimate the mode of the integrand (Bayes estimates of $\boldsymbol{b}_{i,t}$ in Equation (3.35)). Instead, the approximate AGQ put a larger weight on plausible values like $\boldsymbol{b}_{i,t}^0$ estimated by Equation (3.41). In the numerical runs we studied (results in Appendix), this approximation is reasonable, even for limited numbers of $L \times D$ for near symmetrical distributions of b, and moderate numbers of $L \times D$ for highly skewed distributions. The compromise proposed here means that when computing the quadrature points, we do not account for the information in the last term in Equation (3.35). Extensive simulation runs were also conducted to evaluate the proposed algorithm in estimating both the design/fixed effects and random effects parameters. Details of the simulation runs and results are provided in the Appendix. Overall, the proposed AGQ-EM algorithm is able to estimate both the fixed and random effects parameters with higher precision and accuracy over a Gaussian quadrature EM approach. In addition, the flexibility of the SNP random effects enables accurate capture of non-normal (asymmetrical and skewed) random effects and the proposed AGQ-EM algorithm is able to provide good parameter estimates of the model.

In cases where the count state is modeled by a NB distribution in the ZI model, there is an extra dispersion parameter r to be estimated. The estimation of $\boldsymbol{\theta}_l$ and $\boldsymbol{\delta}$ via the proposed approximate EM-AGQ algorithm assumes that r is known. In practice, r is updated and estimated iteratively in accordance with

the updated estimates of $\boldsymbol{\theta}_l$ and $\boldsymbol{\delta}$ by maximizing the loglikelihood function in Equation (3.29). More details about estimating the NB dispersion parameter can be found in Piegorsch (1990).

Standard errors of parameter estimates

To obtain the EM standard errors, bootrapping is commonly used. However, for a complex multilevel ZI model, bootstrapping can be computationally prohibitive. Here, we apply the Empirical Information method (Givens and Hoeting (2012)) to compute the standard errors for the EM estimates. The appeal of it is that all the terms of the *empirical information* (Givens and Hoeting (2012)) are by-products of the M-step in the EM algorithm and hence, no additional computation is required.

We register $\boldsymbol{\varsigma} = (\boldsymbol{\psi}, r)$ and when there is no over-dispersion parameter, $\boldsymbol{\varsigma} = \boldsymbol{\psi}$. Under the proper regularity assumptions, asymptotically as the number of observations $n \to \infty$, the EM estimates $\hat{\boldsymbol{\varsigma}}$ of $\boldsymbol{\varsigma}$ is a consistent, efficient, and asymptotically normal estimator of the true value of $\boldsymbol{\varsigma}$. Its asymptotic variance is the inverse of the Fisher information matrix

$$H(y;\boldsymbol{\varsigma}) = E(I(y;\boldsymbol{\varsigma})) = E(S(y;\boldsymbol{\varsigma})S^T(y;\boldsymbol{\varsigma})) \tag{3.43}$$

where $S(y;\boldsymbol{\varsigma}) = l'(y;\boldsymbol{\varsigma})$ is the score function and $I(y;\boldsymbol{\varsigma}) = -l''(y;\boldsymbol{\varsigma})$ is the Fisher information. To be more general, we write the observed response as $y = (y_1, \ldots, y_I)$ for I lots, and $y_i = (y_{i1}, \ldots, y_{in_i})$ as within lot observations. On condition the data are *i.i.d* observations, the score function is the sum of individual observation score:

$$S(y;\boldsymbol{\varsigma}) = \sum_{i=1}^{I}\sum_{j=1}^{n_i} S(y_{ij};\boldsymbol{\varsigma}) \tag{3.44}$$

Since the Fisher information $H(y;\boldsymbol{\varsigma})$ is defined to be the variance of $S(y;\boldsymbol{\varsigma})$, this suggests estimating $H(y;\boldsymbol{\varsigma})$ using the sample variance of the individual scores $S(y_{ij};\boldsymbol{\varsigma})$, that is the *empirical Fisher information* $\hat{H}(y;\hat{\boldsymbol{\varsigma}})$ (Givens and Hoeting

(2012)), with

$$\hat{H}(y;\boldsymbol{\varsigma}) = \frac{1}{n}\sum_{i=1}^{I}\sum_{j=1}^{n_i} S(y_{ij};\boldsymbol{\varsigma})S(y_{ij};\boldsymbol{\varsigma})^T - \frac{1}{n^2}S(y;\boldsymbol{\varsigma})S(y;\boldsymbol{\varsigma})^T \tag{3.45}$$

Here n is the total number of observations and $n = \sum_{i=1}^{m} n_i$. Note that in the EM algorithm, $\boldsymbol{\varsigma}^t$ maximize $Q(\boldsymbol{\varsigma}|\boldsymbol{\varsigma}^t) - l(\boldsymbol{\varsigma}|y)$ with respect to $\boldsymbol{\varsigma}$ in the t_{th} step. Therefore,

$$Q'(\boldsymbol{\varsigma}|\boldsymbol{\varsigma}^t)|_{\boldsymbol{\varsigma}=\boldsymbol{\varsigma}^t} = S(y;\boldsymbol{\varsigma})|_{\boldsymbol{\varsigma}=\boldsymbol{\varsigma}^t} \tag{3.46}$$

Since in the M step of EM algorithm, we calculate $Q'(\boldsymbol{\varsigma}|\boldsymbol{\varsigma}^t)|_{\boldsymbol{\varsigma}=\boldsymbol{\varsigma}^t}$ to get the optimum value of the parameters, we get $S(y;\boldsymbol{\varsigma})|_{\boldsymbol{\varsigma}=\boldsymbol{\varsigma}^t}$ as by-products of the M step, so no additional computation is required to get the individual terms in 3.45.

3.5.3 Modeling remarks

In our analysis, we derive the count state distribution $g(\cdot)$ based on the knowledge of hillocks growth process for generating the data. However, when such knowledge is lacking, model selection techniques such as BIC criterion should be used to decide the distribution $g(\cdot)$. Count distributions such as the Poisson, binomial, negative binomial, and logarithmic series distributions could be used for $g(\cdot)$ depends on the data characteristics in hand.

In other semiconductor experiment, the state shift may happen at other levels of the multilevel structure. For example, when it happens at the wafer level, a two-level random effects ZI model with response variable y_{ilwd} could be built as:

$$\text{logit }(p_{iwd}) = Z'_{1iwd}\boldsymbol{\beta} + b_{1iw} + b_{1i} \qquad \log(\mu_{iwd}) = Z'_{2iwd}\boldsymbol{\alpha} + b_{2iw} + b_{2i} \tag{3.47}$$

where (b_{1iw}, b_{2iw}) are the wafer level SNP random effects. However, if the shift occurs at site level where the data is binary, there is no way that we can tell which state an observed zero is generated from. Other methods such as a logistic

regression model with sub-sampling (King and Zeng (2001)) need to be applied. Otherwise, repeated measures at the site level would be required. If there are additional levels of variability that need to be captured, higher dimension of the random effects $\boldsymbol{b}_i (q > 2)$ can be applied. Although we describe a single-level random effect in our case study, the dimension of the integral in the proposed approximate AGQ-EM algorithm can be large (see Schilling and Bock (2005), who considered integration with AGQ up to 8 dimensions).

Although the above multilevel ZI model with SNP random effects is derived based on our ICs experiment, certain aspects of it can be generalized and applied to other fields where multilevel ZI data is common, such as in sociology and health care. Examples include high school dropout numbers, amounts of insurance, decayed teeth of 12 years old. These data generally contain excessive zeros and are measured within a hierarchical social structure such as households, schools, provinces, etc (see examples from Tooze et al. (2002); Moghimbeigi et al. (2008).

3.6 Simulation studies

To evaluate the performance of the proposed algorithm in estimating both the design/fix effects and random effects parameters, we performed simulations under 5 different distributions for random effects b_i. We also compared the algorithm with one that uses the Gauss-Hermite quadrature to approximate the integrals in the EM algorithm (GH-EM). The computational advantage of this approximation method is that it does not require the estimation of the empirical Bayes estimate of $\boldsymbol{b}_i$ at each iteration. We report on the logistic component of the ZI regression model. To be more general, we drop the layer index l and use $j = 1, \cdots, n_i$ to represent observations within lot i. In each of 100 Monte Carlo data sets, for each of $i = 1, \ldots, I = 200$ lots, $M_{ij}, j = 1, \ldots, n_i = 15$ observations were generated as conditionally independent samples according to

$M_{ij}|b_i \sim Bernoulli(p_{ij})$ where

$$\text{logit } (p_{ild}) = \log \left(\frac{p_{ij}}{1 - p_{ij}} \right) = W_{ij}\beta + b_i \tag{3.48}$$

W_{ij} include five design levels with $W_{ij} = (-1, -0.5, 0, 0.5, 1)$ and $\beta = 0.3$. For each design level, three replicates were sampled.

We drew b_i from several different distributions to evaluate the performance of the proposed algorithm. These include the Normal distribution (skewness =0), the Gamma distribution (skewness=1.633), the lognormal distribution (skewness=2.260), a symmetrical mixture normal mixture (weight=0.5) and an asymmetrical mixture normal mixture (weight=0.8). For these simulation scenarios, p_{ij} is set at 0.2, which is consistent with the case study. For each data set, Equation (3.48) was the first fit using the approximate AGQ-EM with the SNP assumptions, for $K = 0, 1$ and 2. The GH-EM was also applied for $K = 0, 1$ and 2. In both the AGQ-EM and GH-EM, the BIC was used to select the best fit. As previous studies indicate that $K = 2$ is sufficient to describe a broad class of densities (Chen et al. (2002)), larger K were not considered in the interest of computation speed.

The estimation results are summarized in Table 3.4. As we can see from the numerical studies, the fix effect parameter β is estimated with more precision than the elements associated with the random effects distribution for both approximation methods. This is likely because the accuracy of estimates of β is determined by the total number of observations, while the precision of estimates of elements associated with random effect distribution is determined by the total number of lots. As we can see, the efficiency in the estimation of $E(b_i)$ and $var(b_i)$ under a misspecified normal random effects model (K=0) is compromised for both the AGQ-EM and GH-EM algorithms as compared to their counterparts selected by BIC. The estimates in the BIC selected to model for approximate AGQ-EM are nearly unbiased with relatively small standard errors, and the models estimated by GH suffer a higher bias. The AGQ-EM rescales and updates the quadrature points after each iteration. Hence, the algorithm

is better able to evaluate the Q function (and obtain better estimates of the parameters in the M step) as the parameters and distributions are updated after every iteration. The GH-EM however, determines the quadrature points at the start, which are then fixed throughout the EM iterations. The evaluations and approximations can be poor if the initial estimates of the parameters are far from the "true" parameters. These observations highlight the importance of a proper assumption of the random effect distribution, as well as the usefulness of an efficient approximation, especially when the total number of lots is not large. Here, the significant gain in precision of using approximate AGQ is the centering of the quadrature mass points to points near the modes of the integrand and scaling it using the estimated Hessian at every iteration as the distribution gets updated.

We also note that when the random effect has a distribution with large skewness (log-normal with skewness=2.260), both the fix effect parameter β estimate and the random effects mean $E(b_i)$ suffer from a slightly larger bias. This is likely due to the poorer approximation to the integrand applied in the approximate AGQ for highly skewed distributions. This is because the points are centered at $\boldsymbol{b}_{i,t}^0$, may not approximate the true mode of the integrand $\boldsymbol{b}_{i,t}$ very well, especially when the observations per lot are small, especially for skewed distributions cannot be ignored). However, this situation is rare since the observations within one lot are sufficient to make inference about the fixed effects. Additional runs were conducted for this case where the observations per lot were increased to n_i=30, and the estimates improved, reducing both the standard derivation of β and the bias of $E(b_i)$ by around 50 percent. In situations where observations are limited, importance sampling can be used instead to approximate the integrand, but this method will require much more computational effort.

For further comparison, we consider the case where the true random effects density is normal. The estimates from both approximate AGQ-EM and GH-EM are almost all unbiased. The BIC criteria selected the true model (K=0) 77% of the time with the AGQ-EM, indicating that the SNP can detect the true random

symmetrical mixture normal mixture weight=0.5				
para(true)		β (0.300)	$E(b_i)$ (-0.475)	var(b_i) (0.630)
approx-AGQ (SE)	normal	0.300 (0.059)	-0.470 (0.065)	0.661 (0.102)
	SNP	0.300(0.059)	-0.474 (0.065)	0.651 (0.107)
GH(SE)	normal	0.300 (0.059)	-0.470 (0.064)	0.660 (0.107)
	SNP	0.290 (0.065)	-0.440 (0.082)	0.460 (0.164)
asymmetrical mixture normal mixture weight=0.8				
para(true)		β (0.300)	$E(b_i)$ (-0.470)	var(b_i) (1.035)
approx-AGQ (SE)	normal	0.294 (0.068)	-0.531(0.089)	1.103 (0.165)
	SNP	0.300 (0.068)	-0.457 (0.084)	1.055 (0.158)
GH (SE)	normal	0.307 (0.054)	-0.515 (0.083)	1.146 (0.159)
	SNP	0.282 (0.051)	-0.429 (0.068)	0.588 (0.07)
Gamma distribution: skewness=1.633				
para(true)		β (0.300)	$E(b_i)$ (-0.450)	var(b_i) (1.000)
approx-AGQ (SE)	normal	0.299 (0.068)	-0.505 (.0.077)	0.871 (0.141)
	SNP	0.300 (0.068)	-0.46 (0.080)	0.900 (0.174)
GH(SE)	normal	0.300 (0.068)	-0.505 (0.077)	0.879 (0.148)
	SNP	0.284 (0.064)	-0.430 (0.060)	0.541 (0.165)
lognormal distribution skewness=2.260				
para(true)		β (0.300)	$E(b_i)$ (-0.450)	var(b_i) (1.000)
approx-AGQ (SE)	normal	0.303 (0.059)	-0.519 (0.084)	0.939 (0.144)
	SNP	0.303 (0.059)	-0.466 (0.088)	0.996 (0.200)
GH(SE)	normal	0.304 (0.059)	-0.520 (0.084)	0.951 (0.151)
	SNP	0.288 (0.055)	-0.474 (0.075)	0.646 (0.286)
Normal distribution: skewness=0				
para(true)		β (0.300)	$E(b_i)$ (-0.450)	var(b_i)(1.000)
approx-AGQ (SE)	normal	0.300 (0.053)	-0.450 (0.077)	0.979 (0.131)
	SNP	0.300 (0.053)	-0.453 (0.079)	0.988 (0.141)
GH(SE)	normal	0.300 (0.053)	-0.449 (0.076)	0.994 (0.138)
	SNP	0.300 (0.054)	-0.453 (0.089)	0.883 (0.259)

Table 3.4: Simulation results for 100 datasets: Approx-AGQ(SE) are the average of estimated values and the respective standard errors computed from approximate AGQ-EM, GH(SE) are those computed from GH-EM. SNP represents the best model selected by the BIC criterion when using SNP representation

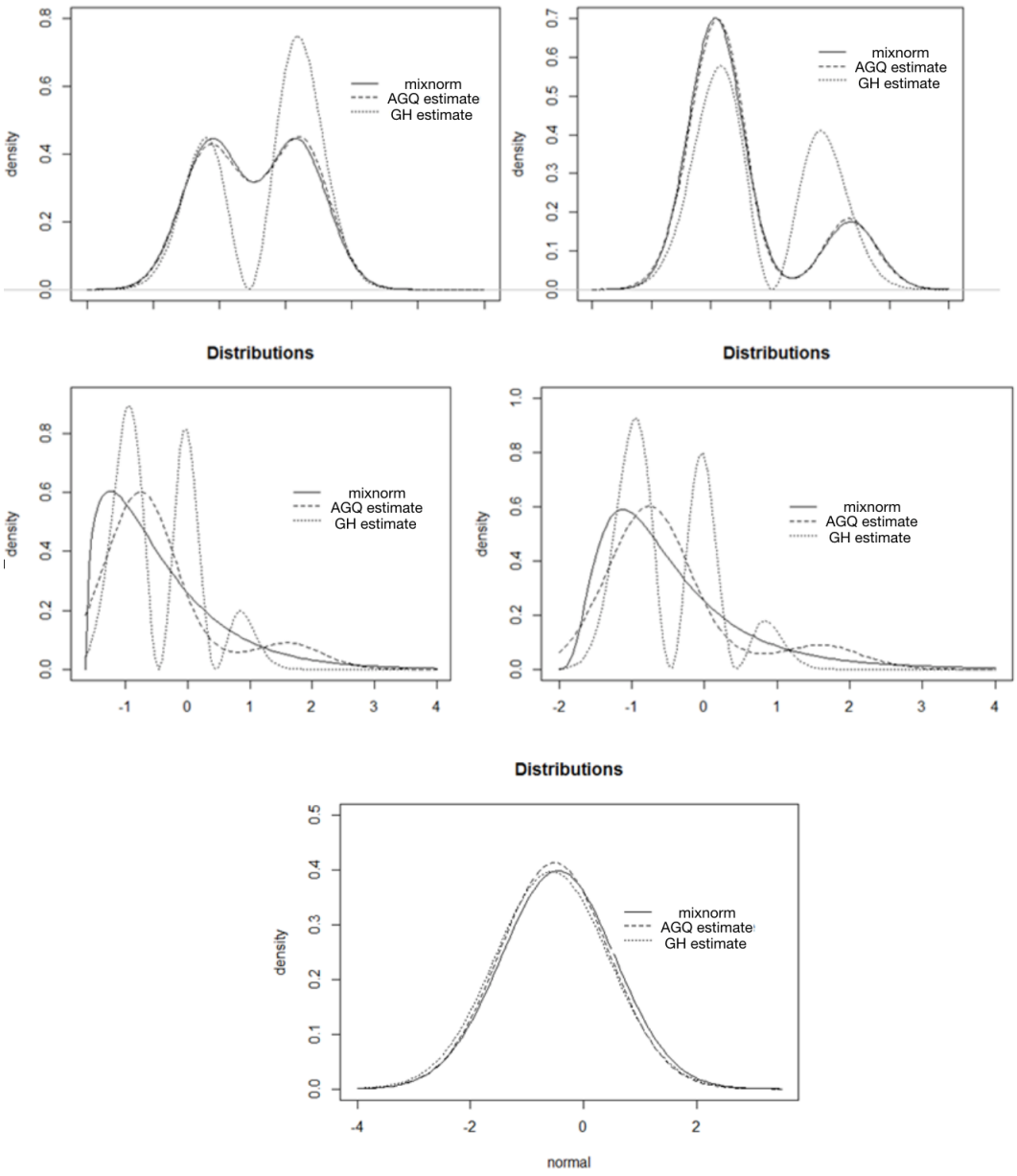

Figure 3.8: Simulation results based on 100 datasets:true density (solid line) compare with average estimated densities for 100 data sets fitted by approximate AGQ-EM preferred by BIC (long dashed line), and fitted by GH-EM preferred by BIC (dotted line)

effects distribution effectively in this multilevel ZI model. Figure 3.8 shows the Monte Carlo average of the estimated SNP densities selected by BIC over the 100 datasets computed from the approximate AGQ-EM algorithm, along with that estimated from the GH-EM algorithm and the true density. The figure shows that the SNP can capture relatively accurately the features of the random effects b_i, and the proposed approximate AGQ-EM provides good estimates of the model. From Figure 3.8, we see that the SNP density (with K up to 2) can approximate both the symmetrical mixture normal and the asymmetrical mixture normal quite well. However, for skewed densities like the Gamma and the lognormal distribution, the SNP approximations are poorer, especially at the tails. This can be due to the limited samples and lots observed, especially at the tails, and considerations of K up to only 2 for the SNP density. The SNP density fit improves when the number of lots is increased, and K = 3 is used (figure not shown here). It is noted however that the parameter estimates of the model do not improve much, albeit much higher computational expense. From Figure 3.8, it is also obvious that the SNP density estimated from GH-EM deviates quite a bit from the true density. Because as the algorithm iterates, the estimates of the mode of the random effect distribution change. Hence, "GH estimate" would potentially locate the highly weighted point in the wrong place, leading to a poor approximation of the integrand in the E-step of Equation 3.30. This also demonstrates the advantages of adopting the proposed approximate AGQ procedure to approximate the integral involved in the EM algorithm.

3.7 Analysis and interpretation of the copper hillocks problem

In this case study, we are interested in looking into the metal dimensions and layer factors that cause harmful copper hillocks to facilitate a better understanding of the growth process phenomenon and recommend design settings to minimize harmful hillock formation.

3.7.1 Analysis of design factors' effect on hillock growth

Based on the domain knowledge and experiment design presented in Table 3.1, we identify the potential regressors as Width, Width^2 and Length. Adopting the multilevel ZI negative binomial (ZI-NB) developed in the previous sections with these predictors, we have:

$$\begin{aligned}\text{logit } (p_{ild}) &= \beta_{0l} + \beta_{1l} * \text{Width} + \beta_{2l} * \text{Width}^2 + \beta_{3l} * \text{Length} + b_{1i} \\ \log\ (\mu_{ild}) &= \alpha_{0l} + \alpha_{1l} * \text{Width} + \alpha_{2l} * \text{Width}^2 + \alpha_{3l} * \text{Length} + b_{2i}\end{aligned} \tag{3.49}$$

for layers $l = 1, \ldots, L$. We also assume lot random effects for the two components are independent, with $b_{i1} \sim \varphi_K(b_{i1}; \boldsymbol{\delta}_1)$ and $b_{i2} \sim \varphi_K(b_{i2}; \boldsymbol{\delta}_2)$, where $\varphi_K(\cdot)$ is the SNP density in Equation (3.27).

In order to determine the significant design factors that affect the hillocks growth and shorts, the full model with all design factors in the four layers was first estimated for $K = 0, 1, 2$ of the SNP. The significant factors were then determined, and the reduced model re-estimated, for each K. Based on the BIC criterion, $K = 2$ is preferred for both b_{1i} and b_{2i}, and Table 3.5 presents the results of fit for K=2.

As a comparison, we also fitted the ZI model with $g(\mu)$ as a Poisson and also a Binomial for $K = 0, 1, 2$. The BIC value for the best fitting ZI Binomial (ZIB), ZI Poisson (ZIP) and ZI Negative Binomial (ZINB) are shown in Table 3.6. As we can see, the BIC values of ZIB and the ZIP models are much larger than that of ZINB. Hence, the ZINB model that was derived based on an understanding of the mechanisms of the process gives a much better fit to the data. As the ZINB model is able to capture the wafer variation through the extra over-dispersion parameter, where the ZIP and ZIB models are unable, this result further confirms the existence of wafer variations that cannot be ignored.

Table 3.7 shows the comparison of the observed and fitted frequencies from ZI_NB with SNP random effects (ZI_NB_SNP) and normal random effects

Logistic (p_{ild}) model (K=2)			
Parameter		Estimate (SE)	t-value
Layer1 intercept	(β_{10})	0.633 (0.207)	3.058
Layer1 width	(β_{11})	0.363 (0.122)	2.975
Layer1 length	(β_{13})	0.209 (0.117)	1.786
Layer2 length	(β_{23})	-0.292 (0.119)	-2.453
Layer3 width	(β_{31})	0.278 (0.124)	2.242
Layer4 intercept	(β_{40})	0.174 (0.171)	1.018
mean(b_{i1})		-0.924 (0.137)	-6.744
sd(b_{i1})		1.172 (0.123)	9.528
NB mean (μ_{ild}) model (K=2)			
Parameter		Estimate (SE)	t-value
Layer2 width	α_{21}	0.223 (0.152)	1.467
Layer3 intercept	α_{30}	-0.518 (0.217)	-2.387
Layer3 width	α_{31}	0.182 (0.151)	1.205
Layer4 intercept	α_{40}	-0.754 (0.397)	-1.899
Layer4 width	α_{41}	0.640 (0.269)	2.379
Layer4 width^2	α_{42}	0.783 (0.316)	2.3791
Layer4 length	α_{43}	0.503 (0.229)	2.197
dispersion parameter	r	0.270 (0.047)	5.744
mean(b_{i2})		3.051 (0.137)	22.270
sd(b_{i2})		0.984 (0.204)	4.823

Table 3.5: Parameter estimates and standard errors for multilevel ZI-NB model with K=2

Model	ZIB	ZIP	ZINB
BIC	31867	25427	6982

Table 3.6: BIC values for model selection

(ZI_NB_Norm). From this table, we can clearly see that the problem of overestimating the zero events of ZI_NB_Norm is greatly reduced by ZI_NB_SNP, and meanwhile, ZI_NB_SNP provides a better fit to the large count. This confirms that the extra flexibility of SNP allows the model to fit the data much better than the normal counterpart.

Table 3.7: Observed and fitted frequencies(rounded)

shorts/lot	observed	SNPpred	SNPDev	Normpred	NormDev
0	1090	1112.3	22.3	1328.6	238.6
1	59	54.5	-4.5	50.9	-8.1
2	37	35.5	-1.5	29.1	-7.9
3	30	26.6	-3.4	22.1	-7.9
4	24	22.2	-1.8	17.9	-6.1
5	19	17.6	-1.4	14.5	-4.5
6	16	15	-1	12.7	-3.3
>6	405	351.1	-53.9	275.3	-129.7
>40	238	194.6	-43.4	179.7	-58.3
>150	13	7.1	-5.9	4.2	-8.8

3.7.2 Interpreting the growth features

Recall that p_{ild} is the probability of the hillocks' height coming from the count state density and the model determines the effect of the design factor on the hillocks height. Specifically, a higher p_{ild} implies a higher chance of having a height density with the maximum value larger than the threshold. The model for the conditional mean number of shorts μ_{ild} (conditioned that the process is in the count state), determines the effect of the design factors on both hillocks height and number.

First we examine the design factors' effect on hillocks height through p_{ild}.

We see from Table 3.5 that the design factors have the most significant effects on p_{ild} in layer 1, and with almost no effect on p_{ild} for layer 4. During processing, the wafers undergo several chemical and physical processes, and the heating cycles that occur in these processes is believed to affect the growth of hillocks. As the metal/insulating layers are stacked one on top of another, earlier metal

layers undergo more heat treatment as more layers are processed above it. During heating, the metals and surrounding dielectric materials have different coefficient of thermal expansion and will expand at different rates and subsequently cooled down, and the cycle continues until four layers are build up. This creates cyclic stress in the layers, and the results show that this will affect the growth of hillocks. Since layer 1 goes through the most heating cycles, and layer 4 the least, the effect of design factors on these two layers suggests that the height distribution is directly linked to the heating cycles, making it more sensitive to the values used in the design factors. This means that certain design settings can result in a higher chance of shifting to a count state height density. Hence, careful determination of the design settings for layer 1 (specifically the width and length of the metal layer) can significantly reduce the chance of growing high hillocks.

We also noticed that the design factors' effect of layer 2 on p_{ild} has a different direction (sign of β) from the other three layers. In the manufacturing process, layer 2 goes through an additional procedure after its processing. Specifically, after processing layer 2, the wafers are placed on hold for electrical testing (ET) to determine the conformance of the wafer up to that stage. This causes a delay in the wafer processing as the wafers spend additional time in this step waiting for and going through the ET. During this waiting time, the copper can self-anneal (Lagrange et al. (2000)), even at room temperature. We see that after this self-annealing process, the larger length would reduce the chance of having a count state hillocks density (harmful density), and this is different from the length's effect on other layers. This finding has led to the further investigation on the self-annealing behavior of copper by the design engineers and has the potential to change the design and manufacturing process of the ICs.

Next, we investigate the design factors' effect on μ_{ild} through both hillocks height and number.

For layer 1 and layer 2, we note that the significant factors affecting p_{ild} through hillocks height do not affect μ_{ild}. Hence, we infer that these design

factors' affect on the number of hillocks grown more significantly. It is also noted that in layer 4, the design factors affect μ_{ild} most significantly. The process feature in layer 4 is that it has the least number of layers capping above it. After each metal layer is processed, it is capped with a layer of hard nitride dielectric material to prevent copper diffusion. As more layers are stacked on top, the pressure from the higher layers and the hardness of this nitride layer makes it harder for the hillocks to grow upwards. So there is much less pressure/stress on layer 4. Hence we can conclude that with less pressure, the number of hillocks grown becomes more sensitive to the design settings. We also note that in this layer, the squared term of width has a significant effect on μ_{ild}. The larger the width, the larger number of sites would be available for hillock growth (Puttlitz et al. (1989)). However, this is balanced by an opposing effect. The larger the width, there would be less thermal stress, and hence the mismatch between the surrounding dielectric and the metal would be less. This reduces the impulse for hillock formation and thus reduces the number of hillocks. Here we notice that layer 4 is the only layer that has a significant width squared effect, and at the same time is the layer undergoing the least number of thermal heating cycles. This observation could imply that only under certain low amounts of thermal heating, the hillock growth number is sensitive to the mismatch effect caused by thermal heating.

3.7.3 Optimum design setting and ICs design recommendations

With the estimated model, we now calculate the optimum design setting which minimizes the number of shorts. We register the optimum setting as d_{optim} =(width$_{optim}$, length$_{optim}$), and restrict the rescaled width value between -1.48 and 0.94, and rescaled length value between -1.83 and 0.68 according to the experiment design range. Table 3.8 presents the calculated d_{optim} for each layer $l = 1, 2, 3, 4$ and the corresponding optimum value. As a comparison, we also present the minimum shorts value predicted by the design settings used in the current fabrication. We can see that layer 1 and layer 4 have the potential

to be better designed to achieve higher reliability.

From the optimal design setting, we can observe that the first three layers

	width_{optim}	length_{optim}	$\text{prediction}_{optim}$	prediction_{best}
Layer1	-1.48	-1.83	7.032	10.267
Layer2	-1.48	0.68	5.607	5.607
Layer3	-1.48	[0.68, -1.83]*	3.288	3.288
Layer4	-0.42	-1.83	2.080	6.124

Table 3.8: Optimal design settings: * any value between the range is optimal since length effect is not significant; prediction_{best} are predictions for the experiment settings which produce the least shorts (current best design)

favor having a smaller width. Thus, in design rules, we should strive to minimize the width of metal lines on these layers. If however, bigger metal lines are required (for electrical circuitry purposes) in these layers, to achieve this, the designers may need to ensure that the layer directly above is clear of metal lines to minimize the probability of inter-layer shorts. On layer four however, the optimal width is slightly increased to -0.42. This result indicates to the design engineers that they might be able to relax the design rules for the top layers (layer 4 in this case). Currently from experience, design engineers put in increasing layered thickness on both the metal and dielectric layers for highly complicated multilayered designs. For example, the Intel Broadwell chip has 13 layers with the topmost layer 15 times thicker than the first four layers (which have a constant thickness). Our findings provide more engineering insights to the current practice.

It was also observed that in most layers that -1.831 was the optimal length for metal lines. While certain customer requirements can make it infeasible to limit all metal lines to -1.831, there are methods that can be employed to achieve this. The first is to design the metal lines with turns every -1.831 if the space on the chip allows the turns. Another feasible scheme is to insert slots within the metal lines which do not cut off the metal lines completely. These can be thought of as holes within the metal lines to allow space for expansion and reduce stress.

Layer 2 shows that we can have much longer metal lines. This is suspected to be related to the E-test done at layer two which allows the metal to have time

to self-anneal and in a limited way, relieving the pressure. However, regarding design specifications, more experiments are needed to before we can safely change the design rules to allow for longer metal lines.

In summary, the key findings and design insights are:

1. More heating cycles make the hillocks height distribution more sensitive to the design factors' values, where certain design settings can result in a higher chance of shifting to a count state height density. Hence, careful determination of the design settings for layer 1 can significantly reduce the chance of having harmful hillocks.

2. For the designs on layer 2, larger length, will reduce the chance of having a count state hillocks density (harmful density), and this is very different from the length's effect on other layers. As the wafers are placed through an additional electrical testing step after processing layer 2, the additional time on hold for the test provides the opportunity for the copper to self-anneal. This finding has led to the further investigation on the self-annealing behavior of copper by the design engineers and has the potential to change the design and manufacturing process of the ICs.

3. With less pressure (on higher layers), the number of hillocks grown becomes more sensitive to the design settings.

4. Under certain low amounts of thermal heating, the hillock growth number can become sensitive to the mismatch effect caused by thermal heating, for example, the case in layer 4.

5. In design rules, we should strive to minimize the width of metal lines on the first three layers. If bigger metal lines are required on these layers, the designers may need to ensure that the layer directly above is clear of metal lines to minimize the probability of inter-layer shorts. More relaxed design rules can be applied to layer 4 and possibly on the layers above it.

6. In most layers, -1.831 is the optimal length for metal lines. While certain

customer requirement makes it infeasible to limit all metal lines to -1.831, there are still few methods can be employed to achieve this. The first is to design the metal lines with turns every -1.831 as long as the space on the chip allows to. Another feasible scheme is to insert slots within the metal lines which do not cut off the metal lines completely.

3.8 Conclusion

In this chapter, we develop a multilevel zero-inflated model to analyze the zero-inflated data arising from a multilevel ICs manufacturing line. The model is derived based on the characteristics of the data (zero-inflation and multilevel variations) and the physical understanding of the manufacturing process. We analyzed the mechanisms causing the excessive zeros and derived the model's count distribution based on the number of hillocks grown and the individual hillock heights.

Although the model was derived specifically for capturing the uncertainties and modeling the experiment result of the ICs manufacturing process, the proposed multilevel ZI model can be extended to model other zero inflated data with multilevel structures with non normal random effects distributions. The proposed approximate AGQ-EM algorithm can also be applied to estimate the parameters from these model structures and is especially useful in cases where the random effects are not normal and estimated with a SNP distribution.
From practical point, the built model enabled us to draw a better understanding of the uncertainties in hillock growth process. The model and results have provided the designers with new insights on the copper wire layer designs that can improve the yield of the process and reliability of the chips. Additionally, through this analysis, it was discovered that an increased waiting time between processes (specifically waiting time to undergo electrical testing) could reverse the effects of some design factors, and this has prompted further investigations into the self-annealing properties of copper during this waiting time.

CHAPTER 4

BAYESIAN EXPERIMENTAL DESIGNS FOR ESTIMATING THE OPTIMUM POINT WITH GENERALIZED LINEAR MODELS

The purpose of engineering optimization is to choose a set of settings for the design variables of the system such that the system performance is optimized. In some cases, the estimated optimum setting can suffer from large uncertainties, especially where the data used for estimating the optimum setting is limited and noisy. In such cases, the design engineer may allocate additional runs to conduct a follow-up experiment to reduce the uncertainty associated with the estimator of optimum setting. In this chapter, we proposed a Bayesian experimental design framework for collecting data to reduce the estimation uncertainty of the optimum point with generalized linear models.

4.1 Introduction

When the initial understanding of a system, a process, or a new product is poor, a preliminary experiment is usually conducted first to learn the shape of the response surface. This preliminary experiment may be designed using a simple screening experiment or an optimal design such as the D-optimal design. Based on the knowledge obtained from the preliminary experiment, a follow-up

design may then be chosen to collect data for more specific objectives. Among the various objectives of planned experiments, an important and realistic one is to find the optimum point (design factors' setting) yielding the best system performance over a certain region of interest (Box and Wilson (1951); Gontard et al. (1992); Soltani and Soltani (2016)). For example, an auto manufacturer may first adopt a simple screening design to identify which of eight or nine factors have the greatest effect on the drying time of the paint on a new car product. Once the most important two or three factors have been identified, the manufacturer can design a more specific follow-up experiment to estimate the optimum point for those important factors. Other applications in which estimating the optimum point are of particular interest include the investigation of an Integrated Circuit back-end design, an industrial chemical, or a new compound (Li et al. (2015); Tye (2004)).

As computational power has evolved over the decades, the development of Bayesian experimental design is facilitating more complex design problems to be solved. The Bayesian framework provides a unified approach for incorporating prior information regarding the statistical model, with a utility function describing the experimental objectives.

Currently, most of the research on batch experimental design has been focusing on a globally well-estimated model or the model parameter vector as a whole. For example, the well-known D-optimality criterion (Chaloner and Verdinelli (1995); Dror and Steinberg (2008); Gotwalt et al. (2009); Russell et al. (2009)) seeks to maximize the determinant of the information matrix of the parameter vector $\boldsymbol{\theta}$. This criterion puts equal attention to all elements of $\boldsymbol{\theta}$, regardless of their influence on the quantity of interest. However, the optimal designs focusing on the estimation of $\boldsymbol{\theta}$ may not still be the 'best' with regards to the estimation of the optimum point. In this chapter, we develop the methods of finding the batch optimal design for efficient estimation of the optimum point with generalized linear models(GLMs), allowing the optimum point to locate at either boundary points or stationary points.

To develop an efficient experimental design framework for GLMs, the *dependence problem* (Khuri et al. (2006)) has to be considered. Khuri et al. (2006) reviewed design issues for GLMs and pointed that efficient designs for GLMs is dependent on the unknown parameter values of the model. In such cases, traditional way of conducting the optimal design is to choose the experiment based on a *best guess* of the parameter values, which leads to *locally optimal* designs (Russell et al. (2009); Wang et al. (2006)). A more coherent way is to use a Bayesian formulation to capture the uncertainty in the parameters(Chaloner and Verdinelli (1995)). Moreover, specific information is usually available prior to the experimentation. For example, the posterior distribution of parameter estimates from the preliminary experiment can serve as a prior distribution for the follow-up design. Therefore, in this work we adopt a Bayesian formulation to build the optimal design framework for estimating the optimum point.

One of the most commonly used formation of utility function for Bayesian design criteria is the mutual information (Lindley et al. (1972)). From a Bayesian point of view, Lindley et al. (1972) suggested that an efficient way of experimental design is to specify a utility function reflecting the value of the experiment, regard the design choice as a decision problem, and select a design that maximizes the utility.

Specifically, the Bayesian optimal design $\boldsymbol{e}^*$, maximizes the expected utility function $U(\boldsymbol{e})$ over the experimental design space $\mathcal{X}^E$ with respect to the future observations $\boldsymbol{y_e} \in \mathcal{Y}$ and model parameter $\boldsymbol{\theta} \in \mathcal{R}^p$:

$$\begin{aligned} \boldsymbol{e}^* &= argmax_{\boldsymbol{e}\in\mathcal{X}^E} E\{U(\boldsymbol{e}, \boldsymbol{\theta}, \boldsymbol{y_e})\} \\ &= argmax_{\boldsymbol{e}\in\mathcal{X}^E} \int_{\mathcal{Y}} \int_{\mathcal{R}^p} U(\boldsymbol{e}, \boldsymbol{\theta}, \boldsymbol{y_e}) p(\boldsymbol{\theta}|\boldsymbol{e}, \boldsymbol{y_e}) p(\boldsymbol{y_e}|\boldsymbol{e}) d\boldsymbol{y_e} d\boldsymbol{\theta} \end{aligned} \tag{4.1}$$

For example, the well-known Bayesian D-optimality criterion (Chaloner and Verdinelli (1995); Dror and Steinberg (2008); Cook et al. (2008); Lewi et al. (2009); Drovandi et al. (2013); Huan and Marzouk (2013); Ryan et al. (2014)) seeks to maximize the mutual information between the observations and the parameter vector. It is of great importance that the utility function incorporates

the specific experimental objectives and is specific to the application of interest. For example, the utility function for efficient estimation of parameter may not perform well when the design objective is to reduce the prediction uncertainty. Therefore, other utility functions such as utilities for model discrimination (Box and Hill (1967); Ng and Chick (2004); Cavagnaro et al. (2010); McGree et al. (2012)) and utilities for prediction of future observations (Zidek et al. (2000); Solonen et al. (2012); Liepe et al. (2013) have been proposed to incorporate specific design objectives.

Nevertheless, the literature on Bayesian optimal designs for estimating optimum points is scarce despite the fact that many engineering problems have estimation of optimum settings as their ultimate goal.

Although many published articles are available on finding the optimum point in a sequential experiment (Box and Wilson (1951); Chatterjee and Mandal (1981); Liyana-Pathirana and Shahidi (2005)), these algorithms can not be used when the experiment is not sequential in nature, as dictated by practical constraints. Box and Wilson (1951) initiated the research on sequentially attaining optimum point by estimating the first derivatives of the response surface and moving toward the optimum with the path of steepest ascent defined by previous estimates. However, this sequential search method would not be applicable to many manufacturing and clinical experiments where measurements are carried out simultaneously in a batch (for example, see Millette et al. (1995); Ruiz et al. (2013)). In such cases, all the design points have to be chosen without feedback information. On the other hand, research on batch experimental design for this topic has been limited to assuming the optimum point being a stationary point (Chaloner (1989); Mandal and Heiligers (1992); Pronzato and Walter (1993); Fedorov and Müller (1997)). For example, Chaloner (1989); Mandal and Heiligers (1992) studied the problem with linear regression models, and assumed that the optimum point was a stationary point and can be written as a closed form function of the model parameters. However, in many practical instances, the design region and hence the optimum point is limited within a constrained region of in-

terest. In such cases, the optimum point can be located at the boundaries when the stationary point is a saddle point or be located outside the region of interest. Currently there are no design criteria that relax the restrictive stationary point assumption on the optimum point.

The reason that Bayesian optimal design has been limited to simple utility functions mainly because of the computational burden to perform the integration and maximization of equation 4.1. To evaluate the Bayesian utility function, one must estimate the posterior distribution $p(\boldsymbol{\theta}|\boldsymbol{e}, \boldsymbol{y_e})$. Generally, thousands of these posterior distributions must be calculated for each potential future experimental observations $\boldsymbol{y_e}$, which is drawn from the prior predictive distribution $p(\boldsymbol{y_e}|\boldsymbol{e}, \boldsymbol{\theta})p(\boldsymbol{\theta})$. To evaluate these posterior distributions, many computational strategies have been proposed. These include Laplace approximation Chaloner and Verdinelli (1995); Long et al. (2013); smoothing of Monte Carlo simulations (Müller (2005)), Markov Chain Monte Carlo (MCMC) (Ryan (2003); Müller (2005)); and sequential Monte Carlo methods (Amzal et al. (2006)).

In the case where the utility function represents the information gain on the optimum point, the posterior distributions of the optimum point are required to be calculated. Since we allow the optimum point to be the boundary point, the conditions for normal approximation are no longer satisfied, the Chaloner and Verdinelli (1995)'s method can not be directly followed. On the other hand, it can be too computationally intensive to perform Monte Carlo to estimate the posterior distribution of optimum point for each of the thousands of iterations required in the optimal search algorithms.

In this work, we propose an alternative approximation method to the proposed criterion based on decomposing the criterion into the utility measure for D-optimal criterion and a 'missing information' term which can be estimated using Monte Carlo without the nested structure. This approximation greatly reduces the computational burden of a pure MCMC algorithm and makes searching for the optimal design feasible.

The remainder of this chapter is organized as follows: Section 2 introduces

the motivating example from a semiconductor experiment. Section 3 reviews other Bayesian optimality criteria for GLMs and the criterion evaluation methods. In Section 4, we develop the optimality criterion for estimating the optimum point and provide an approximation procedure for the evaluation the developed criterion. In Section 5, we provide an optimization procedure based on genetic algorithms (GAs) to optimize the developed criterion and search for the optimal design. In Section 6, we return to the motivating example to illustrate the effectiveness of the developed framework in practical problems. A brief summary is included as Section 7.

4.2 A motivating example

Semiconductor wafers usually undergo many microfabrication process steps, one of which is plasma etching. This step involves a high-speed stream of plasma (an appropriate gas mixture) being shot at a sample, in which the RF power (RF) and factors pressure are among those design factors that can be controlled. Sometimes, the anode-cathode gap and gas species are investigated as well, but those factors were fixed in this experiment. Suppose the design objective is to find the optimum setting of these control factors such that the wafer surface defects is minimized.

On the manufacturing line, these operational control factors are bounded by physical conditions of the process, and so a bounded design space typically applies. Moreover, the design factors like the RF power and factors pressure can only be controlled up to a precision of certain decimal places. In practice, when little is known about the response function, a preliminary experiment is first conducted to estimate the functional relationship and determine the significant factors. This preliminary experiment usually takes the form of a factorial or a space filling design, and are constrained by the operating / manufacturing conditions. With the preliminary experimental results, a regression form is then determined and the coefficients of this model estimated through methods like the maximum likelihood approach. With the estimated coefficients, the

expected number of defects per wafer can be predicted for any setting of the design factors. The optimum setting (of the design factors) can then be determined through minimizing this estimated response surface. Often, however, as the preliminary experiments are conducted only at a few fixed design points, the optimum setting can be inadequately estimated (suffering from large variances). When this is observed, additional budgets for conducting follow-up experiments can be allocated to improve this estimate to better control the manufacturing process. In such cases, as prior information has been obtained from the initial experiment, it is natural to adopt a Bayesian approach to incorporate the prior information into the follow-up experiment. In this work, we adopt the prior distribution and regression form reported by Johnson and Montgomery (2009) in a similar plasma etching experiment. With this initial prior distribution and model form, we study the problem of designing a follow-up batch experiment with 15 runs to better estimate the optimum setting. Based on the preliminary experiment result, Johnson and Montgomery (2009) reported the following second-order Poisson regression model

$$\log(defects) = \theta_0 * intercept + \theta_1 * RF + \theta_2 * pressure + \theta_{11} * RF^2 + \theta_{22} * pressure^2 + \theta_{12} * RF \times pressure \quad (4.2)$$

And a bounded normal prior with means and $\pm 2\boldsymbol{\sigma}(\boldsymbol{\sigma} = (\sigma_1, \sigma_2, \sigma_3, \sigma_4, \sigma_5))$ ranges on the coefficient parameters are specified as follows:

$$1 \leqslant \theta_0 \leqslant 4, \quad 0.22 \leqslant \theta_1 \leqslant 0.8, \quad -1.5 \leqslant \theta_2 \leqslant 0.5, \quad 0.25 \leqslant \theta_{11} \leqslant 0.75, \quad 0.25 \leqslant \theta_{22} \leqslant 0.75, \quad 0.25 \leqslant \theta_{12} \leqslant 0.75 \quad (4.3)$$

4.3 A review of Bayesian experimental designs for GLMs

Here we review the existing Bayesian experimental designs for GLMs. We begin with the construction and evaluation of the expected utility for the Bayesian D-optimality criterion, then review other utility functions for alternative design objectives.

From a Bayesian point of view, Lindley et al. (1972) suggested that an efficient way of experimental design is to specify a utility function reflecting the value of the experiment, regard the design choice as a decision problem, and select a design that maximizes the utility. Following Lindley (1956)'s suggestion, several authors (Stone (1959); DeGroot (1962); Bernardo (1979)) considered the expected gain in Shannon information (Shannon (1948)) given by an experiment as a utility function. Suppose an E run experimental design $\boldsymbol{e} = (e_1, \cdots, e_E)$ must be chosen from $\mathcal{X}^E$, and response $\boldsymbol{y_e} = (y_1, \cdots, y_E)$ will be observed. The density function of $\boldsymbol{y_e}$ is indexed by coefficients $\boldsymbol{\theta} \in \mathcal{R}^p$ and represented by $p(\boldsymbol{y_e}|\boldsymbol{\theta})$. To better estimate $\boldsymbol{\theta}$, these authors (Stone (1959); DeGroot (1962); Bernardo (1979)) proposed choosing an experimental design that maximizes the expected gain in Shannon information on $\boldsymbol{\theta}$:

$$U_D(\boldsymbol{e}) = \int\int \log \frac{p(\boldsymbol{y_e}, \boldsymbol{\theta})}{p(\boldsymbol{y_e})p(\boldsymbol{\theta})} p(\boldsymbol{y_e}, \boldsymbol{\theta}) d\boldsymbol{\theta} d\boldsymbol{y_e} \tag{4.4}$$

$$= \int\int p(\boldsymbol{y_e}, \boldsymbol{\theta}) \log p(\boldsymbol{y_e}|\boldsymbol{\theta}) d\boldsymbol{y_e} d\boldsymbol{\theta} - \int p(\boldsymbol{y_e}) \log p(\boldsymbol{y_e}) d\boldsymbol{y_e} \tag{4.5}$$

$$= \int\int p(\boldsymbol{y_e}, \boldsymbol{\theta}) \log p(\boldsymbol{\theta}|\boldsymbol{y_e}) d\boldsymbol{\theta} d\boldsymbol{y_e} - \int p(\boldsymbol{\theta}) \log p(\boldsymbol{\theta}) d\boldsymbol{\theta} \tag{4.6}$$

When the model is not linear, for example, a Poisson regression model, the expected utility above is often a complicated integral and approximations must typically be used. Most analytical approximations to $U_D(\boldsymbol{e})$ involve using a normal approximation to the posterior distribution $p(\boldsymbol{\theta}|\boldsymbol{y_e})$. A well-known estimator

provided by Chaloner and Verdinelli (1995) is:

$$\widehat{U_D}(\boldsymbol{e}) = -\frac{p}{2}\log(2\pi) - \frac{p}{2} + \frac{1}{2}\int \log\det\{\mathcal{I}(\boldsymbol{\theta}, \boldsymbol{e}) + R\}p(\boldsymbol{\theta})d\boldsymbol{\theta} \\ - \int \log[p(\boldsymbol{\theta})]p(\boldsymbol{\theta})d\boldsymbol{\theta} \quad (4.7)$$

where $\mathcal{I}(\boldsymbol{\theta}, \boldsymbol{e})$ denote the expected Fisher information matrix for a model with unknown parameters $\boldsymbol{\theta}$ and a design $\boldsymbol{e}$. R is the matrix of negative second derivatives of the logarithm of the prior density function, or the precision matrix of the prior distribution. Since the prior distribution $p(\boldsymbol{\theta})$ does not depend on the design $\boldsymbol{e}$, the experiment maximizing the estimator Equation (4.7) is the one that maximizes:

$$\phi_D(\boldsymbol{e}) = \int \log\det\{\mathcal{I}(\boldsymbol{\theta}, \boldsymbol{e}) + R\}p(\boldsymbol{\theta})d\boldsymbol{\theta} \quad (4.8)$$

which is referred as the Bayesian D-optimality criterion (Chaloner and Verdinelli (1995)).

Note that when designing follow-up experiments, the posterior distribution of the first stage experiment can serve as the prior distribution of the follow-up ones. In such cases, the prior precision matrix R represent for the information obtained from the first stage experiment, which is identical to the augmentation of a previous design in the non-Bayesian design literature (Chaloner and Verdinelli (1995)).

Another approach to approximating $U_D(e)$ is to evaluate Equation (4.5) by an MC estimator (Ryan (2003)):

$$\frac{1}{N}\sum_{i=1}^{N}\{\log[p(\boldsymbol{y}_{\boldsymbol{e}}^i|\boldsymbol{\theta}^i)] - \log[\hat{p}(\boldsymbol{y}_{\boldsymbol{e}}^i)]\} \quad (4.9)$$

where $(\boldsymbol{y}_{\boldsymbol{e}}^i, \boldsymbol{\theta}^i)$ for $i = 1, \cdots, N$ is a sample of size N from joint distribution $p(\boldsymbol{y}_{\boldsymbol{e}}, \boldsymbol{\theta})$ and $\hat{p}(\boldsymbol{y}_{\boldsymbol{e}}^i)$ is a suitable estimate for $p(\boldsymbol{y}_{\boldsymbol{e}}^i)$. To obtain a (dependent) pair $(\boldsymbol{y}_{\boldsymbol{e}}^i, \boldsymbol{\theta}^i)$ from $p(\boldsymbol{y}_{\boldsymbol{e}}, \boldsymbol{\theta})$, they suggested to first draw $\boldsymbol{\theta}^i$ from distribution $p(\boldsymbol{\theta})$, then $\boldsymbol{y}_{\boldsymbol{e}}^i$ from distribution $p(\boldsymbol{y}_{\boldsymbol{e}}|\boldsymbol{\theta}^i)$. To estimate $\hat{p}(\boldsymbol{y}_{\boldsymbol{e}}^i)$, they also provide a MC

estimator as

$$\hat{p}(\boldsymbol{y}_{\boldsymbol{e}}^i) = \frac{1}{N_2}\sum_{j=1}^{N_2} p(\boldsymbol{y}_{\boldsymbol{e}}^i|\boldsymbol{\theta}^{ij}) \tag{4.10}$$

where $\boldsymbol{\theta}_{ij}$ $(i = 1, \cdots, N,\ j = 1, \cdots, N_2)$ are N samples of size N_2 from $p(\boldsymbol{\theta})$ obtained independently of the N pairs $(\boldsymbol{y}_{\boldsymbol{e}}^i, \boldsymbol{\theta}^i)$ used in estimator Equation (4.9). Although straightforward, enormous computational resources are required to evaluate this estimator since there is a nested structure when evaluating $p(\boldsymbol{y}_{\boldsymbol{e}}^i)$: for each $i = 1, \cdots, N$, a sample of size M from $p(\boldsymbol{\theta})$ needs to be generated and the likelihood $p(\boldsymbol{y}_{\boldsymbol{e}}|\boldsymbol{\theta})$ would be evaluated $N(N_2 + 1)$ times.

The D-optimal criterion Equation (4.5) is effective when the experiment objective is to obtain a globally well-estimated model. Other than this objective, there are also situations where predictions are of interest. In these cases, the expected Shannon information gain on a future observation y_0 is used rather than that on $\boldsymbol{\theta}$. For example, Verdinelli et al. (1993) used the following expected utility for predictions in accelerated life-testing:

$$\int \log \frac{p(\boldsymbol{y}_{\boldsymbol{e}}, y_0)}{p(y_0)p(\boldsymbol{y}_{\boldsymbol{e}})} p(\boldsymbol{y}_{\boldsymbol{e}}, y_0) d\boldsymbol{y}_{\boldsymbol{e}} dy_0 \tag{4.11}$$

In addition to the interest to the predictions, estimating the optimum point is also a very important objective of many practical design problems. However, there is currently no procedure for constructing Bayesian optimal designs for estimating the optimum point with GLMs. This gap is mainly due to two difficulties. First, in most cases, the optimum point is not a closed form function of the model parameters, which leads to many difficulties in defining the design criterion. Second, as can be seen from the MC estimator in Equation (4.9), evaluating the integrals in the expected utility requires enormous computational efforts. In the following section, we provide a solution to this problem through a Shannon information utility measure and reduce the computational burden by a decomposition of the proposed utility measure.

4.4 Bayesian design formulation for estimating optimum point

The motivating application presented in Section 4.2 is a special case of a much more general problem in optimal design. In this section, we begin by formally defining the problem of optimal design for estimating optimum setting in GLMs and then derive the expected utility for the Bayesian design criterion, followed by proposing an evaluation algorithm to the expected utility.

To set the stage, let $\boldsymbol{y_x}$ be a response variable whose expectation $\mu(\boldsymbol{x}, \boldsymbol{\theta})$ depends on d controllable factors $\boldsymbol{x} = (x_1, \cdots, x_d)'$ and p parameters $\boldsymbol{\theta} = (\theta_1, \cdots, \theta_p)$. Suppose $\boldsymbol{\theta} \in \mathbb{R}^p$ and has prior density $p(\boldsymbol{\theta})$. In most of the practical applications, $\boldsymbol{x}$ can only be controlled up to a certain precision or decimal points and should be limited to be inside of a constrained region of interest. Hence we assume the design space $\mathcal{X}$ is a closed discrete set, and to be concrete, we also assume that the actual factors have been scaled such that $\mathcal{X} = [-1, 1]^d$. The response $\boldsymbol{y_x}$ follows an exponential family with

$$E_{\boldsymbol{y_x}|\boldsymbol{\theta}}[\boldsymbol{y_x}] = \mu(\boldsymbol{x}, \boldsymbol{\theta}), \text{ and } \mu(\boldsymbol{x}, \boldsymbol{\theta}) = g[z(\boldsymbol{x})^T \boldsymbol{\theta}] \tag{4.12}$$

where g is a monotonic link function for the model and $z(\boldsymbol{x})^T \boldsymbol{\theta}$ is the linear predictor. When the initial understanding of a system is poor and the functional form of $\mu(\boldsymbol{x}, \boldsymbol{\theta})$ is unknown, some preliminary experiments using a simple screening experiment could be used. Based on the knowledge obtained from the preliminary experiments, a follow-up design may then be chosen to collect data for more specific objectives such as estimating the optimum point. Consideration of bias due to misspecification of $\mu(\boldsymbol{x}, \boldsymbol{\theta})$ is beyond the scope of this work.

4.4.1 Optimum point

Suppose the experimenter is interested in attaining the optimum setting $\boldsymbol{x}^* \in \mathcal{X}$ which yields the optimum system value. Here attaining $\boldsymbol{x}^*$ includes first estimate $\boldsymbol{\theta}$ by $\hat{\boldsymbol{\theta}}$ and predicting the deterministic part of $\boldsymbol{y_x}$, $\mu(\boldsymbol{x}, \hat{\boldsymbol{\theta}})$, for any

admissible value of $\boldsymbol{x} \in \mathcal{X}$, and then finding the optimum setting $\boldsymbol{x}^*$ such that

$$\boldsymbol{x}^* := \underset{\boldsymbol{x}\in\mathcal{X}}{argmin}\, \mu(\boldsymbol{x}, \hat{\boldsymbol{\theta}}) \tag{4.13}$$

For every possible value of $\boldsymbol{\theta} \in \mathcal{R}^p$, we have an optimum setting solution set

$$\Psi(\boldsymbol{\theta}) := \underset{\boldsymbol{x}\in\mathcal{X}}{argmin}\, \mu(\boldsymbol{x}, \boldsymbol{\theta}) \tag{4.14}$$

We now consider the problem of determining the batch experimental design $\boldsymbol{e} = \{e^1, \cdots, e^E\}$, from design space $\mathcal{X}^E$, which is optimal for estimating $\boldsymbol{x}^*$. In this context, a globally well-estimated model or the model coefficients vector as a whole is not the main interest. Instead, the experimental design should collect data in the most 'efficient' way regarding the inference of $\boldsymbol{x}^*$.

Assuming $\mu(\boldsymbol{x}, \boldsymbol{\theta})$ is quadratic and strictly convex, Mandal and Heiligers (1992) wrote $\boldsymbol{x}^*$ as a close form function of $\boldsymbol{\theta}$ and proposed minimax designs for estimating $\boldsymbol{x}^*$. Similarly, Pronzato and Walter (1993) provided various optimality criterion by assuming $\boldsymbol{x}^*$ as a stationary point. However, as pointed by Peterson et al. (2002), these assumptions are often not well aligned with the practical needs to calculate $\boldsymbol{x}^*$ within a bounded region. In some cases, the stationary point is a saddle point rather than an optimum in the experimental region. For example, suppose $\log(\mu(\boldsymbol{x}, \boldsymbol{\theta})) = \theta_0 + \theta_1 * x + \theta_2 * x^2, x \in [-1, 1]$. When $\theta_1 = 1, \theta_2 = -1$, the stationary point $-\frac{\theta_1}{2\theta_2} = -0.5$ is a saddle point and $\boldsymbol{x}^* = -1$;when $\theta_1 = 4, \theta_2 = 1$, the stationary point $-\frac{\theta_1}{2\theta_2} = -2$ locates outside the feasible set and $\boldsymbol{x}^* = -1$. In this work, we relax the assumptions of $\boldsymbol{x}^*$ being a stationary point, and only assume that $\boldsymbol{x}^*$ comes from a finite set of points, e.g., a bounded discrete set $\mathcal{G} = \{\boldsymbol{x}^1, \cdots, \boldsymbol{x}^m\}$. This is reasonable and practical since the optimum setting can only be controlled up to certain precision in a real application. Moreover, to make the problem well defined, the $\boldsymbol{x}^*$ needs to be guaranteed to be unique with probability one. Here, we prove that $\boldsymbol{x}^*$ is unique with probability one under the assumption $\boldsymbol{x}^* \in \mathcal{G}$ by the following theorem.

Theorem 1 *Let $\mathcal{X} \in \mathcal{R}^p$ be the compact experiment region and $\mathcal{G} = \{\boldsymbol{x}^1, \cdots, \boldsymbol{x}^m\}$*

be a finite set of points (e.g., grid points). Let $g[\boldsymbol{\theta}^T z(\boldsymbol{x})]$ *be the objective function, where* $\boldsymbol{\theta} \in \mathbb{R}^p$, $z : \mathbb{R}^d \to \mathbb{R}^p$, *and* $g : \mathbb{R} \to \mathbb{R}$ *is strictly monotonic link function. Suppose* $\boldsymbol{x}^* \in \mathcal{G}$ *is a point such that* $g[\boldsymbol{\theta}^T z(\boldsymbol{x}^*)] = min\ \{g[\boldsymbol{\theta}^T z(\boldsymbol{x}^1)], \cdots, g[\boldsymbol{\theta}^T z(\boldsymbol{x}^m))]\}$. *Then,* $\boldsymbol{x}^*$ *is unique with probability one if the following two conditions hold:*

1. $\boldsymbol{\theta}$ *is a random vector with a density function on* $\mathbb{R}^p$.

2. $z(\boldsymbol{x}^i) - z(\boldsymbol{x}^j) \neq \mathbf{0},\ \forall (\boldsymbol{x}^i, \boldsymbol{x}^j) \in \mathcal{X} \times \mathcal{X}, \boldsymbol{x}^i \neq \boldsymbol{x}^j$.

Proof*:*

Note that $\{\widetilde{\boldsymbol{\theta}} \in \mathbb{R}^p : \widetilde{\boldsymbol{\theta}}^T \boldsymbol{a} = \mathbf{0}\}, \boldsymbol{a} \neq \mathbf{0}$ *defines a hyperplane in* $\mathbb{R}^p$, *which have Lebesgue measure zero (Page 232 of Aliprantis and Tourky (2007)). Since conditions 1 and 2 above imply that* $P\{\boldsymbol{\theta}^T z(\boldsymbol{x}^i) = \boldsymbol{\theta}^T z(\boldsymbol{x}^j)\} = P\{\boldsymbol{\theta}^T [z(\boldsymbol{x}^i) - z(\boldsymbol{x}^j)] = \mathbf{0}] = 0$ *if* $i \neq j$, *we have* $P[\boldsymbol{\theta}^T z(\boldsymbol{x}^i) = \boldsymbol{\theta}^T z(\boldsymbol{x}^j)$ *for some* $i \neq j, 1 \leqslant i \leqslant j \leqslant m] \leqslant \sum_{1 \leqslant i \leqslant j \leqslant m} P[\boldsymbol{\theta}^T z(\boldsymbol{x}^i) = \boldsymbol{\theta}^T z(\boldsymbol{x}^j)] = 0$. *Since* g *is strictly monotonic,* $g[\boldsymbol{\theta}^T z(\boldsymbol{x}^i)] = g[\boldsymbol{\theta}^T z(\boldsymbol{x}^j)]$ *if and only if* $\boldsymbol{\theta}^T z(\boldsymbol{x}^i) = \boldsymbol{\theta}^T z(\boldsymbol{x}^j)$. *Thus,* $P\{g[\boldsymbol{\theta}^T z(\boldsymbol{x}^i)] = g[\boldsymbol{\theta}^T z(\boldsymbol{x}^j)]$ *for some* $i \neq j, 1 \leqslant i \leqslant j \leqslant m\} = 0$. *This implies that the minimum point* $\boldsymbol{x}^*$ *must be unique with probability one.*

Remark 1: Suppose $d = 2$, $g(\cdot) = \exp(\cdot)$, and $\boldsymbol{\theta}^T z(\boldsymbol{x}) = \theta_0 + \theta_1 x_1 + \theta_2 x_2 + \theta_3 x_1 x_2 + \theta_4 x_1^2 + \theta_5 x_2^2$, then Theorem 1 holds since $z(\boldsymbol{x}^i) - z(\boldsymbol{x}^j) = (0, x_1^i - x_1^j, x_2^i - x_2^j, x_1^i x_2^i - x_1^j x_2^j, (x_1^i)^2 - (x_1^j)^2, (x_2^i)^2 - (x_2^j)^2) \neq \mathbf{0}\ \forall \boldsymbol{x}^i, \boldsymbol{x}^j \in [-1, 1]^2, \boldsymbol{x}^i \neq \boldsymbol{x}^j$.

Remark 2: There exist a subset Λ such that $\boldsymbol{x}^*$ is not unique and $P(\boldsymbol{\theta} \in \Lambda) = 0$, while when $\boldsymbol{\theta} \in \mathbb{R}^p \backslash \Lambda$, $\boldsymbol{x}^*$ is unique and $P(\boldsymbol{\theta} \in \mathbb{R}^p \backslash \Lambda) = 1$. When $\boldsymbol{x}^*$ is unique, $\boldsymbol{x}^*$ would be a function of $\boldsymbol{\theta}$,

$$\boldsymbol{\theta} \mapsto x^*(\boldsymbol{\theta}) \in \Psi(\boldsymbol{\theta}), \quad \boldsymbol{\theta} \in \mathbb{R}^p \backslash \Lambda \tag{4.15}$$

4.4.2 Bayesian design criterion for estimating the optimum point

Now we construct the Bayesian design criterion for estimating the optimum setting. In a similar spirit with Lindley (1956), we can define the expected utility for estimating $\boldsymbol{x}^*$ based on expected Shannon information gain on $\boldsymbol{x}^*$ from an experiment. For a prior distribution $p(\boldsymbol{x}^*)$, the Shannon information (Shannon

(1948)) is defined to be

$$H(\boldsymbol{x}^*) = -\int p(\boldsymbol{x}^*)\log p(\boldsymbol{x}^*)d\boldsymbol{x}^* \tag{4.16}$$

whenever the integral exists. For any $\boldsymbol{x}^*$ for which $p(\boldsymbol{x}^*) = 0$, define $p(\boldsymbol{x}^*)\log p(\boldsymbol{x}^*)$ to be zero.

After the experiment has been performed and the response $\boldsymbol{y}_{\boldsymbol{e}}^i$ observed, the posterior distribution of $\boldsymbol{x}^*$ is $p(\boldsymbol{x}^*|\boldsymbol{y}_{\boldsymbol{e}}^i) = p(\boldsymbol{y}_{\boldsymbol{e}}^i|\boldsymbol{x}^*)p(\boldsymbol{x}^*)/p(\boldsymbol{y}_{\boldsymbol{e}}^i)$, and the corresponding Shannon information is

$$H(\boldsymbol{x}^*|\boldsymbol{y}_{\boldsymbol{e}} = \boldsymbol{y}_{\boldsymbol{e}}^i) = -\int \log p(\boldsymbol{x}^*|\boldsymbol{y}_{\boldsymbol{e}}^i)p(\boldsymbol{x}^*|\boldsymbol{y}_{\boldsymbol{e}}^i)d\boldsymbol{x}^* \tag{4.17}$$

(If $p(\boldsymbol{x}^*|\boldsymbol{y}_{\boldsymbol{e}}^i) = 0$, define the integrand to be zero.)

Definition 1 *The amount of information (uncertainty) reduced by the experiment $\boldsymbol{e}$, with prior knowledge $p(\boldsymbol{x}^*)$ and observation $\boldsymbol{y}_{\boldsymbol{e}}^i$, is*

$$H_\Delta(\boldsymbol{x}^*|\boldsymbol{y}_{\boldsymbol{e}}^i) = H(\boldsymbol{x}^*) - H(\boldsymbol{x}^*|\boldsymbol{y}_{\boldsymbol{e}}^i) \tag{4.18}$$

In the experimental design problem, however, $\boldsymbol{e}$ must be selected before $\boldsymbol{y}_{\boldsymbol{e}}^i$ is observed. Hence, $H_\Delta(\boldsymbol{x}^*|\boldsymbol{y}_{\boldsymbol{e}}^i)$ need to be averaged with respect to the marginal distribution of $\boldsymbol{y}_{\boldsymbol{e}}$. Hence, we have

Definition 2 *The average amount of information reduced by the experiment $\boldsymbol{e}$, with prior knowledge $p(\boldsymbol{x}^*)$ is*

$$E_{\boldsymbol{y}_{\boldsymbol{e}}}[H(\boldsymbol{x}^*) - H(\boldsymbol{x}^*|\boldsymbol{y}_{\boldsymbol{e}} = \boldsymbol{y}_{\boldsymbol{e}}^i)] = H(\boldsymbol{x}^*) - H(\boldsymbol{x}^*|\boldsymbol{y}_{\boldsymbol{e}}) \tag{4.19}$$

where $H(\boldsymbol{x}^*|\boldsymbol{y}_{\boldsymbol{e}}) := E_{\boldsymbol{y}_{\boldsymbol{e}}}[H(\boldsymbol{x}^*|\boldsymbol{y}_{\boldsymbol{e}} = \boldsymbol{y}_{\boldsymbol{e}}^i)]$.

This measure is also defined as the mutual information between $\boldsymbol{x}^*$ and $\boldsymbol{y}_{\boldsymbol{e}}$: $I(\boldsymbol{x}^*; \boldsymbol{y}_{\boldsymbol{e}}) := H(\boldsymbol{x}^*) - H(\boldsymbol{x}^*|\boldsymbol{y}_{\boldsymbol{e}})$, and satisfies $I(\boldsymbol{x}^*; \boldsymbol{y}_{\boldsymbol{e}}) \geqslant 0$ (MacKay (2003)). Intuitively, the mutual information reflects the dependency of two random variables, it is a measure of the 'amount of information' obtained about one random

variable, through observations of the other random variable. Using this information measure to define the expected utility, we have

$$\begin{aligned} U(\boldsymbol{e}) &= \int\int \log[\frac{p(\boldsymbol{y_e}, \boldsymbol{x}^*)}{p(\boldsymbol{y_e})p(\boldsymbol{x}^*)}]p(\boldsymbol{y_e}, \boldsymbol{x}^*)d\boldsymbol{x}^* d\boldsymbol{y_e} \\ &= \int\int \log[p(\boldsymbol{y_e}|\boldsymbol{x}^*)]p(\boldsymbol{x}^*, \boldsymbol{y_e})d\boldsymbol{x}^* d\boldsymbol{y_e} - \int \log[p(\boldsymbol{y_e})]p(\boldsymbol{y_e})\boldsymbol{y_e} \end{aligned} \quad (4.20)$$

The optimal design problem is then to find the experiment $\boldsymbol{e}^* \in \mathcal{X}^E$ such that $U(\boldsymbol{e}^*) = \underset{\boldsymbol{e}\in\mathcal{X}^E}{max}\, U(\boldsymbol{e})$. We call this criterion for estimating the optimum setting as the *Bayesian OP optimality criterion.*

4.4.3 An algorithm to evaluate the proposed criterion

When the model belongs to the class of GLMs, the utility function, Equation (4.20) is often a complicated integral and approximations must typically be used. In the optimization procedure of searching for the optimal design, for each searched candidate design, the expected utility associated with this design needs to be recalculated. This requires substantial computation. As we reviewed in Section 4.3, for Bayesian D-optimality criterion, Chaloner (1989) provided an asymptotic normal approximation to the posterior distribution of $\boldsymbol{\theta}$, while Ryan (2003) suggested a MCMC estimator. The approximation proposed by Chaloner and Verdinelli (1995) reduces the computational burden by using a normal approximation to the posterior distribution $p(\boldsymbol{\theta}|\boldsymbol{y_e})$. However, when calculating $\boldsymbol{x}^*$ from minimizing $\mu(\boldsymbol{x}, \boldsymbol{\theta})$ over the bounded region $[-1, 1]^d$, some of the posterior value of $\boldsymbol{\theta} \in \mathcal{R}^p$ can lead to the same value of $\boldsymbol{x}^*$ located at the boundary points. This violates the conditions to approximate $p(\boldsymbol{x}^*|\boldsymbol{y_e})$ by normal distribution(the value of the first derivative of the posterior $p(\boldsymbol{x}^*|\boldsymbol{y_e})$ may no longer be zero at the posterior mode). Hence, we can not directly resemble Chaloner and Verdinelli (1995)'s method to approximate the expected utility, Equation (4.20). The alternative MC estimator Equation (4.9) provided by Ryan (2003) requires enormous computational effort, making it infeasible to be applied for optimizing the expected utility and searching for an optimal design. This observation is

also made by the authors of this MC estimator for their case study in Ryan (2003) . In this subsection, we propose an algorithm to evaluate the expected utility, Equation (4.20) based on (1) an approximation to the expected utility for D-optimality criterion $U_D(\boldsymbol{e})$ provided by Chaloner and Verdinelli (1995); (2) the data processing inequality (Cover and Thomas (2012)) to decompose the expected utility Equation (4.20) into two separate terms, where the first term equals to $U_D(\boldsymbol{e})$ and the second term can be estimated by the N sample pairs $(\boldsymbol{y}_{\boldsymbol{e}}^i, \boldsymbol{\theta}^i)$, as used in Equation (4.9). This avoids the nested MC structure for estimating $\int \log[p(\boldsymbol{y_e})]p(\boldsymbol{y_e})\boldsymbol{y_e}$ required by the MC estimator in Equation (4.10).

Recall that the expected utility defines the information gain on $\boldsymbol{x}^*$ through observing $\boldsymbol{y_e}$; in other words, the mutual information between $\boldsymbol{x}^*$ and $\boldsymbol{y_e}$. We have the explicit relationship between $\boldsymbol{\theta}$ and $\boldsymbol{y_e}$ from $E_{\boldsymbol{y_x}|\boldsymbol{\theta}}[\boldsymbol{y_x}] = \mu(\boldsymbol{x}, \boldsymbol{\theta})$, but not for $\boldsymbol{x}^*$ and $\boldsymbol{y_e}$. As mentioned, to attain the value of $\boldsymbol{x}^*$, first we need to estimate $\boldsymbol{\theta}$ by $\hat{\boldsymbol{\theta}}$ from observations of $\boldsymbol{y_e}$, then calculate $\boldsymbol{x}^*$ from Equation (4.13). When we calculating $\boldsymbol{x}^*$ from various estimates of $\boldsymbol{\theta}$, some different values of $\hat{\boldsymbol{\theta}}$ may map to the same value of $\boldsymbol{x}^*$. For example, suppose $\hat{\boldsymbol{\theta}}|\boldsymbol{y}_{\boldsymbol{e}}^1 = \boldsymbol{\theta}_1$ and $\hat{\boldsymbol{\theta}}|\boldsymbol{y}_{\boldsymbol{e}}^2 = \boldsymbol{\theta}_2$, but $\boldsymbol{\theta}_1$ and $\boldsymbol{\theta}_2$ lead to the same value of $\boldsymbol{x}^*$ such that: $(\boldsymbol{x}^*)^1 = \underset{\boldsymbol{x}\in\mathcal{X}}{argmin}\, \mu(\boldsymbol{x}, \boldsymbol{\theta}_1), (\boldsymbol{x}^*)^1 = \underset{\boldsymbol{x}\in\mathcal{X}}{argmin}\, \mu(\boldsymbol{x}, \boldsymbol{\theta}_2)$. In such cases, knowing $\boldsymbol{x}^* = (\boldsymbol{x}^*)^1$ would no longer provide the explicit information on whether we observe $\boldsymbol{y}_{\boldsymbol{e}}^1$ or $\boldsymbol{y}_{\boldsymbol{e}}^2$; on the contrary, measuring two samples $\boldsymbol{y}_{\boldsymbol{e}}^1$ and $\boldsymbol{y}_{\boldsymbol{e}}^2$ would be equivalent to measuring one sample $\boldsymbol{y}_{\boldsymbol{e}}^1$ with respect to gaining knowledge on $\boldsymbol{x}^*$. This argument is described by the *Data processing inequality* theorem (Cover and Thomas (2012)) from information theory. In the following, we will introduce this theorem and use this theorem to decompose the mutual information between $\boldsymbol{x}^*$ and $\boldsymbol{y_e}$ into mutual information between $\boldsymbol{\theta}$ and $\boldsymbol{y_e}$ and the 'information loss'.

Definition 3 (Markov Chain) *(Cover and Thomas (2012)) Given three random variables X, Y, Z, they form a Markov chain denoted as $X \to Y \to Z$ iff X and Z are conditionally independent given Y. I.e., $p(z, x|y) = p(z|y)p(x|y), \forall x, y, z$*

.

Proposition 1 *For $\boldsymbol{\theta} \in \mathbb{R}^p \backslash \Lambda$, $\boldsymbol{y_e}$, $\boldsymbol{\theta}$ and $\boldsymbol{x}^*$ form a Markov chain: $\boldsymbol{y_e} \to \boldsymbol{\theta} \to \boldsymbol{x}^*$.*

***Proof**: From Equation (4.15), we have: $p(\boldsymbol{y_e}|\boldsymbol{\theta}, \boldsymbol{x}^*) = p(\boldsymbol{y_e}|\boldsymbol{\theta}, x^*(\boldsymbol{\theta})) = p(\boldsymbol{y_e}|\boldsymbol{\theta}), \boldsymbol{\theta} \in \mathbb{R}^p \backslash \Lambda$. Thus,*

$$\begin{aligned} p(\boldsymbol{y_e}, \boldsymbol{x}^*|\boldsymbol{\theta}) &= \frac{p(\boldsymbol{y_e}|\boldsymbol{x}^*, \boldsymbol{\theta}) p(\boldsymbol{x}^*, \boldsymbol{\theta})}{p(\boldsymbol{\theta})} \\ &= \frac{p(\boldsymbol{y_e}|\boldsymbol{\theta}) p(\boldsymbol{x}^*, \boldsymbol{\theta})}{p(\boldsymbol{\theta})} = p(\boldsymbol{y_e}|\boldsymbol{\theta}) p(\boldsymbol{x}^*|\boldsymbol{\theta}), \boldsymbol{\theta} \in \mathbb{R}^p \backslash \Lambda \end{aligned}$$

and $\boldsymbol{y_e} \to \boldsymbol{\theta} \to \boldsymbol{x}^*, \boldsymbol{\theta} \in \mathbb{R}^p \backslash \Lambda$.

Theorem (2.8.1 of Cover and Thomas (2012)) *(Data-processing inequality) If $X \to Y \to Z$, then $I(X;Y) \geqslant I(X;Z)$.*

From Equation 2.121 of the proof of this theorem, we also have: $I(X;Y) = I(X;Z) + I(X;Y|Z)$, where

$$I(X;Y|Z) = E_{p(x,y,z)} \log \frac{p(X,Y|Z)}{p(X|Z)p(Y|Z)} \tag{4.21}$$

is the expected value of the mutual information of X and Y given the value of Z.

Proposition 2 *For $\boldsymbol{\theta} \in \mathbb{R}^p \backslash \Lambda$, we have $I(\boldsymbol{y_e}, \boldsymbol{\theta}) \geqslant I(\boldsymbol{y_e}, \boldsymbol{x}^*)$ and $I(\boldsymbol{y_e}; \boldsymbol{\theta}) = I(\boldsymbol{y_e}; \boldsymbol{x}^*) + I(\boldsymbol{y_e}; \boldsymbol{\theta}|\boldsymbol{x}^*)$, where*

$$I(\boldsymbol{y_e}; \boldsymbol{\theta}|\boldsymbol{x}^*) = E_{p(\boldsymbol{y_e}, \boldsymbol{\theta}, \boldsymbol{x}^*)} \log \frac{p(\boldsymbol{y_e}, \boldsymbol{\theta}|\boldsymbol{x}^*)}{p(\boldsymbol{y_e}|\boldsymbol{x}^*)p(\boldsymbol{\theta}|\boldsymbol{x}^*)} \tag{4.22}$$

Proof: According to Proposition 1, $\boldsymbol{y_e} \to \boldsymbol{\theta} \to \boldsymbol{x}^*, \boldsymbol{\theta} \in \mathbb{R}^p \backslash \Lambda$ forms a Markov chain.

Based on the above Proposition, instead of directly approximating the expected utility in Equation (4.5), we decompose it to

$$\begin{aligned} U(\boldsymbol{e}) = I(\boldsymbol{y_e}; \boldsymbol{x}^*) &= I(\boldsymbol{y_e}; \boldsymbol{\theta}) - I(\boldsymbol{y_e}; \boldsymbol{\theta}|\boldsymbol{x}^*) \\ &= U_D(\boldsymbol{e}) - E_{p(\boldsymbol{y_e}, \boldsymbol{\theta}, \boldsymbol{x}^*)} \log \frac{p(\boldsymbol{y_e}, \boldsymbol{\theta}|\boldsymbol{x}^*)}{p(\boldsymbol{y_e}|\boldsymbol{x}^*)p(\boldsymbol{\theta}|\boldsymbol{x}^*)} \end{aligned} \tag{4.23}$$

where the first term in the right side of the equation equals to the utility $U_D(\boldsymbol{e})$ for the D-optimality criterion and measures the information gain on the overall regression model; while the second term measures the information loss when transmitting the information through $\boldsymbol{\theta}$ to $\boldsymbol{x}^*$ by function $x^*(\boldsymbol{\theta})$. For $U_D(\boldsymbol{e})$, we directly adopt the approximation used for Bayesian D-optimality criterion by Chaloner and Verdinelli (1995) in Equation (4.7). Specifically, for GLMs, we have

$$\widehat{U_D}(\boldsymbol{e}) = -\frac{p}{2}\log(2\pi) - \frac{p}{2} + \frac{1}{2}\int \log\det\{Z'QZ + R\}p(\boldsymbol{\theta})d\boldsymbol{\theta} - \int \log[p(\boldsymbol{\theta})]p(\boldsymbol{\theta})d\boldsymbol{\theta} \quad (4.24)$$

where $Z = (z(\boldsymbol{x})_1, \cdots, z(\boldsymbol{x})_E)'$ is the experiment covariate matrix, $Q = \text{diag}\{w_e\}_{e=1}^E$, and $w_e = 1/\{\text{var}(y_i|\mu_i)[h'(\mu_i)]^2\}$ are weights associated with the eth observation, $e = 1, \cdots, E$. The first element in the weights is the variance of the ith observations condition on its expectation, and the second term is the first derivative of the inverse link function, $h(\cdot) = g^{-1}(\cdot)$. We can see that the information matrix depends on the unknown parameter values through the weights.

As there is no analytical form for $I(\boldsymbol{y_e}; \boldsymbol{\theta}|\boldsymbol{x}^*)$, we proposed a MC procedure to approximate it. To obtain a computationally efficient estimator, we first rewrite Equation (4.22) as

$$I(\boldsymbol{y_e}; \boldsymbol{\theta}|\boldsymbol{x}^*) = E_{p(\boldsymbol{y_e},\boldsymbol{\theta},\boldsymbol{x}^*)} \log \frac{p(\boldsymbol{y_e}, \boldsymbol{\theta}|\boldsymbol{x}^*)}{p(\boldsymbol{y_e}|\boldsymbol{x}^*)p(\boldsymbol{\theta}|\boldsymbol{x}^*)} \quad (4.25)$$

$$= E_{p(\boldsymbol{y_e},\boldsymbol{\theta},\boldsymbol{x}^*)} \log \frac{p(\boldsymbol{y_e}|\boldsymbol{\theta})}{p(\boldsymbol{y_e}|\boldsymbol{x}^*)} \quad (4.26)$$

$$= E_{p(\boldsymbol{x}^*)}[E_{p(\boldsymbol{y_e},\boldsymbol{\theta}|\boldsymbol{x}^*)} \log \frac{p(\boldsymbol{y_e}|\boldsymbol{\theta})}{p(\boldsymbol{y_e}|\boldsymbol{x}^*)}], \boldsymbol{\theta} \in \mathbb{R}^p \backslash \Lambda \quad (4.27)$$

where the second equation holds as $p(\boldsymbol{y_e}, \boldsymbol{\theta}|\boldsymbol{x}^*) = p(\boldsymbol{y_e}|\boldsymbol{\theta})p(\boldsymbol{\theta}|\boldsymbol{x}^*), \boldsymbol{\theta} \in \mathbb{R}^p \backslash \Lambda$ (from Proposition 1). Note that as $\boldsymbol{x}^*$ is a random variable with discrete sample

space $\mathcal{G}$, this suggests a MC estimator as

$$\sum_{(\boldsymbol{x}^*)^i \in \mathcal{G}} \hat{p}[(\boldsymbol{x}^*)^i] \frac{1}{m_i} \sum_{j=1}^{m_i} \log \frac{p(\boldsymbol{y}_{\boldsymbol{e}}^{(i,j)} | \boldsymbol{\theta}^{(i,j)})}{\hat{p}[\boldsymbol{y}_{\boldsymbol{e}}^{(i,j)} | (\boldsymbol{x}^*)^i]} \tag{4.28}$$

where $\hat{p}[(\boldsymbol{x}^*)^i]$ is a suitable estimate for $p[(\boldsymbol{x}^*)^i)]$, $(\boldsymbol{y}_{\boldsymbol{e}}^{(i,j)}, \boldsymbol{\theta}^{(i,j)})$ for $j = 1, \cdots, m_i$ is a sample of size m_i from $p[\boldsymbol{y}_{\boldsymbol{e}}, \boldsymbol{\theta} | (\boldsymbol{x}^*)^i]$ and $\hat{p}[\boldsymbol{y}_{\boldsymbol{e}}^{(i,j)} | (\boldsymbol{x}^*)^i]$ is a suitable estimate for $p[\boldsymbol{y}_{\boldsymbol{e}}^{(i,j)} | (\boldsymbol{x}^*)^i]$.

First we look into the distribution $p(\boldsymbol{x}^*)$. Although $\boldsymbol{x}^*$ can be uniquely decided with probability one for each value of $\boldsymbol{\theta} = \boldsymbol{\theta}^k$, analytically deducing the distribution of $\boldsymbol{x}^*$ is generally infeasible. Instead, using the MC procedure, we can obtain a large sample of $\boldsymbol{x}^*$, and use the empirical probability to approximate $p(\boldsymbol{x}^*)$. Specifically, we first simulate $\boldsymbol{\theta}^1, \cdots, \boldsymbol{\theta}^N$ from $p(\boldsymbol{\theta})$, and these samples will be distinct with probability one. Then for each $\boldsymbol{\theta}^k$, we can compute $(\boldsymbol{x}^*)^k \in \mathcal{G}$. Here, since $\mathcal{G}$ is a finite set of points, different $\boldsymbol{\theta}^k$ may result in same value of $\boldsymbol{x}^*$. Suppose $\widehat{\mathcal{G}} = \{(\boldsymbol{x}^*)^1, \cdots, (\boldsymbol{x}^*)^M\}$ are the distinct values of $\boldsymbol{x}^*$ and $(\boldsymbol{x}^*)^i$ is obtained from $\{\boldsymbol{\theta}^{(i,1)}, \cdots, \boldsymbol{\theta}^{(i,m_i)}\}$, where $\sum_{i=1}^{M} m_i = N$. Then we can estimate $p[(\boldsymbol{x}^*)^i]$ with its empirical probability $\hat{p}[(\boldsymbol{x}^*)^i] = m_i/N$.

Then, to generate random sample pairs from $p[\boldsymbol{y}_{\boldsymbol{e}}, \boldsymbol{\theta} | \boldsymbol{x}^* = (\boldsymbol{x}^*)^i]$, we draw $\boldsymbol{y}_{\boldsymbol{e}}^k$ from $p(\boldsymbol{y}_{\boldsymbol{e}} | \boldsymbol{\theta}^k)$ for $k = 1, \cdots, N$, $p(\boldsymbol{y}_{\boldsymbol{e}} | \boldsymbol{\theta})$ is known and is given in Equation (4.12). $(\boldsymbol{y}_{\boldsymbol{e}}^k, \boldsymbol{\theta}^k)$ is hereby a sample pair from $p(\boldsymbol{y}_{\boldsymbol{e}}, \boldsymbol{\theta})$. Condition on $\boldsymbol{x}^* = (\boldsymbol{x}^*)^i$, the sample pairs $\{(\boldsymbol{y}_{\boldsymbol{e}}^{(i,1)}, \boldsymbol{\theta}^{(i,1)}), \cdots, (\boldsymbol{y}_{\boldsymbol{e}}^{(i,m_i)}, \boldsymbol{\theta}^{(i,m_i)})\}$ would be independent samples from $p[\boldsymbol{y}_{\boldsymbol{e}}, \boldsymbol{\theta} | (\boldsymbol{x}^*)^i]$. To approximate $p[\boldsymbol{y}_{\boldsymbol{e}} | (\boldsymbol{x}^*)^i]$, we use the MC estimator

$$\hat{p}[\boldsymbol{y}_{\boldsymbol{e}} | (\boldsymbol{x}^*)^i] = \sum_{t=1}^{m_i} p[\boldsymbol{y}_{\boldsymbol{e}} | \boldsymbol{\theta}^{(i,t)}] p[\boldsymbol{\theta}^{(i,t)} | (\boldsymbol{x}^*)^i] = \sum_{t=1}^{m_i} p[\boldsymbol{y}_{\boldsymbol{e}} | \boldsymbol{\theta}^{(i,t)}]/m_i \tag{4.29}$$

When $m_i = 1$, the above estimator equals to $\hat{p}[\boldsymbol{y}_{\boldsymbol{e}} | (\boldsymbol{x}^*)^i] = p[\boldsymbol{y}_{\boldsymbol{e}} | \boldsymbol{\theta}^{(i,1)}]$.

Hence, the MC estimator, Equation (4.28) can be written as:

$$\sum_{i}^{M} \frac{m_i}{N} \{ \frac{1}{m_i} \sum_{j=1}^{m_i} \log \frac{p[\boldsymbol{y}_{\boldsymbol{e}}^{(i,j)} | \boldsymbol{\theta}^{(i,j)}]}{\hat{p}[\boldsymbol{y}_{\boldsymbol{e}}^{(i,j)} | (\boldsymbol{x}^*)^i]} \} = \frac{1}{N} \sum_{i}^{M} \sum_{j=1}^{m_i} \log \frac{p[\boldsymbol{y}_{\boldsymbol{e}}^{(i,j)} | \boldsymbol{\theta}^{(i,j)}]}{\hat{p}[\boldsymbol{y}_{\boldsymbol{e}}^{(i,j)} | (\boldsymbol{x}^*)^i]} \}$$

where $\hat{p}[\boldsymbol{y}_{\boldsymbol{e}}^{(i,j)}|(\boldsymbol{x}^*)^i] = \sum_{t=1}^{m_i} p[\boldsymbol{y}_{\boldsymbol{e}}^{(i,j)}|\boldsymbol{\theta}^{(i,t)}]/m_i$. Note that when $m_i = 1$,

$$\log \frac{p[\boldsymbol{y}_{\boldsymbol{e}}^{(i,j)}|\boldsymbol{\theta}^{(i,j)}]}{\sum_{t=1}^{m_i} p[\boldsymbol{y}_{\boldsymbol{e}}^{(i,j)}|\boldsymbol{\theta}^{(i,t)}]/m_i} = \log \frac{p[\boldsymbol{y}_{\boldsymbol{e}}^{(i,1)}|\boldsymbol{\theta}^{(i,1)}]}{p[\boldsymbol{y}_{\boldsymbol{e}}^{(i,1)}|\boldsymbol{\theta}^{(i,1)}]} = 0 \tag{4.30}$$

this simplifies the computation.

Overall, the proposed estimation procedure can be summarized as

---

Simulation procedure for estimating $I(\boldsymbol{y}_{\boldsymbol{e}}; \boldsymbol{\theta}|\boldsymbol{x}^*)$

Step 1. Sample $\boldsymbol{\theta}^1, \cdots, \boldsymbol{\theta}^N$ from $p(\boldsymbol{\theta})$.

Step 2: For each $\boldsymbol{\theta}^k$, compute $(\boldsymbol{x}^*)^k \in \mathcal{G}$. Let $\widehat{\mathcal{G}} = \{(\boldsymbol{x}^*)^1, \cdots, (\boldsymbol{x}^*)^M\}$ be the distinct values of $\boldsymbol{x}^*$ and suppose that $(\boldsymbol{x}^*)^i$ is obtained from $\Theta_i = \{\boldsymbol{\theta}^{(i,1)}, \cdots, \boldsymbol{\theta}^{(i,m_i)}\}$ in Step 1.

Step 3: Sample $\boldsymbol{y}_{\boldsymbol{e}}^{(i,j)}$ from $p(\boldsymbol{y}_{\boldsymbol{e}}|\boldsymbol{\theta}^{(i,j)})$ for $\boldsymbol{\theta}^{(i,j)} \in \Theta^i$.

Then, approximate $I(\boldsymbol{y}_{\boldsymbol{e}}; \boldsymbol{\theta}|\boldsymbol{x}^*)$ with

$$\frac{1}{N} \sum_{i}^{M} \sum_{j=1}^{m_i} \log \frac{p[\boldsymbol{y}_{\boldsymbol{e}}^{(i,j)}|\boldsymbol{\theta}^{(i,j)}]}{\hat{p}[\boldsymbol{y}_{\boldsymbol{e}}^{(i,j)}|(\boldsymbol{x}^*)^i]}$$

where $\hat{p}[\boldsymbol{y}_{\boldsymbol{e}}^{(i,j)}|(\boldsymbol{x}^*)^i] = \sum_{t=1}^{m_i} p[\boldsymbol{y}_{\boldsymbol{e}}^{(i,j)}|\boldsymbol{\theta}^{(i,t)}]/m_i$.

Remark: when $m_i = 1$, $\log \frac{p[\boldsymbol{y}_{\boldsymbol{e}}^{(i,j)}|\boldsymbol{\theta}^{(i,j)}]}{\hat{p}[\boldsymbol{y}_{\boldsymbol{e}}^{(i,j)}|(\boldsymbol{x}^*)^i]} = 0$, this simplifies the computation.

Combining with the estimator in Equation (4.24) for the *regression information term*, we obtain the overall MC estimator as

$$\begin{aligned}\widehat{U(\boldsymbol{e})} = &-\frac{p}{2}\log(2\pi) - \frac{p}{2} + \frac{1}{2}\sum_{k=1}^{N} \frac{1}{2N} \log\det\{[Z'Q^kZ + R]\} \\ &+ \int \log[p(\boldsymbol{\theta})]p(\boldsymbol{\theta})d\boldsymbol{\theta} - \frac{1}{N}\sum_{i}^{M}\sum_{j=1}^{m_i} \log \frac{p[\boldsymbol{y}_{\boldsymbol{e}}^{(i,j)}|\boldsymbol{\theta}^{(i,j)}]}{\hat{p}[\boldsymbol{y}_{\boldsymbol{e}}^{(i,j)}|(\boldsymbol{x}^*)^i]}\end{aligned} \tag{4.31}$$

where $Z = (z(\boldsymbol{x})_1, \cdots, z(\boldsymbol{x})_E)'$ is the experiment covariate matrix, $Q^k = \text{diag}\{\exp[z(\boldsymbol{x})_e'\boldsymbol{\theta}^k]\}_{e=1}^E$, and $\hat{p}[\boldsymbol{y}_{\boldsymbol{e}}^{(i,j)}|(\boldsymbol{x}^*)^i] = \sum_{t=1}^{m_i} p[\boldsymbol{y}_{\boldsymbol{e}}^{(i,j)}|\boldsymbol{\theta}^{(i,t)}]/m_i$. Note that because the integration in Equation (4.24) is generally intractable, the same N samples of $\boldsymbol{\theta}$ is also used to approximate this integration.

Since the prior distribution $p(\boldsymbol{\theta})$ does not depend on the design $\boldsymbol{e}$, so the

experiment maximizing the estimator, Equation (4.31) for OP optimal design criterion is the one that maximizes:

$$\widehat{\phi}(\boldsymbol{e}) = \frac{1}{2}\sum_{k=1}^{N}\frac{1}{2N}\log\det\{[Z'Q^kZ+R]\} - \frac{1}{N}\sum_{i}^{M}\sum_{j=1}^{m_i}\log\frac{p[\boldsymbol{y}_{\boldsymbol{e}}^{(i,j)}|\boldsymbol{\theta}^{(i,j)}]}{\hat{p}[\boldsymbol{y}_{\boldsymbol{e}}^{(i,j)}|(\boldsymbol{x}^*)^i]} \quad (4.32)$$

And the experiment maximizing the D-optimal design criterion in Equation (4.8) is the one that maximizes:

$$\widehat{\phi_D}(\boldsymbol{e}) = \frac{1}{2}\sum_{k=1}^{N}\frac{1}{2N}\log\det\{[Z'Q^kZ+R]\} \quad (4.33)$$

In the case where comparing two different designs $\boldsymbol{e}_1$ and $\boldsymbol{e}_2$ is the objective, one should use the same N samples for the $\boldsymbol{\theta}^k$, for that positive correlation between $\widehat{\phi}(\boldsymbol{e}_1)$ and $\widehat{\phi}(\boldsymbol{e}_2)$ would reduce the estimation variance of their difference (see Ryan (2003)). Remark: The proposed two components approximation algorithm decomposes the original criterion and deterministically approximates the component involving the evaluation of $\int\log[p(\boldsymbol{y_e})]p(\boldsymbol{y_e})\boldsymbol{y_e}$ in Equation 4.5 and 4.20. This avoids the nested structure to estimate $\log[p(\boldsymbol{y_e})]$ with $N(N_2+1)$ samples in Equation 4.9. Compared to a pure Monte Carlo simulation, the computational burden is reduced.

4.5 A genetic algorithm for searching optimal design

To search the optimal design for the proposed Bayesian OP optimality criteria, we apply the Genetic Algorithms (GAs) (Mitchell (1998)). GAs are evolutionary based algorithms that are suitable for searching irregular, poorly characterized constrained/unconstrained spaces. More importantly, GAs can also be parallelized quite easily (Cantú-Paz (1998)), making the search for a near-optimal design for various design criteria feasible. For these reasons, GAs have become quite effective in searching of optimal designs (Broudiscou et al. (1996); Hamada et al. (2001)).

In GAs, a population of candidate solutions (individuals) is evolved toward

solutions with higher fitness values. These individuals are made of units (genes) which can be mutated and exchanged. The fitness of each individual is evaluated and only the individuals with superior fitness values are selected to pass their genetic information to offsprings. When optimizing an optimal design criterion, each individual is a candidate design $\boldsymbol{e}$, and the length of it is the product of the number of control factors d and the number of runs E. For example, a candidate individual could be $[(1,-1),(1,1),(-1,1),(1,1)]$ for a batch experiment with two control factors and four runs, where $(1,-1)$ is a unit. For more details in applying GAs to the search of optimal designs, see Hamada et al. (2001).

Upon the efficient use of GAs for searching optimal designs, there are several optimization algorithm inputs that need to be specified by the user: the population size $popSize$, the mutation probability pmu, the elitism rate $Elit$ and the maximum number of generations to run (evolve) before the search is halted $maxiter$. Our simulation studies show that the convergence of GAs exhibit similar behavior for optimizing the Bayesian D-optimal and the OP optimal criterion. This is probably because these two criteria share the same search space and that $\widehat{\phi_D}(\boldsymbol{e})$ in Equation (4.33) accounts for a large part of $\widehat{\phi}(\boldsymbol{e})$ in Equation (4.32). Since a single optimization procedure using GAs to optimize $\widehat{\phi_D}(\boldsymbol{e})$ can be done in a much shorter time than to optimize $\widehat{\phi}(\boldsymbol{e})$, one can progressively tune the GAs inputs for optimizing $\widehat{\phi_D}(\boldsymbol{e})$ until obtaining a relatively fast and satisfactory convergence behavior. Thereafter, the obtained GAs inputs can be used for optimizing $\widehat{\phi}(\boldsymbol{e})$. More details of the setting of these algorithm inputs are provided in Section 4.6.2.

4.6 Examples

4.6.1 A simple numerical example

Here we use a simplified one-dimensional problem to study the characteristics of the OP optimal design and compare them with the traditional Bayesian D optimal design. We assume that the response variable $\boldsymbol{y_x}$ follows a Poisson

distribution with mean $\mu(x, \boldsymbol{\theta})$ where the design variable $x \in [-1, 1]$ can only be controlled precisely up to two decimal place. And

$$\log(\mu(x, \boldsymbol{\theta})) = \theta_0 + \theta_1 * x + \theta_2 * x^2 + \theta_3 * x^3 \tag{4.34}$$

A bounded normal prior with means and $\pm 2\boldsymbol{\sigma}$ ranges on the coefficient parameters are specified as follows:

$$3.04 \leqslant \theta_0 \leqslant 3.56, \quad -2.68 \leqslant \theta_1 \leqslant -1.32,$$
$$-0.6 \leqslant \theta_2 \leqslant 0.2, \quad 1.2 \leqslant \theta_{11} \leqslant 2.8 \tag{4.35}$$

The response function with the mode of the prior parameter is plotted in Figure 4.1. As can be seen from this figure, the minimum point of the response surface is highly possible to be located in the range of $[0, 1]$ based on the prior information. Intuitively, in order to collect more informative about the location of the minimum point, more points should be put close to 0.6. Here, we run the GAs to search for a 9-run OP optimal design and a 9-run D-optimal design.

The D-optimal criterion estimator in Equation (4.33) can be write as

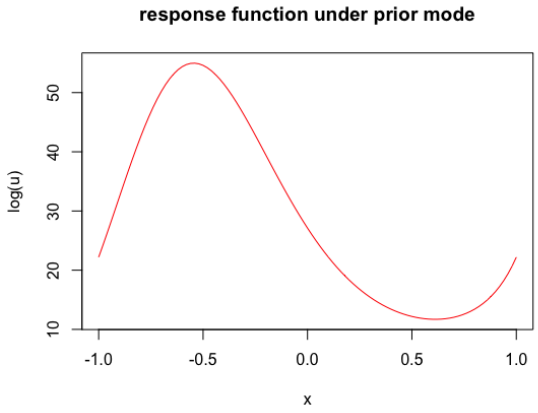

Figure 4.1: Prior response function of toy example

$$\widehat{\phi_D}(\boldsymbol{e}) = \sum_{k=1}^{N} \frac{1}{2N} \log \det\{[Z' Q^k Z + R]\} \tag{4.36}$$

where $Z = [z(\boldsymbol{x})_1, \cdots, z(\boldsymbol{x})_E]'$ is the experiment covariate matrix with $z(\boldsymbol{x}) = (1, x, x^2, x^3)$ and the prior precision matrix $R = \text{diag}(1/\boldsymbol{\sigma^2})$. The weight matrix $Q^k = \text{diag}\{\exp[z(\boldsymbol{x})'_e \boldsymbol{\theta}^k]\}_{e=1}^E$, where $\boldsymbol{\theta}^k = (\theta_0^k, \theta_1^k, \theta_2^k, \theta_3^k)$ is a random sample from the prior distribution. And the OP optimal criterion estimator Equation (4.32) is

$$\widehat{\phi}(\boldsymbol{e}) = \sum_{k=1}^{N} \frac{1}{2N} \log\det\{[Z'Q^kZ + R]\} - \frac{1}{N}\sum_{i}^{M}\sum_{j=1}^{m_i} \log \frac{p[\boldsymbol{y}_{\boldsymbol{e}}^{(i,j)}|\boldsymbol{\theta}^{(i,j)}]}{\widehat{p}[\boldsymbol{y}_{\boldsymbol{e}}^{(i,j)}|(\boldsymbol{x}^*)^i]} \quad (4.37)$$

In this application, a sample size of $N = 1e^5$ is chosen for a trade-off between computability and estimation error. A bootstrap procedure shows that the estimation standard derivation of $\widehat{\phi}(\boldsymbol{e})$ in Equation (4.42) for $N = 1e^5$ is $1.2e^{-3}$ for this application. Thereafter, we adopt a real-valued GA procedure to optimize $\widehat{\phi}(\boldsymbol{e})$ and $\widehat{\phi_D}(\boldsymbol{e})$ and the optimum design points are rounded to two decimal places. The GAs inputs for optimizing both $\widehat{\phi}(\boldsymbol{e})$ and $\widehat{\phi_D}(\boldsymbol{e})$ are $popSize = 20, pmu = 0.2, Elit = 2$ and $maxiter = 400$.

Figure 4.2 and 4.3 plot how the fitness ($\widehat{\phi_D}(\boldsymbol{e})$ or $\widehat{\phi}(\boldsymbol{e})$) increases over the

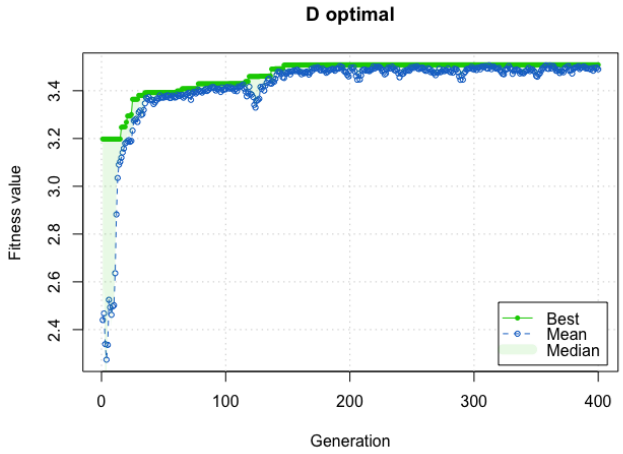

Figure 4.2: Toy example: evolution process of GAs for D-optimal

400 generations during the optimization process of the GAs for searching the D-optimal and OP-optimal design points. As can be seen from the plot, the best fitness value of the 20 individual population almost stays the same after 300 generations for both $\widehat{\phi_D}(\boldsymbol{e})$ and $\widehat{\phi}(\boldsymbol{e})$, hence we deem the GAs convergence

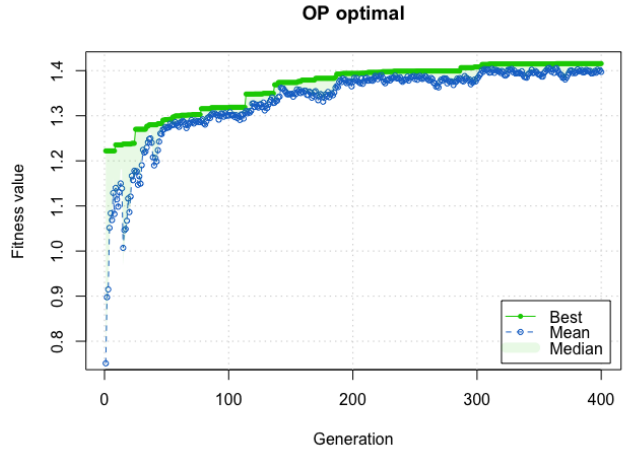

Figure 4.3: Toy example: evolution process of GAs for OP-optimal design

after 400 generations.

The obtained D-optimal points are

$$x = -0.99, -0.98, -0.98, -0.53, -0.53, -0.52, 0.97, 0.98, 1.00 \tag{4.38}$$

and OP optimal points are

$$x = -0.97, -0.44, -0.31, 0.10, 0.98, 0.99, 0.99, 0.99, 1.00 \tag{4.39}$$

In this example, we see that the D-optimal design puts more points in the range of $[-1, -0.5]$ because the shape of the function changes the most sharply in this area. On the other hand, the OP optimal design places most of the points in the upper bound of the design space near $x = 1$. This is because with its initial fit with the prior information, the minimum point is estimated to be near 0.6.

To compare the design efficiency in respect to estimating the optimum point, the design efficiency measure is also calculated with :

$$\text{eff}(\boldsymbol{e}) = \frac{\widehat{\phi}(\boldsymbol{e})}{\widehat{\phi}(\boldsymbol{e}^*)} = \frac{1.137}{1.695} = 0.67 \tag{4.40}$$

This result implies that if the Bayesian D-optimal design $\boldsymbol{e}_D$ (9 run) is used for the Poisson regression model in Equation (4.34) with prior described in Equation (4.35), the (asymptotic) variance of estimating $\boldsymbol{x}^*$ is 33 percent larger than the variance, which can be obtained from the OP optimal design $\boldsymbol{e}^*$.

4.6.2 Bayesian OP optimal design for the motivating experiment

The objective of the motivating problem is to find a batch experiment leading to an efficient estimation of the optimum point. To make the notation simple, we denote $(RF, pressure) = (x_1, x_2)$, hence $\boldsymbol{x}^* = (RF^*, pressure^*) = (x_1^*, x_2^*)$. Since the value of $\boldsymbol{x}^*$ can only be controlled precisely up to two decimal place, $\boldsymbol{x}^*$ falls in a discrete set $\mathcal{G} \subset [-1, 1]^2$. For the Poisson regression in Equation (4.2) with prior distribution described in Equation (4.3), the D-optimal criterion estimator in Equation (4.33) can be write as

$$\widehat{\phi_D}(\boldsymbol{e}) = \sum_{k=1}^{N} \frac{1}{2N} \log\det\{[Z'Q^kZ + R]\} \tag{4.41}$$

where $Z = [z(\boldsymbol{x})_1, \cdots, z(\boldsymbol{x})_E]'$ is the experiment covariate matrix with $z(\boldsymbol{x}) = (1, x_1, x_2, x_1^2,\ x_2^2, x_1x_2)$ and the prior precision matrix $R = \mathrm{diag}(1/\boldsymbol{\sigma^2})$. The weight matrix $Q^k = \mathrm{diag}\{\exp[z(\boldsymbol{x})_e'\boldsymbol{\theta}^k]\}_{e=1}^{E}$, where $\boldsymbol{\theta}^k = (\theta_0^k, \theta_1^k, \theta_2^k, \theta_{11}^k, \theta_{22}^k, \theta_{12}^k)$ is a random sample from the prior distribution. And the OP optimal criterion estimator Equation (4.32) is

$$\widehat{\phi}(\boldsymbol{e}) = \sum_{k=1}^{N} \frac{1}{2N} \log\det\{[Z'Q^kZ + R]\} - \frac{1}{N}\sum_{i}^{M}\sum_{j=1}^{m_i} \log \frac{p[\boldsymbol{y}_{\boldsymbol{e}}^{(i,j)}|\boldsymbol{\theta}^{(i,j)}]}{\widehat{p}[\boldsymbol{y}_{\boldsymbol{e}}^{(i,j)}|(\boldsymbol{x}^*)^i]} \tag{4.42}$$

In this application, a sample size of $N = 1e^5$ is chosen for a trade-off between computability and estimation error. A bootstrap procedure shows that the estimation standard derivation of $\widehat{\phi}(\boldsymbol{e})$ in Equation (4.42) for $N = 1e^5$ is $3.16e^{-3}$ for this application. Thereafter, we adopt a real-valued GA procedure to optimize $\widehat{\phi}(\boldsymbol{e})$ and the optimum design points are rounded to two decimal places. As a comparison, the D-optimal design is also obtained by optimizing $\widehat{\phi_D}(\boldsymbol{e})$ in

Equation (4.41) using the same real-valued GA procedure. The GAs inputs for optimizing both $\widehat{\phi}(\boldsymbol{e})$ and $\widehat{\phi_D}(\boldsymbol{e})$ are $popSize = 20, pmu = 0.2, Elit = 2$ and $maxiter = 500$.

Figure 4.4 and 4.5 plot how the fitness ($\widehat{\phi_D}(\boldsymbol{e})$ or $\widehat{\phi}(\boldsymbol{e})$) increases over the 500 generations during the optimization process of the GAs for searching the D-optimal and OP-optimal design points. As can be seen from the plot, the best fitness value of the 20 individual population almost stays the same after 450 generations for both $\widehat{\phi_D}(\boldsymbol{e})$ and $\widehat{\phi}(\boldsymbol{e})$, hence we deem the GAs convergence after 500 generations.

The obtained 15-run OP-optimal and D-optimal design points are shown in

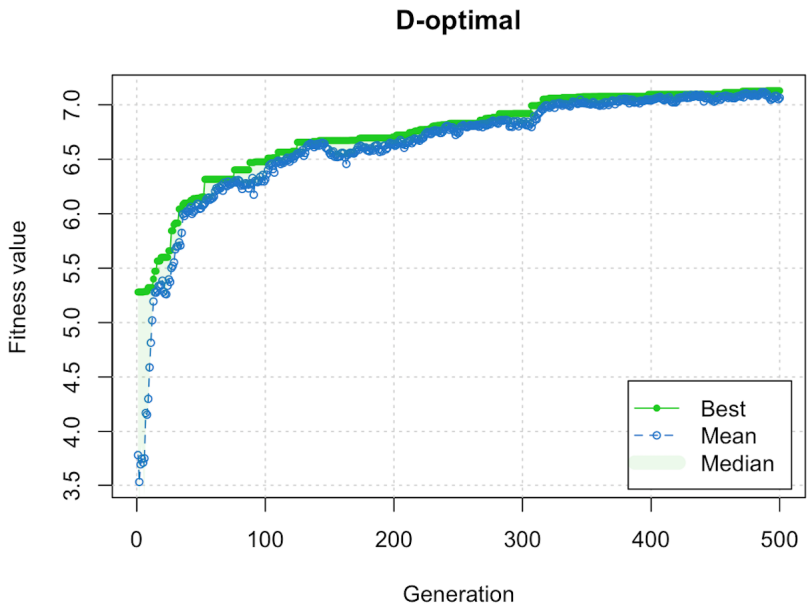

Figure 4.4: Evolution process of GAs for D-optimal design

Table 4.1. To gain more insight on how the OP-optimal design points are different from the D-optimal design points, we also calculate the results for a 12-run experiment. The obtained OP-optimal and D-optimal design points are plotted for both the 12-run experiment (Figure 4.6) and 15-run experiment (Figure 4.7). As can be seen from the plot, the OP optimal design of both the 12-run and 15-run experiment move one point of D-optimal design from the lower level of x_2 to the middle level of x_2 (e.g. from -1 to 0). This implies that the observations in

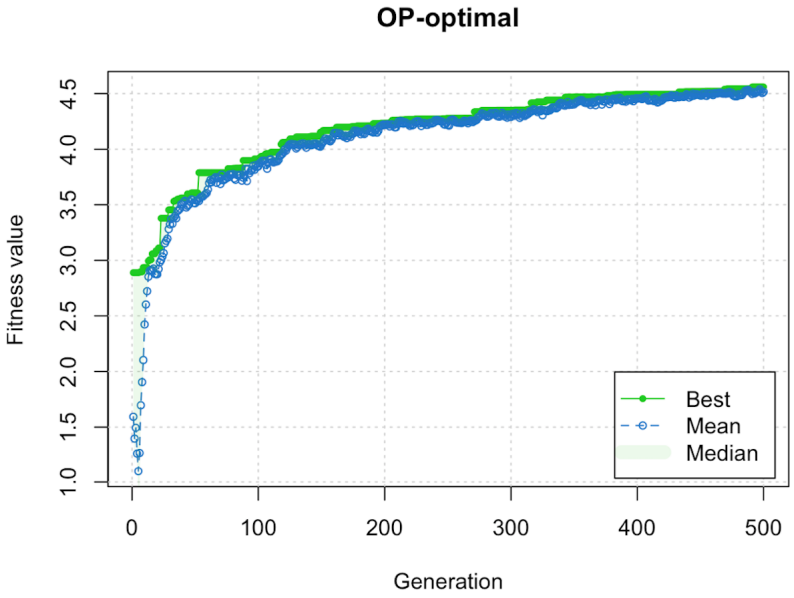

Figure 4.5: Evolution process of GAs for OP-optimal design

Table 4.1: The D-optimal and OP-optimal design points

D-optimal			OP optimal		
run	x_1	x_2	run	x_1	x_2
1	0.96	-0.9	1	0.97	-0.05
2	-0.95	1	2	0.95	-0.98
3	0.92	-0.02	3	0.24	0.95
4	0.98	0.98	4	0.98	0.99
5	-0.97	-0.97	5	-0.97	-0.97
6	0.94	0.1	6	-0.99	0.94
7	0.9	0.97	7	0.99	-0.99
8	0.05	0.96	8	-0.01	-0.97
9	-1	-0.96	9	-0.94	0.96
10	0.05	-0.94	10	0.09	-0.02
11	0.98	-0.98	11	0.96	0.03
12	0.11	-0.97	12	0.09	-0.96
13	-0.94	-0.9	13	-0.96	-0.96
14	-0.96	0.89	14	-0.94	0.04
15	0.16	-0.2	15	0.88	0.96

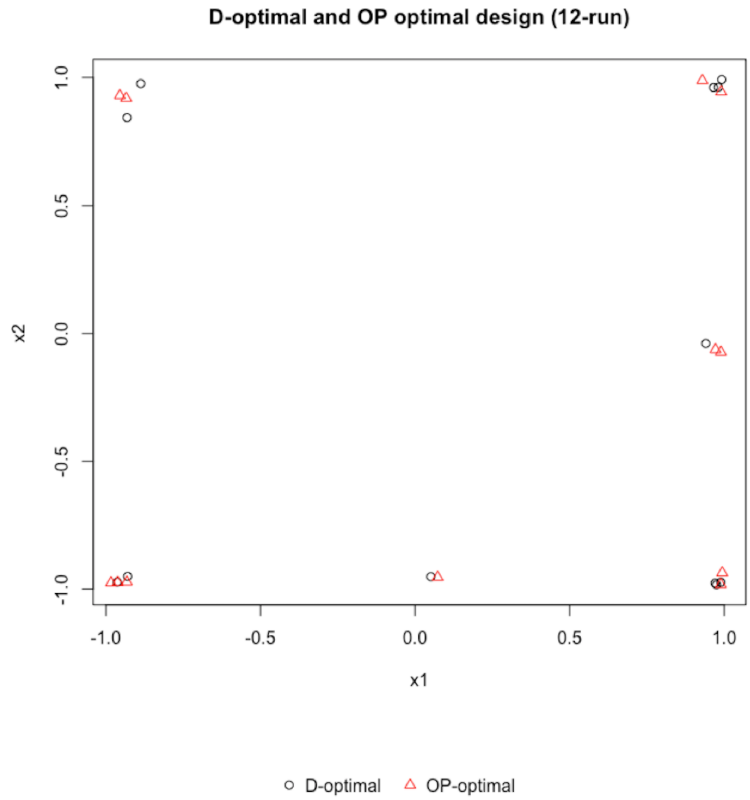

Figure 4.6: The D-optimal and OP-optimal design points (12 run)

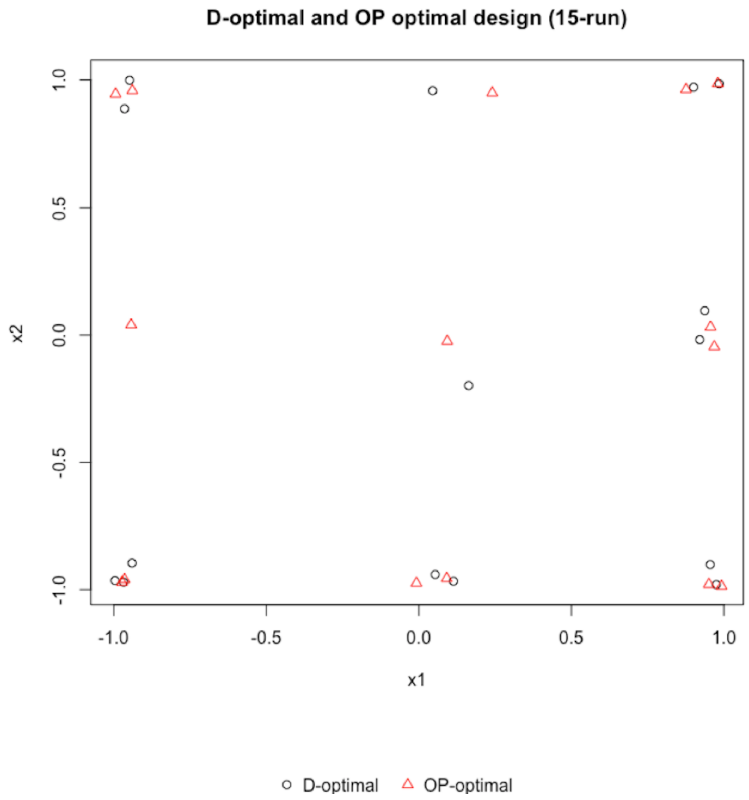

Figure 4.7: The D-optimal and OP-optimal design points (15 run)

the middle level of x_2 is more informative than the observations in the lower level of x_2 to obtain an efficient estimator of $\boldsymbol{x}^*$. To intuitively understand this, we fix the x_1 value as $x_1 = \overline{x_1}$ and plot the defect response function $\mu(\overline{x_1}, x_2, \widehat{\boldsymbol{\theta}}_{mle})$ with its dependence on x_2, conditioning on the coefficients $\boldsymbol{\theta}$ equal to the prior mode $\widehat{\boldsymbol{\theta}}_{mle}$. In Figure 4.8, we plot three functions of $\mu(\overline{x_1}, x_2, \widehat{\boldsymbol{\theta}}_{mle})$ by setting $\overline{x_1} = -1, 0, 1$ respectively. In this three functions, for $\overline{x_1} = -1, 0, 1$, the corresponding ξ_2^* equals to $1, 0.5, 0$. This means that for fixed $x_1 \in [-1, 1]$, the 'prior mode' of x_2^* locates in the range $[0, 1]$. In other words, based on prior information, x_2^* would have higher chance to belong to $[0, 1]$. Therefore, observations in the range $[0, 1]$ would be more informative with respect to estimating the posterior value of x_2^* than observations in the range $[-1, 0]$. This explains why both the 12-run and the 15-run OP-optimal design move one point of the D-optimal design from the lower level $x2 \approx -1$ to the middle level $x2 \approx 0$.

Now we check the efficiency of the obtained OP optimal design and D opti-

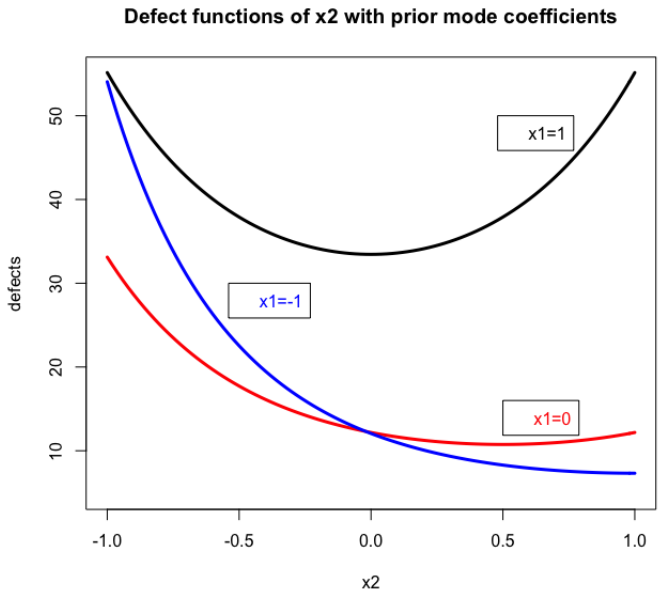

Figure 4.8: Response functions for fixed x1

mal design in respect of estimating the optimum point $\boldsymbol{x}^*$. Let $\boldsymbol{e}^*$ denotes the obtained OP-optimal design and $\boldsymbol{e}_D$ denotes the D-optimal design. From the estimator in Equation (4.42), we obtained the expected utility value these two

designs are $\widehat{\phi}(\boldsymbol{e}^*) = 4.638$ and $\widehat{\phi}(\boldsymbol{e}_D) = 4.098$ respectively. These optimal values mean that the maximum information one can gain on $\boldsymbol{x}^*$ from conducting a 15-run experiment is 4.657 and the information gain on $\boldsymbol{x}^*$ from conducting a 15-run D-optimal design is 4.098. To compare the efficiency of a design $\boldsymbol{e} \in \mathcal{X}^E$ with the optimal design $\boldsymbol{e}^*$ for the OP optimality criterion $\phi(\cdot)$, we use the following measure similar with Dette et al. (2008)

$$\text{eff}(\boldsymbol{e}) = \frac{\widehat{\phi}(\boldsymbol{e})}{\widehat{\phi}(\boldsymbol{e}^*)} \tag{4.43}$$

And in this example, this efficiency measure $\text{eff}(\boldsymbol{e}_D) = 0.880$. This result implies that if the Bayesian D-optimal design $\boldsymbol{e}_D$ (15 run) is used for for the Poisson regression model in Equation (4.2) with prior described in Equation (4.3), the (asymptotic) variance of estimating $\boldsymbol{x}^*$ is 12 percent larger than the variance, which can be obtained from the OP optimal design $\boldsymbol{e}^*$.

4.7 Conclusion

In this chapter, a Bayesian optimal design framework is built for estimating the optimum point. A Bayesian OP optimality criterion is derived based on expected Shannon information gain (uncertainty reduction) on the optimum point. To evaluate the proposed criterion, we derive an estimator based on decomposing the criterion into two separate terms, where the first term equals to the D-optimal criterion and the second term can be estimated with Monte Carlo without a nested structure. The proposed approximation greatly reduces the computational burden of a pure MC algorithm and makes searching for the near-optimal design more feasible. Moreover, the proposed framework employs a general treatment of the regression model and could be used to obtain optimal designs for any kind of regression function in the regressor.

CHAPTER 5

METAMODEL-BASED OPTIMIZATION OF STOCHASTIC COMPUTER MODELS UNDER UNCERTAIN OBJECTIVE FUNCTION

In this chapter, we focus on the quantification of the parameter uncertainty in the objective function through computationally efficient tools.

5.1 Introduction

With the constantly upgraded computing power, stochastic computer models are becoming important tools for understanding and optimizing engineering systems that are analytically intractable and subject to random fluctuations. Typically, a stochastic computer model is constructed based on technical knowledge of how the engineering system operates. The purpose of engineering optimization is to choose a set of settings for the design variables of the system such that the system performance is optimized. These tools have been recently successfully applied to many engineering optimization applications including the integrated photonic filters design in electrical engineering (Weng et al. (2017)), aerospike nozzle design in aerospace engineering(Stevens and Branam (2015)), continuous stirred-tank (CSTR) reactor design in chemical engineering (Ding et al. (2010)), etc.

An ideal case would be such that the design engineer or the investigator has complete knowledge for determining the objective functions for optimizing the system performance. However, this may not always be true especially when analyzing complex engineering systems. In many areas of applications, there are multiple objectives or difficult-to-evaluate parameters in the objective functions (for example Ristow et al. (2005); Pant et al. (2011); Bozsak et al. (2015)). When multiple objectives need to be optimized simultaneously, the most popular method is to form a composite objective function through weighted sum (Marler and Arora (2010)) or desirability functions (Wu (2004); Park and Kim (2005)), where a weight or scale parameter proportional to the user preference is assigned to a particular objective. However, the determination of these preference parameters is usually highly subjective and not straightforward. It requires an investigation of the qualitative and experience-driven information to determine the quantitative preference parameter values. Without the possible trade-off optimal solutions in hand, this is an even more challenging task. Besides these uncertain preference parameters, the uncertainty in an objective function may also come from the difficult-to-evaluate parameters. For example, when designing a nuclear power plant building, the cost incurred by varying rates of leakage of radioactive material can be hard to quantify (Korsakissok et al. (2013)). And a change in the potential cost will possibly result in a totally different optimal solution. This objective function uncertainty problem appears in various areas of application and brings many challenges in both concept and computation.

When dealing with this uncertainty problem, the current development of stochastic computer models mainly focuses on replacing the uncertain parameters by some estimates and assuming the objective function is precisely determined, for example, see Humphrey and Wilson (2000); Cao et al. (2004); Ristow et al. (2005); Kleijnen (2014); Weng et al. (2017). By such a choice, the uncertainty is pushed out of sight through approximating the uncertain parameters by some particular estimates, such as decision maker's preference information, expert judgment, historical records, or a sample mean. Meanwhile, the inferen-

tial procedure for other choices of the uncertain parameters is simply ignored. However, unless a reliable preference or accurate estimate is available, the optimal solution obtained by such methods would be highly subjective to the specific investigator or largely sensitive to the choice of the estimates(Wurl and Albin (1999)).

In the optimization literature, an ideal procedure for a multi-objective problem is the *posteriori approach* (Burke and Kendall (2013)), in which a set of different trade-off optimal solutions is first obtained and then a multiple-criterion decision-making technique (such as using high-level information) (Deb and Sundar (2006)) is used to analyze the solutions to choose a most preferred solution. This is because any two different optimal solutions (such as Pareto-points) represent different trade-offs among the objectives, and the decision maker would be in a better position to balance risk when such choices are presented. Likewise, when the objective function contains some difficult-to-evaluate parameters, a rational procedure is to conduct *sensitivity analysis* (post-optimality analysis) (Wallace (2000)). For example, when the cost of failure is uncertain, it is important for the investigator to know how profit would be affected by a change in the potential failure cost. The results of *sensitivity analysis* provide how sensitive the optimal solution is to the change in the uncertain parameters and establish the upper and lower bounds for the uncertain parameters within which they can vary without causing violent changes in the current optimal solution.

As pointed by Burke and Kendall (2013), the classical methods use a different philosophy such that the objective function uncertainty is artificially forced out of sight, mainly due to a lack of suitable optimization tools to obtain many optimal solutions efficiently. To properly capture this uncertainty, the most straightforward method should be to optimize the system many times with various settings of the uncertain parameters. However, for a time-consuming stochastic computer model, this would usually incur extensive computational burden. In the context of multi-objective optimization, an alternative solution is the *interactive approach* (Deb et al. (2010); Boyle and Shin (1996)), in which the decision

maker's responses to specific questions were used iteratively to guide the solution towards the preferred part of the Pareto-optimal region. Although this method reduces the computational burden of optimizing the system repeatedly for many different uncertain parameter choices, it requires a lot of cognitive efforts of the decision maker. Moreover, when the modeler and the decision maker is not the same person, this method can be infeasible or very inefficient.

In short, it is important to capture the uncertainty in the objective function to offer the decision maker desired flexibility in making a more informed and rational decision. However, capturing this uncertainty means the investigator has to optimize the computer model repeatedly for many different choices of the uncertain parameters, which is very time-consuming. In this work, we proposed a computationally efficient solution to this problem from an experimental design and metamodeling point of view. This solution first constructs a Cartesian product design over the space of both design variables and uncertain parameters. Thereafter, a radial basis function metamodel is used to provide a smooth prediction surface of the objective value over the design variables and uncertain parameters spaces. In addition, based on the Cartesian product design structure, a fast fitting algorithm is also derived for fitting the metamodel. To illustrate the effectiveness of the proposed method for solving practical problems, we use the optimization of drug release from a polymer matrix (Schiesser (2012)) as a test example, where the developed tools are used to facilitate a robust selection of the scale parameters in the desirability function.

The remainder of this chapter is organized as follows: Section 3.2 introduces some examples of uncertainty parameters in general classes of objective functions and stresses its importance in practical applications. Section 3.3 first introduces the interpolation of an objective function estimate with fixed objective function parameters with an RBF metamodel, and then proposes design and modeling techniques for conveniently capturing the uncertainty in the objective function. In Section 3.4, the developed tools are used to solve a practical problem and demonstrate how a more informed and rational decision can be made. Finally,

Section 3.5 concludes the chapter.

5.2 Objective functions with uncertain parameters

In this section, to demonstrate the practical scenarios where the proposed framework is helpful, we present some of the major cases where there are uncertain parameters in the objective functions. Following each specific case, the corresponding post-optimal decision-making tools are also discussed. Most of these tools require optimizing the objective function under many different choices of the uncertain parameters, which motivates the development of computationally efficient tools for conducting such post-optimal analysis for time-consuming stochastic computer models.

5.2.1 Uncertain failure cost in structural design

In structural design, stochastic computer models are usually used to predict the degree of deformation or the probability of damage (see Papadrakakis and Lagaros (2002); Deng et al. (2003)). Using the *cost-benefit analysis* tools (Kanda and Shah (1997)), the optimal structural design is determined, where the 'cost' is the price of increasing safety and the 'benefit' is the reduced risk in terms of expected failure cost. An example of the total cost C_T defined by Kanda and Shah (1997) is

$$C_T = C_I + C_F \int_0^1 \frac{\eta - \eta_0}{1 - \eta_0} P(\eta) d\eta \tag{5.1}$$

where C_I is the initial cost, $\eta \in [0, 1]$ is the damage level, η_0 is the initial damage level, and C_F is the failure cost at ultimate limit state $\eta = 1$. The quantity $p(\eta)$ is the probability for different damage levels to happen which is the output of the computer model. In this objective function, the ultimate limit state failure cost C_F is an uncertain parameter which varies from building to building and contains some difficult-to-evaluate parts such as casualties caused by the collapse of buildings or serious failure of nuclear power plants. Note that in this example,

although the stochastic computer model may have captured the random fluctuations in loads and structural resistance, the failure cost parameter C_F is not part of the stochastic computer model and do not affect the computer model output $P(\eta)$. Instead, it is an uncertain parameter in the objective function.

The simplest solution is to choose C_F based on subjective judgments or historical records. However, the optimal solution could be very sensitive to the choice of C_F and hence result in very unreliable and subjective decisions. A more rational decision can be made if the structural designer can conduct a *sensitivity analysis* (post-optimality analysis) (Wallace (2000)) of the optimal design solution with respect to the uncertainty in C_F. This involves re-optimizing the system under alternative choices of C_F to decide how sensitive the optimal solution is to the change in the C_F. If significant changes of the optimal solution are identified and associated with the changes in C_F, more attention and effort should, therefore, be made to select the value of C_F in order to increase the robustness of the decision.

When there are difficult-to-evaluate parameters in the objective function, conducting *sensitivity analysis* can also enhance the communication from modeler to decision makers (e.g. by making recommendations more informative, credible or understandable). For example, the result of *sensitivity analysis* would provide information to the manager on how profit would be affected by a change in the potential failure cost. If the results are insensitive to changes in uncertain parameters, the manager can be quite confident that the decision made is good. Note that to efficiently conduct *sensitivity analysis* for time-consuming stochastic computer models, a procedure for optimizing the system with a low computing budget is desired.

5.2.2 Pareto-optimal front

Suppose there are S objective functions, denoted as $J_s(x), s = 1, \cdots, S$. For multi-objective optimization problems, an ideal procedure is first to find multiple trade-off solutions with a wide range of values(Pareto-optimal front), and then

a multiple-criteria decision-making technique (such as using high-level information) (Deb and Sundar (2006)) is used to analyze the solutions to choose a most preferred solution. Specifically, the Pareto-optimal front consists of solutions with the property that none of the objective values can be improved without degrading some of the other objective values. The simplest way to obtain the Pareto-optimal front is the weighted sum method, where the solution x^* optimizing the objective $J(x) = \sum_{s=1}^{S} w_s J_s(x)$ is Pareto-optimal if $w_s > 0, s = 1, \cdots, S$ and $\sum_{s=1}^{S} w_s = 1$. Under some assumptions, every different choice of the weight parameters under the constraints $w_s > 0, s = 1, \cdots, S$ and $\sum_{s=1}^{S} w_s = 1$ would produce different points in the Pareto-optimal front (Miettinen (2012)). In this case, the weights $w_s > 0, s = 1, \cdots, S$ are uncertain parameters in the objective function $J(x)$, and a procedure allowing convenient optimization of $J(x)$ under different weight values would save considerable computational effort.

5.2.3 Desirability function

The desirability function (Harrington (1965); Derringer (1980)) is one of the most widely used methods for the optimization of multiple responses or multiple objective engineering systems. This approach first transforms the different objectives into a common scale $[0, 1]$ and then combines them into an overall objective using the geometric mean. Suppose there are S objective functions, denoted as $J_s(\boldsymbol{x}), s = 1, \cdots, S$. For each of the S functions, a corresponding desirability score function is constructed which is high when $J_s(x)$ is at a desirable level (such as minimum, maximum, or target) and low when $J_s(\boldsymbol{x})$ is at an undesirable level. For example, for minimization of $J_s(\boldsymbol{x})$, Derringer (1980) construct the desirability function as

$$D_s^{min}(\boldsymbol{x}; \theta_s) = \begin{cases} 0 & \text{if } J_s(\boldsymbol{x}) > B \\ [\frac{J_s(\boldsymbol{x}) - B}{A - B}]^{\theta_s} & \text{if } A \leqslant J_s(\boldsymbol{x}) \leqslant B \\ 1 & J_s(\boldsymbol{x}) < A \end{cases} \tag{5.2}$$

where A, B, and the scale parameters θ_s are chosen by the investigator. For target-the-best situations, the desirability function is

$$D_s^{target}(\boldsymbol{x};\theta_s) = \begin{cases} [\frac{J_s(\boldsymbol{x})-A}{T_0-A}]^{\theta_{s1}} & \text{if } A \leqslant J_s(\boldsymbol{x}) \leqslant T_0 \\ [\frac{J_s(\boldsymbol{x})-B}{T_0-B}]^{\theta_{s2}} & \text{if } T_0 < J_s(\boldsymbol{x}) \leqslant B \\ 0 & \text{otherwise} \end{cases} \tag{5.3}$$

where $\theta_s = (\theta_{s1}, \theta_{s2})$ and T_0 is the target value chosen by the investigator. And for maximization, the desirability function is given in Wu (2004).

Given that the S desirability functions $D_1, \cdots, D_S$ are on the same scale($[0, 1]$), they can be combined to produce an overall desirability function through the geometric mean:

$$D(\boldsymbol{x};\boldsymbol{\theta}) = [\prod_{s=1}^{S} D_s(\boldsymbol{x};\theta_s)]^{1/S} \tag{5.4}$$

where $\boldsymbol{\theta} = (\theta_1, \cdots, \theta_S)$. In this overall objective function $D(\boldsymbol{x};\boldsymbol{\theta})$, the scale parameters $\boldsymbol{\theta}$ have to be chosen such that the desirability measure is easier or harder to satisfy. For example, choosing $\theta_{s1} > 1$ in Equation (5.3) would place more rewards on being close to the target value, and choosing $0 < \theta_{s1} < 1$ would make this less important.

This desirability-based method is easy to understand and is available in many data analysis software packages. It has been extensively used in optimization of industrial problems, such as Elsayed and Lacor (2013); Zhang et al. (2009); Yalcınkaya and Bayhan (2009). However, to use this method, the investigator needs to choose values of the shape parameters to represent the trade-off preferences. This is not a trivial task and the choices may possibly be made without awareness of the fact that different values of these scale parameters would possibly produce very different optimal solutions. Other than specifying these scale parameters subjectively, Jeong and Kim (2009) proposed an *interactive approach* to select the values for these parameters. They proposed to first initialize the scale parameter and obtain an initial optimal solution, then interact with the

decision maker to find his reaction to this solution and thereafter adjust the scale parameter value until some stopping criterion is satisfied. Although this method reduced the computational burden of optimizing the system repeatedly for many different scale parameter settings, it requires a lot of cognitive efforts of the decision maker.

An alternative solution to this uncertain scale parameter problem is to select the most 'robust' choice of the scale parameter. Specifically, for a particular choice of the scale parameter, one would obtain the corresponding optimal solution depending on $\boldsymbol{\theta}$ as $\boldsymbol{x}^*(\boldsymbol{\theta}) := \text{argmax}_{\boldsymbol{x}} D(\boldsymbol{x}; \boldsymbol{\theta})$. To select the most 'robust' $\boldsymbol{\theta}$ from the many choices, or equivalently, to choose the most 'robust' corresponding $\boldsymbol{x}^*(\boldsymbol{\theta})$, a reasonable criterion is to measure how $\boldsymbol{x}^*(\boldsymbol{\theta})$ would perform under all the other possible choices of the scale parameter $\boldsymbol{\vartheta} \in \Theta$. Suppose the 'true' scale parameter value is $\boldsymbol{\vartheta}$, the maximum desirability score would be achieved at point $\boldsymbol{x} = \boldsymbol{x}^*(\boldsymbol{\vartheta})$ with value $D[\boldsymbol{x}^*(\boldsymbol{\vartheta}); \boldsymbol{\vartheta}]$; while the desirability score of setting $\boldsymbol{x} = \boldsymbol{x}^*(\boldsymbol{\theta})$ would be $D[\boldsymbol{x}^*(\boldsymbol{\theta}); \boldsymbol{\vartheta}]$. Hence, $\frac{D[\boldsymbol{x}^*(\boldsymbol{\theta}); \boldsymbol{\vartheta}]}{D[\boldsymbol{x}^*(\boldsymbol{\vartheta}); \boldsymbol{\vartheta}]}$ could be used to represent the efficiency of setting $\boldsymbol{x} = \boldsymbol{x}^*(\boldsymbol{\theta})$ when the 'true' scale parameter value is $\boldsymbol{\vartheta}$. By integrating this efficiency over all the possible values of $\boldsymbol{\vartheta} \in \Theta$, one can obtain the overall efficiency score of setting $\boldsymbol{x} = \boldsymbol{x}^*(\boldsymbol{\theta})$. Hence, we propose the following definition to select the robust scale parameter value for a desirability function.

Definition 4 ***(robust scale parameter value of desirability function)*** *For the maximization of a desirability function $D(\boldsymbol{x}; \boldsymbol{\theta})$ with design variable $\boldsymbol{x} \in \mathcal{X}$ and uncertain scale parameter $\boldsymbol{\theta} \in \Theta$, denote the optimal solution for a specific choice of $\boldsymbol{\theta}$ as $\boldsymbol{x}^*(\boldsymbol{\theta}) := argmax_{\boldsymbol{x}} D(\boldsymbol{x}; \boldsymbol{\theta})$. A scale parameter choice $\boldsymbol{\theta}^*$ is called the robust scale parameter value of desirability function $D(\boldsymbol{x}; \boldsymbol{\theta})$, if it is the global maximum solution of the following problem:*

$$\begin{aligned} &\textit{Maximize} \quad \int_{\boldsymbol{\vartheta} \in \Theta} \frac{D[\boldsymbol{x}^*(\boldsymbol{\theta}); \boldsymbol{\vartheta}]}{D[\boldsymbol{x}^*(\boldsymbol{\vartheta}); \boldsymbol{\vartheta}]} d\boldsymbol{\vartheta} \\ &\textit{subject to} \quad \boldsymbol{\theta} \in \Theta \end{aligned}$$

And the corresponding solution $\boldsymbol{x}^*(\boldsymbol{\theta}^*)$ is called a robust optimal solution.

By using this robustness definition, one can select a scale parameter and obtain the corresponding robust optimal solution without depending on subjective and qualitative information. Nonetheless, to obtain the robust choice of the scale parameter value, we need to optimize the computer model under every scale parameter choice $\boldsymbol{\theta} \in \Theta$. In such cases, an integrated and efficient solution to optimizing the time-consuming computer model repeatedly with many different scale parameter settings would be very helpful. Such a solution would make the desirability function method more appealing to the practitioners who have trouble selecting the scale parameter value based on qualitative information.

5.3 Methodology

In this section, we first formally define the computer model based engineering optimization optimization problem with uncertain parameters in the objective function. Thereafter, we introduce a metamodeling method for optimizing stochastic computer models when the uncertain parameters in the objective function are fixed. However, this method would require one to refit the metamodel every time the values of the uncertain parameters are changed, which is time-consuming and unstable. Following that, we propose an alternative solution that provides a smooth prediction of the objective function surface over both the design variables and uncertain parameters spaces.

5.3.1 Engineering optimization under uncertain objective function

In engineering optimization problems, stochastic computer models are often constructed based on technical knowledge of how the engineering system operates. We consider a stochastic computer model that accepts a fixed design variable vector $\boldsymbol{x} = (x_1, \cdots, x_k)^T \in \mathcal{X} \subset \mathbb{R}^k$, a random system fluctuation vector $\boldsymbol{\xi}$, and returns a random output vector $\boldsymbol{Y}(\boldsymbol{x}, \boldsymbol{\xi}) \in \mathbb{R}^p$. For optimization purpose,

the objective function with uncertain parameter $\boldsymbol{\theta}$ can be defined as

$$R(\boldsymbol{x};\boldsymbol{\theta}) = E_{\boldsymbol{Y}}\{J[\boldsymbol{Y}(\boldsymbol{x},\boldsymbol{\xi}),\boldsymbol{x};\boldsymbol{\theta}]\} \tag{5.5}$$

where $\boldsymbol{\theta} \in \Theta \subset \mathbb{R}^q$, $J : \mathbb{R}^p \times \mathcal{X} \times \Theta \to \mathbb{R}$ is a real valued objective function, which measures the system performance and $E_{\boldsymbol{Y}}$ is the expectation operator with respect to the randomness in $\boldsymbol{Y}(\boldsymbol{x},\boldsymbol{\xi})$ (induced by randomness in $\boldsymbol{\xi}$). The optimization problem(for simplicity, minimization is taken to be the standard) depending on $\boldsymbol{\theta}$ is then

$$\text{minimize } R(\boldsymbol{x};\boldsymbol{\theta}) \text{ over all } \boldsymbol{x} \in \mathcal{X} \tag{5.6}$$

When dealing with this uncertainty problem, the current development of stochastic computer models mainly focuses on pushing the uncertainty out of sight through replacing the uncertain parameter $\boldsymbol{\theta}$ by some particular estimate $\hat{\boldsymbol{\theta}}$, and solving a single optimization problem

$$\text{minimize } R(\boldsymbol{x};\hat{\boldsymbol{\theta}}) \text{ over all } \boldsymbol{x} \in \mathcal{X} \tag{5.7}$$

By doing this, the inferential procedure for other choices of $\boldsymbol{\theta} \in \Theta$ is simply disregarded.

As argued in Section 5.2, capturing the uncertainty in $\boldsymbol{\theta}$ is of great importance to make a rational and reliable decision. Therefore, in this work we would regard this as a family of problems where for each different $\boldsymbol{\theta} \in \Theta$, it yields an optimal value

$$\boldsymbol{x}^*(\boldsymbol{\theta}) := \text{argmin}_{\boldsymbol{x}} R(\boldsymbol{x};\boldsymbol{\theta}) \tag{5.8}$$

which needs to be analyzed in its dependence on $\boldsymbol{\theta}$.

5.3.2 Metamodel-based optimization under a fixed objective function

Frequently, computer codes of simulating an engineering system are very time-consuming to run. Consequently, a practically appealing approach is to approximate the computer model by a more computationally efficient metamodel. A metamodel-based optimization strategy requires one to first identify a metamodel form, then design an experiment to collect data by running the expensive computer code, and finally fit and optimize the metamodel (Barton and Meckesheimer (2006)). Metamodels can be built using many regression models with a variety of prediction power. For example, simple linear regression is easy to built and has been used widely. Although simple, this model lacks the ability to model complicated surfaces. By using more sophisticated methods such as Gaussian Process models or radial basis function (RBF) models, one can achieve better prediction. RBF models using simple spline functions can be fit efficiently. They are also applicable to problems with high dimensional design variable space since generally few restrictions are imposed on the location of sample points. In this section, we focus on using the RBF metamodel to predict and optimize the stochastic computer model under a fixed objective function.

Suppose an experiment with n design points $\mathcal{D} = \{\boldsymbol{x}_1, \cdots, \boldsymbol{x}_n\}$ is chosen, and M independent replicates have been obtained from running the computer model at each design point. Denote the data from the experiment by $S_n = \{\boldsymbol{y}_i = [\boldsymbol{y}_1(\boldsymbol{x}_i, \boldsymbol{\xi}), \cdots, \boldsymbol{y}_M(\boldsymbol{x}_i, \boldsymbol{\xi})]'\}_{i=1}^n$. A standard approach to optimizing the objective function $R(\boldsymbol{x}_i, \boldsymbol{\theta})$ Equation (5.5) for predetermined $\boldsymbol{\theta}$ is to first estimate $R(\boldsymbol{x}_i, \boldsymbol{\theta})$ with output observations $\boldsymbol{y_i}$ using some estimator $\widetilde{R}(\boldsymbol{x}_i, \boldsymbol{\theta}) = g(\boldsymbol{y_i})$, then fit an RBF regression model with the control-response data pairs $\{(\boldsymbol{x}_1, \widetilde{R}_1), \cdots, (\boldsymbol{x}_n, \widetilde{R}_n)\}$. Thereafter, the fitted RBF metamodel can be used to predict $R(\boldsymbol{x}, \boldsymbol{\theta})$ for all $\boldsymbol{x} \in \mathcal{X}$ for a predetermined $\boldsymbol{\theta}$, and the problem of optimizing the computer model is transformed to optimizing the RBF metamodel.

A straightforward estimator of $R(\boldsymbol{x}_i, \boldsymbol{\theta})$ would be

$$\widetilde{R}(\boldsymbol{x}_i, \boldsymbol{\theta}) = \sum_{j=1}^{M} J[\boldsymbol{y}_j(\boldsymbol{x}_i, \boldsymbol{\xi}), \boldsymbol{x}_i, \boldsymbol{\theta}]/M \tag{5.9}$$

For simplicity of notation, we use $\widetilde{R}(\boldsymbol{x}_i, \boldsymbol{\theta})$ and $\widetilde{R}_i$ interchangeably. Although averaging over the replicated observations $\boldsymbol{y}_j(\boldsymbol{x}_i, \boldsymbol{\xi})$ reduces the random error in $\widetilde{R}(\boldsymbol{x}_i, \boldsymbol{\theta})$, it is still a noisy version of the true value of $R(\boldsymbol{x}_i, \boldsymbol{\theta})$. Therefore, we include a nugget parameter in the RBF metamodel to mitigate overfitting. An advantage of such a treatment is that the regression form is not restricted to situations where random errors associated with $\widetilde{R}_i, i = 1, \cdots, n$ are independent and identically distributed.

Now we introduce the RBF metamodel form which was extensively studied by Buhmann (2003). This RBF model approximates the unknown function with a linear combination of positive definite kernels and takes the forms of

$$\hat{R}(\boldsymbol{x}, \boldsymbol{\theta}) = \mu + \sum_{i=1}^{n} \beta_i \phi(\boldsymbol{x} - \boldsymbol{x}_i) \tag{5.10}$$

where $\hat{R}(\boldsymbol{x}, \boldsymbol{\theta})$ is the predicted objective value for any $\boldsymbol{x} \in \mathcal{X}$ and $\phi(\cdot)$ is a kernel basis function. Many choices of $\phi(\cdot)$ are available, and examples include multiquadrics, thin plate splines, cubic splines, Gaussian, and inverse multiquadrics. A difficulty with the widely used Gaussian basis function is that the kernel/correlation matrix can often be close to singular, which induces a lot of computational problems. Hence, in this article, we adopt

$$\phi(\boldsymbol{x} - \boldsymbol{z}) = \prod_{j=1}^{k} \exp[-|x_j - z_j|/\gamma_j](|x_j - z_j|/\gamma_j + 1) \tag{5.11}$$

which is a member of the class of Matern correlation functions(Santner et al. (2013)). Note that some authors (Fasshauer and McCourt (2015), page 41) reserve the term RBF for basis functions ϕ that depend on $(\boldsymbol{x} - \boldsymbol{z})$ only through $||\boldsymbol{x} - \boldsymbol{z}||$, and use the term kernel for more general bases that depend on the translates $(\boldsymbol{x} - \boldsymbol{z})$. However, we follow the convention of Buhmann (2003) (page

4) and call Equation (5.11) a radial basis function as well. This basis function avoids numerical difficulties commonly encountered with the Gaussian RBF. It is twice continuously differentiable, but not three times continuously differentiable. Define $\boldsymbol{\beta} = (\beta_1, \cdots, \beta_n)'$, $\boldsymbol{\gamma} = (\gamma_1, \cdots, \gamma_k)'$, $(\boldsymbol{B})_{ij} = \phi(\boldsymbol{x}_i - \boldsymbol{x}_j)$, and $\widetilde{\boldsymbol{R}} = (\widetilde{R}_1, \cdots, \widetilde{R}_n)'$. Then, given $\mu, \boldsymbol{\gamma}$, and the nugget $\lambda > 0$, the vector $\boldsymbol{\beta}$ is determined by solving the linear equations

$$(\boldsymbol{B} + \lambda \boldsymbol{I})\boldsymbol{\beta} = \widetilde{\boldsymbol{R}} - \mu \mathbf{1} \tag{5.12}$$

where $\boldsymbol{I}$ is a $n \times n$ identity matrix.

This RBF model is mathematically equivalent to the posterior mean of a Gaussian Process (GP) with correlation function *Equation* (5.11). Therefore, the correlation length parameters $\boldsymbol{\gamma}$ determine the degree of influence of each observation on the prediction $\hat{R}(\boldsymbol{x}, \boldsymbol{\theta})$: with short correlation length, the prediction at $\boldsymbol{x}$ depends more strongly on nearby observations and weakly on far away observations. And the above system of equations Equation (5.12) for determining $\boldsymbol{\beta}$ with a nugget parameter is similar in spirit with the GP with independent and identically distributed normal errors with unknown variance. Note that if $\lambda = 0$, the coefficients $\boldsymbol{\beta}$ given by Equation (5.12) will make Equation (5.10) interpolate the data $\{(\boldsymbol{x}_1, \widetilde{R}_1), \cdots, (\boldsymbol{x}_n, \widetilde{R}_n)\}$. .

To determine $\mu, \lambda, \boldsymbol{\gamma}$, a common way is to set $\mu = \sum_{i=1}^{n} \widetilde{R}_i/n$ and choose $\boldsymbol{\gamma}, \lambda$ using leave-one-out (LOO) crossed validation. Specifically, let

$$\widetilde{\boldsymbol{R}}_{-i} = (\widetilde{R}_1, \cdots, \widetilde{R}_{i-1}, \widetilde{R}_{i+1}, \cdots, \widetilde{R}_n)' \tag{5.13}$$

Then, the predicted value of the response variable at $\boldsymbol{x}_i$ using the LOO data $\widetilde{\boldsymbol{R}}_{-i}$ is $\hat{R}(\boldsymbol{x}_i, \boldsymbol{\theta})|\widetilde{\boldsymbol{R}}_{-i}$, with prediction error $e_i = \widetilde{R}_i - \hat{R}(\boldsymbol{x}_i, \boldsymbol{\theta})|\widetilde{\boldsymbol{R}}_{-i}$. Then the optimal value of λ and $\boldsymbol{\gamma}$ can be obtained by minimizing the mean square prediction error:

$$E_{LOO} = \sum_{i=1}^{n} e_i^2/n \tag{5.14}$$

The advantage of LOO for linear models such as RBF regression is that the error vector $\boldsymbol{e} = (e_1, \cdots, e_n)'$ can be calculated analytically as (see Tan (2015) for proof)

$$\boldsymbol{e} = \text{diag}\{(\boldsymbol{B} + \lambda \boldsymbol{I})^{-1}\}^{-1}(\boldsymbol{B} + \lambda \boldsymbol{I})^{-1}(\tilde{\boldsymbol{R}} - \mu \boldsymbol{1}) \tag{5.15}$$

This shortcut formula saves substantial computation time over a brute force approach to compute the error vector $\boldsymbol{e}$.

As mentioned, the decision made by using only one predetermined estimate of $\boldsymbol{\theta}$ would result in unforeseeable risk, hence solving the optimization problem under a set of candidate values $\boldsymbol{\theta}_1, \cdots, \boldsymbol{\theta}_K$ would be desired. In such cases, one has to refit the RBF metamodel Equation (5.10) K times. The calculation of $(\boldsymbol{B} + \lambda \boldsymbol{I})^{-1}$ in Equation (5.15) would take $O(n^3)$ arithmetic operations (see O'Leary (2009) Page 70), and hence the fitting of each $\hat{R}(\cdot, \boldsymbol{\theta}_i)$ would take $O(n^3)$ arithmetic operations. Thus, fitting/estimation of all $\hat{R}(\cdot, \boldsymbol{\theta}_1), \cdots, \hat{R}(\cdot, \boldsymbol{\theta}_K)$ would take $O(Kn^3)$ arithmetic operations. For purposes such as calculating the Pareto front, conducting sensitivity analysis or obtaining the robust scale parameter using Definition 4, the required RBF model fitting times could be quite large because K can be very large. Moreover, even if the investigator has the required computational budgets to fit the K RBF models, the predicted value of $\hat{R}(\bar{\boldsymbol{x}}, \boldsymbol{\theta})$ at a fixed design point $\bar{\boldsymbol{x}}$ could possibly be discontinuous over $\boldsymbol{\theta}$. One reason is the existence of many possible local optimizers of function Equation (5.14) when estimating λ and $\boldsymbol{\gamma}$, which is an inevitable problem for fitting RBF and GP model with the current development of these models.

5.3.3 Metamodel-based optimization under uncertain objective function

To capture the uncertainty in $\boldsymbol{\theta}$ in a more efficient way, we now propose a fast fitting solution based on the unique model structure of RBF. The fact that the RBF metamodel is linear in the vector of response data allows us to use the shortcut formula Equation (5.15) to calculate the leave-one-out crossed validation

error. Furthermore, the model form of RBF metamodel is characterized by *separability*: the RBF is a product of functions that each depends on an input variable. This *separability* structure enables the use of a fast matrix inversion formula for calculating $(\boldsymbol{B} + \lambda \boldsymbol{I})^{-1}$ if the design space is a Cartesian product. This fact motivates us to collect data using a Cartesian product design in the $(\boldsymbol{x}, \boldsymbol{\theta})$ space: $\Omega = \{(\boldsymbol{x}_1, \boldsymbol{\theta}_1), \cdots, (\boldsymbol{x}_N, \boldsymbol{\theta}_N)\} \subset \mathcal{X} \times \Theta$. The obtained data can then be used to fit an RBF model for predicting the objective function value over both the space of $\boldsymbol{x}$ and the space of $\boldsymbol{\theta}$. In this way, we can not only reduce the computational burden of fitting the RBF model many times, but also provide a smooth prediction surface of $\hat{R}(\bar{\boldsymbol{x}}, \boldsymbol{\theta})$ over the space of $\boldsymbol{\theta}$ for a fixed design point $\bar{\boldsymbol{x}}$.

Now we describe the design and model fitting strategies in detail. Suppose we use a Cartesian product design

$$\begin{aligned}
\widetilde{\mathcal{D}} &= \{\boldsymbol{x}_1, \cdots, \boldsymbol{x}_n\} \times \{\boldsymbol{\theta}_1, \cdots, \boldsymbol{\theta}_m\} \\
&= \{(\boldsymbol{x}_1, \boldsymbol{\theta}_1), \cdots, (\boldsymbol{x}_1, \boldsymbol{\theta}_m), \cdots, (\boldsymbol{x}_n, \boldsymbol{\theta}_1), \cdots, (\boldsymbol{x}_n, \boldsymbol{\theta}_m)\} \\
&:= \{\boldsymbol{d}_1, \cdots, \boldsymbol{d}_N\}
\end{aligned} \tag{5.16}$$

with $\boldsymbol{d} = (\boldsymbol{x}, \boldsymbol{\theta}) = (x_1, \cdots, x_k, \theta_1, \cdots, \theta_q) = (d_1, \cdots, d_{k+q})$ and $N = n \times m$. Assuming that computer model output data $S_n = \{\boldsymbol{y} = [\boldsymbol{y}_1(\boldsymbol{x}_v, \boldsymbol{\xi}), \cdots, \boldsymbol{y}_M(\boldsymbol{x}_v, \boldsymbol{\xi})]'\}_{v=1}^{n}$ is collected from running the stochastic simulator, we can obtain estimates of $R(\boldsymbol{d}_i)$ for all $\boldsymbol{d}_i \in \widetilde{\mathcal{D}}, i = 1, \cdots, N$ using

$$\widetilde{R}(\boldsymbol{d}_i) = \widetilde{R}(\boldsymbol{x}_v, \boldsymbol{\theta}_l) = \sum_{j=1}^{M} J[\boldsymbol{y}_j(\boldsymbol{x}_v, \boldsymbol{\xi}), \boldsymbol{x}_v, \boldsymbol{\theta}_l]/M \tag{5.17}$$

for $v = 1, \cdots, n, l = 1, \cdots, m$. We emphasize that this estimator is based on the same data as the estimator in Equation (5.9), i.e., no additional computer model runs are needed to estimate the objective function as its parameter vector

$\boldsymbol{\theta}$ varies. Then, the RBF model

$$\begin{aligned}\hat{R}(\boldsymbol{x},\boldsymbol{\theta}) = \hat{R}(\boldsymbol{d}) &= \mu + \sum_{i=1}^{N}\beta_i \prod_{e=1}^{k+q}\exp[-|d_e - d_{ie}|/\gamma_e](|d_e - d_{ie}|/\gamma_e + 1) \\ &= \mu + \sum_{i=1}^{N}\beta_i \prod_{v=1}^{k}\exp[-|x_v - x_{iv}|/\gamma_v](|x_v - x_{iv}|/\gamma_v + 1) \\ &\quad \times \prod_{l=1}^{q}\exp[-|\theta_l - \theta_{il}|/\gamma_{k+l}](|\theta_l - \theta_{il}|/\gamma_{k+l} + 1) \quad (5.18)\end{aligned}$$

is used to construct a predictor of $R(\boldsymbol{x},\boldsymbol{\theta})$ for all $(\boldsymbol{x},\boldsymbol{\theta}) \in \mathcal{X} \times \Theta$, , where x_{iv} is the v_{th} component of $\boldsymbol{x}_i$ and θ_{il} is the l_{th} component of $\boldsymbol{\theta}_i$.

Since $\widetilde{\mathcal{D}}$ in Equation (5.16) is of a Cartesian product design, an algorithm reducing the number of arithmetic operations to fit the RBF model Equation (5.18) can be obtained. Specifically, for design Equation (5.16), it is easy to verify that

$$\boldsymbol{B} + \lambda \boldsymbol{I}_N = \boldsymbol{B}_1 \otimes \boldsymbol{B}_2 + \lambda \boldsymbol{I}_N \quad (5.19)$$

where $\boldsymbol{I}_N$ is $N \times N$ identity matrix, $(\boldsymbol{B})_{ij} = \phi(\boldsymbol{d}_i - \boldsymbol{d}_j)$, $(\boldsymbol{B}_1)_{ij} = \phi(\boldsymbol{x}_i - \boldsymbol{x}_j)$, and $(\boldsymbol{B}_2)_{ij} = \phi(\boldsymbol{\theta}_i - \boldsymbol{\theta}_j)$.

Based on Equation (5.19), we derive a computationally convenient formula for $(\boldsymbol{B} + \lambda \boldsymbol{I}_N)^{-1}$ used in Equation (5.12) and Equation (5.15) when fitting the RBF model. Since $\boldsymbol{B}_1$ and $\boldsymbol{B}_2$ are positive semi-definite matrices, their eigen-decompositions can be denoted by $\boldsymbol{E}_1\boldsymbol{L}_1\boldsymbol{E}_1^T$ and $\boldsymbol{E}_2\boldsymbol{L}_2\boldsymbol{E}_2^T$ respectively, where $\boldsymbol{E}_1^{-1} = \boldsymbol{E}_1^T$ and $\boldsymbol{E}_2^{-1} = \boldsymbol{E}_2^T$. Here, $\boldsymbol{E}_1, \boldsymbol{E}_2$ are the matrices of orthogonal eigenvectors and $\boldsymbol{L}_1, \boldsymbol{L}_2$ are the diagonal matrices of the corresponding eigenvalues. Note that

$$\begin{aligned}\boldsymbol{B}_1 \otimes \boldsymbol{B}_2 + \lambda \boldsymbol{I}_N &= (\boldsymbol{E}_1\boldsymbol{L}_1\boldsymbol{E}_1^T) \otimes (\boldsymbol{E}_2\boldsymbol{L}_2\boldsymbol{E}_2^T) + \lambda \boldsymbol{E}_1\boldsymbol{E}_1^T \otimes \boldsymbol{E}_2\boldsymbol{E}_2^T \\ &= (\boldsymbol{E}_1 \otimes \boldsymbol{E}_2)(\boldsymbol{L}_1 \otimes \boldsymbol{L}_2)(\boldsymbol{E}_1^T \otimes \boldsymbol{E}_2^T) + \lambda(\boldsymbol{E}_1 \otimes \boldsymbol{E}_2)(\boldsymbol{E}_1^T \otimes \boldsymbol{E}_2^T) \\ &= (\boldsymbol{E}_1 \otimes \boldsymbol{E}_2)(\boldsymbol{L}_1 \otimes \boldsymbol{L}_2 + \lambda \boldsymbol{I}_N)(\boldsymbol{E}_1^T \otimes \boldsymbol{E}_2^T)\end{aligned} \quad (5.20)$$

Since $(\boldsymbol{E}_1 \otimes \boldsymbol{E}_2)^{-1} = (\boldsymbol{E}_1^T \otimes \boldsymbol{E}_2^T)$, it is seen that $(\boldsymbol{B} + \lambda \boldsymbol{I}_N)^{-1}$ is given by the formula

$$(\boldsymbol{B} + \lambda \boldsymbol{I}_N)^{-1} = (\boldsymbol{E}_1 \otimes \boldsymbol{E}_2)(\boldsymbol{L}_1 \otimes \boldsymbol{L}_2 + \lambda \boldsymbol{I}_N)^{-1}(\boldsymbol{E}_1^T \otimes \boldsymbol{E}_2^T) \tag{5.21}$$

Denote $\boldsymbol{L}_1 = \text{diag}\{L_{11}, \cdots, L_{1n}\}$ and $\boldsymbol{L}_2 = \text{diag}\{L_{21}, \cdots, L_{2m}\}$. Then note that

$$(\boldsymbol{L}_1 \otimes \boldsymbol{L}_2 + \lambda \boldsymbol{I}_N)^{-1} = \text{diag}\{(\lambda + L_{11}L_{21})^{-1}, \cdots, (\lambda + L_{1n}L_{2m})^{-1}\} \tag{5.22}$$

Thus, if the number of arithmetic operations to obtain the eigendecompositions of $\boldsymbol{B}_1$ and $\boldsymbol{B}_2$ are $O(n^3)$ and $O(m^3)$ respectively (see O'Leary (2009) Page 70), by using the derived formula Equation (5.21), we can compute $(\boldsymbol{B} + \lambda \boldsymbol{I}_N)^{-1}(\widetilde{\boldsymbol{R}} - \mu \boldsymbol{1})$ with $O(n^3 + m^3 + n^2m^2)$ arithmetic operations. On the contrary, we would need $O(N^3) = O(n^3m^3)$ arithmetic operations to compute $(\boldsymbol{B} + \lambda \boldsymbol{I}_N)^{-1}(\widetilde{\boldsymbol{R}} - \mu \boldsymbol{1})$ directly.

As a summary, we list the fitting procedures of RBF models in the following Algorithm

---

Fast fitting of RBF models

Input: $\widetilde{R}(\boldsymbol{d}_i), i = 1, \cdots, N$

Procedure:

Step 1. Setting $\mu = \sum_{i=1}^n \widetilde{R}_i / N$.

Step 2. Choose $\boldsymbol{\gamma}, \lambda$ by minimizing the mean square LOO prediction error in Equation (5.14), with the error vector calculated by Equation (5.15) and Equation (5.21).

Step 3. Calculate $\boldsymbol{\beta}$ from $\boldsymbol{\beta} = (\boldsymbol{B} + \lambda \boldsymbol{I})^{-1}(\widetilde{\boldsymbol{R}} - \mu \boldsymbol{1})$, where calculation of $(\boldsymbol{B} + \lambda \boldsymbol{I})^{-1}$ follows Equation (5.21).

After fitting the RBF model, predictions of $R(\boldsymbol{x}, \boldsymbol{\theta})$ for all $(\boldsymbol{x}, \boldsymbol{\theta}) \in \mathcal{X} \times \Theta$ can be made through equation Equation (5.18). And based on the predictions $\hat{R}(\boldsymbol{x}, \boldsymbol{\theta})$,

the optimal solution $\boldsymbol{x}^*(\boldsymbol{\theta})$ optimizing

$$\hat{R}(\boldsymbol{x};\boldsymbol{\theta}) \text{ over all } \boldsymbol{x} \in \mathcal{X} \text{ for any } \boldsymbol{\theta} \in \Theta \tag{5.23}$$

can be obtained through equation Equation (5.8).

Denote the scalar statistics of interest as $\hat{\Upsilon}$ (for example, $\hat{R}(\boldsymbol{x},\boldsymbol{\theta})$ in Equation (5.18) or the components of $\boldsymbol{x}^*(\boldsymbol{\theta})$ in equation Equation (5.8)). To measure the uncertainty associated with $\hat{\Upsilon}$, approximate confidence intervals can be constructed via the following bootstrap procedure

---

Constructing confidence intervals via Bootstrap

Input: $S_n = \{\boldsymbol{y} = [\boldsymbol{y}_1(\boldsymbol{x}_i), \cdots, \boldsymbol{y}_M(\boldsymbol{x}_i)]'\}_{i=1}^n$

Procedure:

Step 1. Estimate $\hat{\Upsilon}$ based on S_n.

Step 2. Generate an empirical bootstrap sample, by taking random samples with replacement from S_n as : $S_n^* = \{\boldsymbol{y}^{*r} = [\boldsymbol{y}_1^*(\boldsymbol{x}_i,\boldsymbol{\xi}), \cdots, \boldsymbol{y}_M^*(\boldsymbol{x}_i,\boldsymbol{\xi})]'\}_{i=1}^n$

Step 3. Estimate Υ based on S_n^*, and denote the estimator as $\hat{\Upsilon}^*$. Repeat *Step 2* and *Step 3* B^* times.

Step 4. Compute the bootstrap differences $\delta^* = \hat{\Upsilon}^* - \hat{\Upsilon}$. Put these B^* values in order and pick out the 0.975 and 0.025 critical values. Set these values as $\delta^*_{.975}$ and $\delta^*_{.025}$.

Step 5. The estimated 95% bootstrap confidence interval for $\hat{\Upsilon}$ is: $[\hat{\Upsilon} + \delta^*_{.025}, \hat{\Upsilon} + \delta^*_{.975}]$

5.4 Illustration example: design of drug delivery system

5.4.1 A computer model of drug release from polymer matrix devices

With the constantly upgraded computing power, computer models have recently been used extensively to understand the drug release process from poly-

meric devices or Drug-Eluting Stents, see Pant et al. (2011); Ferreira et al. (2012); Groh et al. (2014); Bozsak et al. (2015). Optimizing the drug release process generally involves many conflicting goals: maximizing the drug therapy effect, minimizing the side effect and minimizing the cost of the drug, etc. For example, Pant et al. (2011); Bozsak et al. (2015) reported their pioneering attempts at including multiple design objectives for optimizing the design of Drug-eluting stents, where a sufficiently high drug concentrations in smooth muscle cells and low drug concentration at the endothelial cell surface are to be achieved simultaneously.

To demonstrate the application of our approach, we use the design and

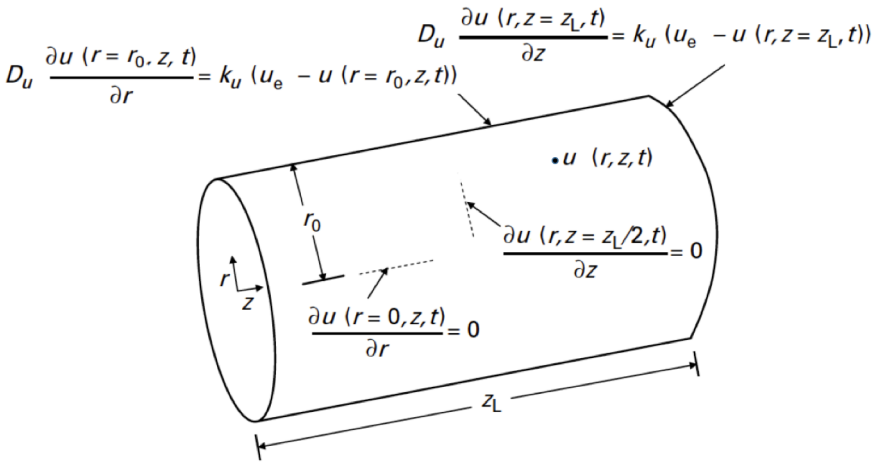

Figure 5.1: Diagram of a drug diffusion system

modeling of drug release from a polymer matrix (Schiesser (2012) page 340) as a test example. The schematic of the drug release stochastic computer model is represented in Figure Equation (5.1) as a polymer matrix (PM), where the PM radius is r_0 (cm), and PM length is z_L (cm). A certain amount of drug is initially administered in the PM, the modeling problem is then to determine how fast the drug will leave the PM and enter the surrounding tissue treated by the drug. Within the PM, the movement of the drug is modeled by diffusion equations, and the transfer rate to the surrounding tissue is described by a mass transfer coefficient. The partial differential equation describing the diffusion in

cylindrical coordinates (r, z, φ) is given by

$$\frac{\partial u}{\partial t} = D_u\left(\frac{\partial^2 u}{\partial r^2} + \frac{1}{r}\frac{\partial u}{\partial r} + \frac{1}{r^2}\frac{\partial^2 u}{\partial \varphi^2} + \frac{\partial^2 u}{\partial z^2}\right) \tag{5.24}$$

Here, $u = u(r, z, \varphi, t)$ is the drug concentration at location (r, z, φ) after a release time of t, and D_u is the drug diffusivity which is a specified constant.

Assuming a uniform external drug concentration, the system in Equation (5.24) is symmetric in φ, so the angular term in Equation (5.24) is dropped. This gives $u = u(r, z, t)$ and

$$\frac{\partial u}{\partial t} = D_u\left(\frac{\partial^2 u}{\partial r^2} + \frac{1}{r}\frac{\partial u}{\partial r} + \frac{\partial^2 u}{\partial z^2}\right) \tag{5.25}$$

Equation Equation (5.25) is first order in t and second order in r and z. Thus, one initial condition (IC) in t and two boundary conditions (BCs) in r and z are required. The IC is:

$$u(r, z, t = 0) = u_0 \tag{5.26}$$

where u_0 is specified constant and represents the initial values of u.

The homogeneous Neumann BC (Schiesser (2012) page 113) for equation Equation (5.25) at $r = 0$ is used to specify symmetry in r:

$$\frac{\partial u(r = 0, z, t)}{\partial r} = 0 \tag{5.27}$$

and the BC at the exterior surface $r = r_0$ is based on mass transfer coefficients k_u:

$$D_u\frac{\partial u(r = r_0, z, t)}{\partial r} = k_u(u_e - u(r = r_0, z, t)) \tag{5.28}$$

where u_e is the external concentration of drug subject to random fluctuation. This equation equate the mass fluxes at the polymer surface $r = r_0$ to the fluxes due to concentration differences at $r = r_0$. Similarly, the BC reflect symmetry

in z and the BC at $z = z_L$ specify the fluxes in the bottom of the polymer:

$$
\begin{aligned}
D_u \frac{\partial u(r, z = z_L/2, t)}{\partial z} &= 0 \\
D_u \frac{\partial u(r, z = z_L, t)}{\partial z} &= k_u(u_e - u(r, z = z_L, t))
\end{aligned}
\tag{5.29}
$$

Equations Equation (5.25) to Equation (5.29) constitute equations of the computer model in the system of Figure Equation (5.1). These partial differential equations(PDEs) are solved by the method of lines (MOL), which proceeds by first discretizing the spatial derivatives and leaving the time variable continuous. This leads to a system of ordinary differential equations (ODEs) to which a numerical method can be applied. In this problem, the PDEs are solved by discretizing r to 11 grid points over the value $0 \leqslant r \leqslant r_0$ and z to 11 grid points over the value $0 \leqslant z \leqslant z_L$. In other words, a system of 11×11 ODEs that approximates the PDE are used. More detailed description of the computer model can be found in Schiesser (2012) page 340.

To conclude the description of this stochastic computer model, we summarize the model design variable, output variable, random fluctuation variable, and the constants in Table Equation (5.1). The value of these variables and parameters are specified following Schiesser (2012) page 340. Note that for concentrations, normalized values $0 \leqslant u(r, z, t), u_0, u_e \leqslant 1$ are used to facilitates their interpretation (e.g., their departure from one). The variable u_e is the exterior drug concentration value which represents the remaining drug concentration

Table 5.1: Summary of the variables and parameters of the drug release stochastic computer model

Variable, parameter	Interpretation
$u(r, z, t) \in [0, 1]$	drug concentration at time t and location (r, z)
$r_0 \in [0.5, 1.5]$	PM radius (cm)
$u_e \sim$ unif $(0, 0.5)$	exterior drug concentration value (normalized)
$z_L = 2$	PM length (cm)
$u_0 = 1$	initial drug concentration value (normalized)
$D_u = 1.0e - 06$	diffusivity (cm^2/ s)
$k_u = 1.0e - 01$	mass transfer coefficient (cm/s)

from the previously administered dose. It is set to be random due to differences in individual patient metabolism.

5.4.2 Objective function for drug design

In this example, we focus on minimizing the cost of drug while keeping the effect of drug therapy close to the desired effect. This joint consideration is typical in drug design (see Lu et al. (1998)). First, the cost of drug is measured by the amount of drug initially administered to the system with $J_1(r_0) = \pi r_0^2 z_L u_0$. Second, the effect of drug therapy is measured by the difference between the desired (target) drug release profile and the actual release profile after $t = 24$ and $t = 48$ hours of the initial drug administration, where the actual total amount of the drug that has released from the PM at t is (see Schiesser (2012) page 340).

$$Q_t(r_0) = \pi r_0^2 z_L u_0 - 2 * 2\pi \int_{z_L/2}^{z_L} \int_0^{r_0} u(r, z, t) r dr dz \tag{5.30}$$

Translating these goals to desirability functions, a smaller-the-better function Equation (5.2) is used for the cost measure with values $A = 0.1$ and $B = 15$

$$d_1^{min}(r_0) = \begin{cases} 0 & \text{if } J_1(r_0) > 15 \\ [\frac{J_1(r_0)-15}{0.1-15}]^{\theta} & \text{if } 0.1 \leqslant J_1(r_0) \leqslant 15 \\ 1 & J_1(r_0) < 0.1 \end{cases} \tag{5.31}$$

for the cost $J_1(r_0)$.

Next, target oriented desirability function Equation (5.3) is used for $Q_{24}(r_0)$ with $A = 1$, $T_0 = 3.5$, $B = 12$, and $Q_{48}(r_0)$ with $A = 1.2$, $T_0 = 9.45$, $B = 13$ as

$$d_2^{target}(r_0) = \begin{cases} [\frac{Q_{24}(r_0)-1}{3.5-1}]^{\theta_{21}} & \text{if } 1 \leqslant Q_{24}(r_0) \leqslant 3.5 \\ [\frac{Q_{24}(r_0)-12}{3.5-12}]^{\theta_{22}} & \text{if } 3.5 \leqslant Q_{24}(r_0) \leqslant 12 \\ 0 & \text{otherwise} \end{cases} \tag{5.32}$$

$$d_3^{target}(r_0) = \begin{cases} [\frac{Q_{48}(r_0)-1.2}{9.45-1.2}]^{\theta_{31}} & \text{if } 1.2 \leqslant Q_{48}(r_0) \leqslant 9.45 \\ [\frac{Q_{48}(r_0)-13}{9.45-13}]^{\theta_{32}} & \text{if } 9.45 \leqslant Q_{48}(r_0) \leqslant 13 \\ 0 & \text{otherwise} \end{cases} \tag{5.33}$$

we can write the overall objective function as

$$J(r_0; \theta, \theta_{21}, \theta_{22}, \theta_{31}, \theta_{32}) = [d_1^{min}(r_0) * d_2^{target}(r_0) * d_3^{target}(r_0)]^{1/3} \tag{5.34}$$

The scale parameters $\theta, \theta_{21}, \theta_{22}, \theta_{31}, \theta_{32}$ are typically uncertain in the above objective function.

5.4.3 Optimization results and discussion

In this section, we describe the computer model and design optimization based on RBF metamodel in detail. The control variable $\boldsymbol{x}$ is the PM radius r_0(cm) in a design space $[0.5, 1.5]$, the model random fluctuation variable $\boldsymbol{\xi}$ is the normalized exterior drug concentration value u_e, which is assumed to be uniformly distributed in $[0, 0.2]$. The model output is the drug concentration $u(r, z, 24)$ and $u(r, z, 48)$ at time $t = 24, 48$h and at position (r, z). For the objective function described in Equation (5.34), we fix $\theta_{21} = 2, \theta_{22} = 1, \theta_{31} = 2, \theta_{32} = 1$ and only treat θ as an uncertain parameter to be adjusted for illustrative purpose. Suppose a 6×6 points Cartesian product design is used over the space of model control variable r_0 and the uncertain parameter θ as

$$\widetilde{\mathcal{D}} = \{0.5, 0.7, 0.9, 1.1, 1.3, 1.5\} \times \{0, 0.6, 1.2, 1.8, 2.4, 3\} \tag{5.35}$$

At each design point of $r_0^v \in \{0.5, 0.7, 0.9, 1.1, 1.3, 1.5\}$, $M = 30$ computer model replications are conducted and the outputs

$$\boldsymbol{y}_j(r_0^v) = (u_j(r, z, 24), u_j(r, z, 48)) | r_0^v, j = 1, \cdots, M \tag{5.36}$$

are obtained for each replication. The sample average of the objective value from the replicates is then computed for each design point $(r_0^v, \theta^l) \in \widetilde{\mathcal{D}}$ as $\widetilde{R}(r_0^v, \theta^l) = \sum_{j=1}^{M} J(\boldsymbol{y}_j(r_0^v), r_0^v, \theta^l)/M$ Using the RBF regression in Equation (5.18) to interpolate the surface of $\widetilde{R}(r_0, \theta)$, we obtain the prediction of $\widetilde{R}(r_0, \theta)$ at all values of $r_0 \in [0.5, 1.5]$ and $\theta \in [0, 3]$.

To check the model fitting efficiency, we compare the model predictions in a larger test design set with the "true value". Specifically, we estimate the "true value" accurately by using the average of $M = 100$ replicates. Figure Equation (5.2) plots the predicted desirability values and the 'true value' versus the grid point number for a 21×21 grid point Cartesian product design over the design space $[0.5, 1.5] \times [0, 3]$. As we can see, the curve of predicted and true value of the desirability is very close to each other, suggesting that the RBF regression model has very good prediction ability.

Then we plot the predicted desirability value surface in Figure Equation (5.3). As can be seen from this plot, using the proposed Cartesian product design and the RBF metamodel, we can predict the smooth surface of the desirability function score in its dependency on both the control variable r_0 and the uncertain scale parameter θ. Based on this prediction, we can conveniently obtain $r_0^*(\theta)$ for any choice of $\theta \in [0, 3]$ through 5.8, while avoiding the burden of

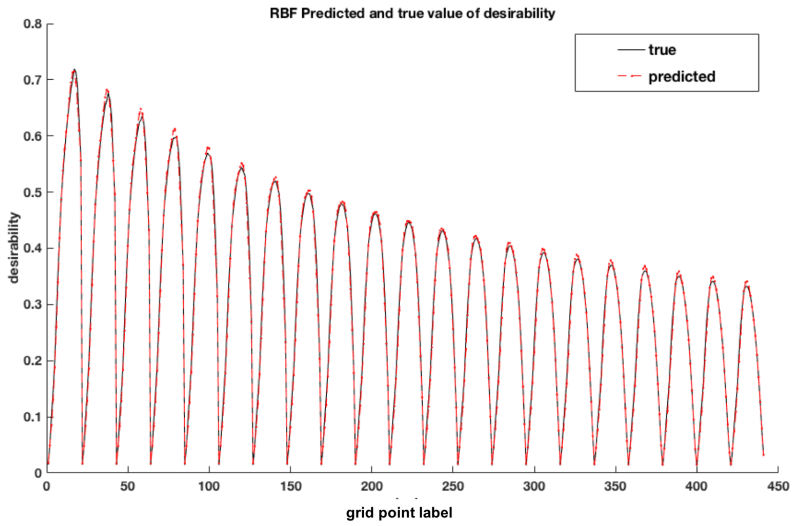

Figure 5.2: RBF predicted versus true desirability value

refitting the RBF metamodel every time θ changes. In Figure Equation (5.4), we plot $r_0^*(\theta)$ for different choices of $\theta \in [0, 3]$, where the black curve is a smoothly changed optimal value curve under different settings of the scale parameter θ. In this plot, the optimal setting r_0^* changes significantly with different values of θ, which supports the argument that it is necessary to analyze the optimal solutions in their dependence on the uncertain objective parameters. In this drug delivery example, θ determines the impact of the cost of the drug on the overall desirability. When multiple optimal solutions are available for different values of θ, high-level information can be used to choose from one of the optimal solutions. For example, if the drug is expensive, the investigator may want to choose a large value for θ to heavily punish high amounts of initial drug $J_1(r_0)$. The calculation shows that all the optimal solution r_0^* fall into the range $[0.99, 1.27]$. If based on experience, r_0 values in the range $[0.9, 1.3]$ are generally acceptable, one can comfortably select a large value of θ without worrying about the potential unsatisfactory treatment effect.

In cases where the qualitative/higher-level information may not be ap-

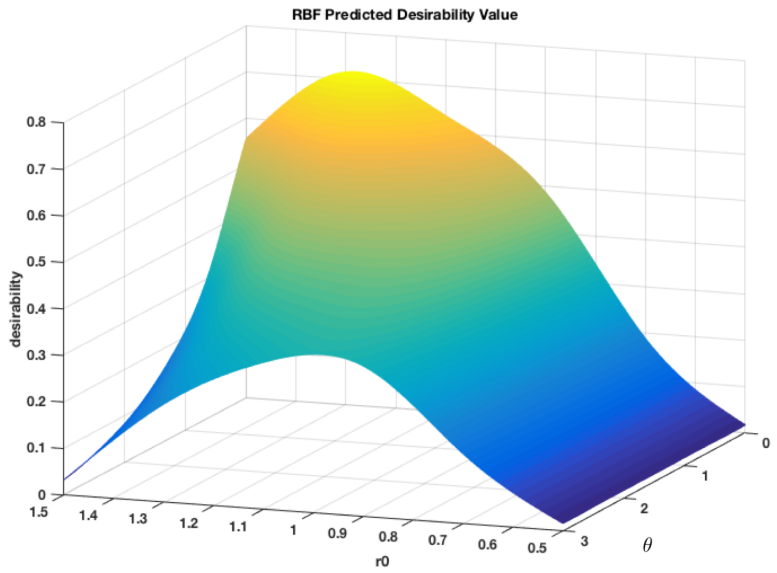

Figure 5.3: Desirability surface

proachable to the investigator, an attractive method is to select the scale parameters using a quantitative procedure. In Definition 4, we proposed such a

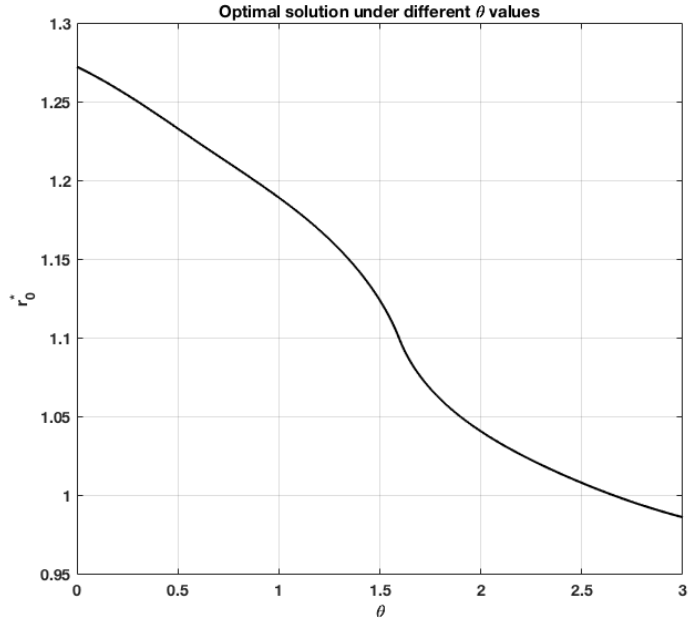

Figure 5.4: Optimal points

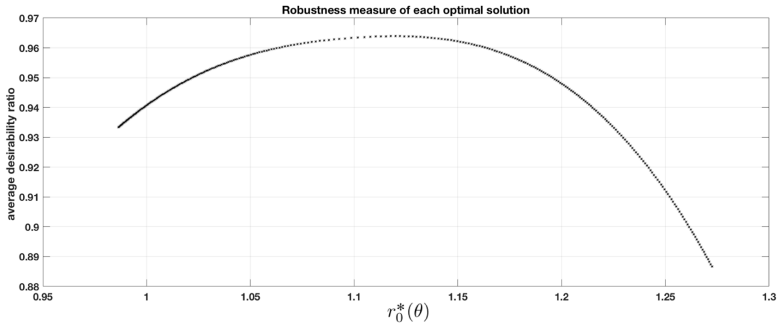

Figure 5.5: Robust measure plot for different r_0^*

solution to select the most "robust" optimal setting r_0^*. Now we illustrate the usefulness of this solution in this practical problem. In figure 5.5, we plot the robust measure $\int_{\boldsymbol{\vartheta}\in\Theta} \frac{D[\boldsymbol{x}^*(\boldsymbol{\theta});\boldsymbol{\vartheta}]}{D[\boldsymbol{x}^*(\boldsymbol{\vartheta});\boldsymbol{\vartheta}]} d\boldsymbol{\vartheta}$ for each optimal setting $r_0^*(\theta)$. The robustness of $r_0^*(\theta)$ reaches its peak at $r_0^*(\theta^*) = 1.1200$ with $\theta^* = 1.52$. Therefore, choosing $\theta^* = 1.52$ as the scale parameter value would produce a robust optimal solution that performs well under other choices of θ. This robust optimal solution can also serve as a compromised solution when there are many different decision makers/patients, and different scale parameter should be used to represent their specific trade-off preference.

5.5 Discussion

In this chapter, we look into metamodel-based optimization of stochastic computer models where the objective functions are uncertain. We presented typical scenarios where the objective function is uncertain and provided the corresponding uncertainty quantification techniques. We leverage on the flexible and efficient radial basis function metamodel, and a novel experimental design approach to model the objective function as a function of both the design factors and the uncertain objective function parameters. By using a design that is a Cartesian product of points in the design variable space and the uncertain parameter space, we developed a fast fitting algorithm to construct the RBF metamodel. These tools provide the system designers more flexibility in making an informed and rational decision than the traditional choice of replacing the uncertain parameter by some estimates.

Although the developed RBF focused on the case where one overall objective function with uncertain parameters is of interest, it can be easily extended for fitting multiple objective functions. For example, in a multi-objective optimization problem, if the manager needs the individual objective function values to guide decision-making, independent metamodels can be used to predict each of the objective functions.

CHAPTER 6

CONCLUSION

This thesis contributes to the modeling of the uncertainties in the engineering optimization problem through regression analysis and experimental design. The main focus of this thesis is the modeling of the inherent uncertainty and the parameter uncertainty in objective function, whereas the modeling uncertainty and parameter uncertainty in inputs of mathematical models are beyond the scope of this thesis.

In this thesis, a multilevel zero-inflated model is first proposed to model the inherent uncertainties in multilevel high-quality manufacturing processes. Thereafter, a Bayesian experiential design framework for reducing the estimation uncertainty of the optimum setting for engineering optimization is proposed. The first two works focus on modeling and reducing the inherent uncertainty in engineering optimization problems. The third work develops a framework for capturing the parameter uncertainty in the objective function of computer models. These three developed methodologies together contribute to the modeling of uncertainties in engineering optimization and robust design decision making.

6.1 Main findings

In the first work, we develop a multilevel zero-inflated model to build the functional relationship between the design factors and the wafer defects with data collected from a multilevel high-quality manufacturing. In this work, the identification of proper distributions for random variables and the estimation of the parameters in these distributions are very important component in the inherent uncertainty analysis. In this model, the excessive zeros are modeled by a random shift between a zero state in which defects are nonexistent and a count state in which defects can occur according to a count distribution. The count state distribution is derived based on the number of hillocks grown and the individual hillock heights. This helps to identify the sources of the inherent uncertainty and provide insights on reducing it. In addition, the wafer level variation is modeled by assuming the mean number of defects for each wafter is itself a random variable with Gamma distribution. The lot level variation is the largest one and shows multi-mode and right-skewed characteristics, hence it is modeled by a semi-nonparametric distribution. Although the count model was derived specifically for capturing the uncertainties and modeling the experiment result of the ICs manufacturing process, the proposed multilevel ZI model can be extended to model other zero inflated data with multilevel structures with non normal random effects distributions. The proposed approximate AGQ-EM algorithm can also be applied to estimate the parameters from these model structures and is especially useful in cases where the random effects are not normal and estimated with a SNP distribution. The identification of proper distributions for random variables in the system and the estimation of the parameters in these distributions are important components in improving the uncertainty analysis of high quality manufacturing processes.

In the second work, a Bayesian optimal design framework is built for collecting data informative on reducing the estimation uncertainty of the optimum point. A Bayesian OP optimality criterion is derived based on expected Shannon information gain (uncertainty reduction) on the optimum point. To evaluate the

proposed criterion, we derive an estimator based on decomposing the criterion into two separate terms, where the first term equals to the D-optimal criterion and the second term can be estimated with Monte Carlo without a nested structure. The proposed approximation greatly reduces the computational burden of a pure MC algorithm and makes searching for the near-optimal design more feasible. Moreover, the proposed framework is not limited to GLMs, it can be easily extended for any kind of non-linear regression models. The developed criterion and estimation approach is an important step towards assisting designers to develop more efficient data collection procedures to improve and optimize the systems under study.

In the third work , we explored metamodel-based optimization of stochastic computer models subject to an objective function with uncertain parameters. We presented typical scenarios where the objective function is uncertain and provided the corresponding uncertainty quantification techniques. We developed an RBF metamodel based optimization method through predicting the objective function as a function of both the design variables and the objective function uncertain parameters. By using a design that is a Cartesian product of points in the design variable space and the uncertain parameter space, we developed a fast fitting algorithm to construct the RBF metamodel. These tools provide the system designers more flexibility in making an informed and rational decision than the traditional choice of replacing the uncertain parameter by some estimates. Although the developed RBF focused on the case where one overall objective function with uncertain parameters is of interest, it can be easily extended for fitting multiple objective functions. For example, in a multi-objective optimization problem, if the manager needs the individual objective function values to guide decision-making, independent metamodels can be used to predict each of the objective functions.

6.2 Future works

There are several topics worth further investigation.

- Chapter 3 deals with zero-inflated count data with multilevel variations. In some cases, the observed data are continuous data but could still characterized by excessive zeros and multilevel variations. For example, in an integrated circuits current leakage experiment, other than the number of short circuits, the value of the leakage current could also be treated as the response variable. In this case, due to the measurement accuracy, current values smaller than a certain precision value can not be accurately measured and hence are labeled as zeros. To model this kind of response variable, a multilevel modeling technique for capturing the inherent uncertainties in continuous 'zero-heavy' data is desirable. To solve this problem, a truncated continuous distribution could potentially be used. The corresponding multilevel randomness modeling method could be developed.

- For the evaluation of the expected utility measure in Chapter 4, the current method is to use a combination of analytical approximation and Monte Carlo (MC) approximation. Although this method has greatly reduced the computational burden from the original pure MC approximation, it still requires a lot of computational resources. Instead, an analytical approximation may release the computational burden of searching for the Bayesian OP optimal design. A potential method could be the Poissonization and depoissonization analytical technique for approximating infinite progression. This would further popularize the developed framework. In a recent work, Saleh and Pan (2016) developed an generalized coordinate exchange algorithm for searching D-optimal experimental designs for GLMs. Using simulation study, they showed that this algorithm performs better than GAs in some specific scenarios. This suggests that exchange algorithm for searching OP optimal designs would also be a potential research area.

- Chapter 5 focus on the quantification of the uncertainties in the objective

function of a stochastic computer model. This work assumes that the input parameters of the computer model are all known without uncertainty. However, when using computer models to conduct engineering optimization, the exact values of the computer model inputs may often be uncertain to the investigator. These inputs may be quantities that are uncertain due to lack of information or limited data. For example, the various material properties in a finite element analysis for engineering may be difficult to obtain. One possible future research is to take into account the computer model inputs uncertainty.

REFERENCES

BIBLIOGRAPHY

Albin, S. L. and Friedman, D. J. (1989). The impact of clustered defect distributions in ic fabrication. *Management Science*, 35(9):1066–1078.

Aliprantis, C. D. and Tourky, R. (2007). *Cones and duality*, volume 84. American Mathematical Soc.

Amzal, B., Bois, F. Y., Parent, E., and Robert, C. P. (2006). Bayesian-optimal design via interacting particle systems. *Journal of the American Statistical Association*, 101(474):773–785.

Arulampalam, W. and Booth, A. L. (1997). Who gets over the training hurdle? a study of the training experiences of young men and women in britain. *Journal of Population Economics*, 10(2):197–217.

Barton, R. R. and Meckesheimer, M. (2006). Metamodel-based simulation optimization. *Handbooks in operations research and management science*, 13:535–574.

Barton, R. R., Nelson, B. L., and Xie, W. (2013). Quantifying input uncertainty via simulation confidence intervals. *INFORMS Journal on Computing*, 26(1):74–87.

Barton, R. R. and Schruben, L. W. (2001). Resampling methods for input

modeling. In *Proceedings of the 33nd conference on Winter simulation*, pages 372–378. IEEE Computer Society.

Bernardo, J. M. (1979). Expected information as expected utility. *The Annals of Statistics*, pages 686–690.

Böhning, D., Dietz, E., Schlattmann, P., Mendonca, L., and Kirchner, U. (1999). The zero-inflated poisson model and the decayed, missing and filled teeth index in dental epidemiology. *Journal of the Royal Statistical Society: Series A (Statistics in Society)*, 162(2):195–209.

Box, G. E. and Hill, W. J. (1967). Discrimination among mechanistic models. *Technometrics*, 9(1):57–71.

Box, G. E. and Wilson, K. (1951). On the experimental attainment of optimum conditions. *Journal of the Royal Statistical Society. Series B (Methodological)*, 13(1):1–45.

Boyle, C. R. and Shin, W. S. (1996). An interactive multiple-response simulation optimization method. *IIE transactions*, 28(6):453–462.

Bozsak, F., Gonzalez-Rodriguez, D., Sternberger, Z., Belitz, P., Bewley, T., Chomaz, J.-M., and Barakat, A. I. (2015). Optimization of drug delivery by drug-eluting stents. *PloS one*, 10(6):e0130182.

Breslow, N. E. and Clayton, D. G. (1993). Approximate inference in generalized linear mixed models. *Journal of the American Statistical Association*, 88(421):9–25.

Broudiscou, A., Leardi, R., and Phan-Tan-Luu, R. (1996). Genetic algorithm as a tool for selection of d-optimal design. *Chemometrics and Intelligent Laboratory Systems*, 35(1):105–116.

Brown, C. J., Pagán, J. A., and Rodriguez-Oreggia, E. (2005). The decision-making process of health care utilization in mexico. *Health Policy*, 72(1):81–91.

Buhmann, M. D. (2003). *Radial basis functions: theory and implementations*, volume 12. Cambridge university press.

Burke, E. K. and Kendall, G. (2013). *Search Methodologies: Introductory Tutorials in Optimization and Decision Support Techniques (page 403)*. Springer Publishing Company, Incorporated, 2nd edition.

Cantú-Paz, E. (1998). A survey of parallel genetic algorithms. In *Calculateurs paralleles*. Citeseer.

Cao, Y., Li, H., and Petzold, L. (2004). Efficient formulation of the stochastic simulation algorithm for chemically reacting systems. *The journal of chemical physics*, 121(9):4059–4067.

Cavagnaro, D. R., Myung, J. I., Pitt, M. A., and Kujala, J. V. (2010). Adaptive design optimization: A mutual information-based approach to model discrimination in cognitive science. *Neural computation*, 22(4):887–905.

Chaloner, K. (1989). Bayesian design for estimating the turning point of a quadratic regression. *Communications in Statistics-Theory and Methods*, 18(4):1385–1400.

Chaloner, K. and Verdinelli, I. (1995). Bayesian experimental design: A review. *Statistical Science*, pages 273–304.

Chatterjee, S. K. and Mandal, N. K. (1981). Response surface designs for estimating the optimal point. *Calcutta Statistical Association Bulletin*, 30(3-4):145–170.

Chen, J., Zhang, D., and Davidian, M. (2002). A monte carlo em algorithm for generalized linear mixed models with flexible random effects distribution. *Biostatistics*, 3(3):347–360.

Chen, S. X. and Liu, J. S. (1997). Statistical applications of the poisson-binomial and conditional bernoulli distributions. *Statistica Sinica*, 7(4):875–892.

Cheung, Y. B. (2002). Zero-inflated models for regression analysis of count data: a study of growth and development. *Statistics in medicine*, 21(10):1461–1469.

Chick, S. E. (2001). Input distribution selection for simulation experiments: accounting for input uncertainty. *Operations Research*, 49(5):744–758.

Cook, A. R., Gibson, G. J., and Gilligan, C. A. (2008). Optimal observation times in experimental epidemic processes. *Biometrics*, 64(3):860–868.

Cover, T. M. and Thomas, J. A. (2012). *Elements of information theory*. John Wiley & Sons.

Deb, K., Sinha, A., Korhonen, P. J., and Wallenius, J. (2010). An interactive evolutionary multiobjective optimization method based on progressively approximated value functions. *IEEE Transactions on Evolutionary Computation*, 14(5):723–739.

Deb, K. and Sundar, J. (2006). Reference point based multi-objective optimization using evolutionary algorithms. In *Proceedings of the 8th annual conference on Genetic and evolutionary computation*, pages 635–642. ACM.

DeGroot, M. H. (1962). Uncertainty, information, and sequential experiments. *The Annals of Mathematical Statistics*, pages 404–419.

Dempster, A. P., Laird, N. M., and Rubin, D. B. (1977). Maximum likelihood from incomplete data via the em algorithm. *Journal of the Royal Statistical Society. Series B (Methodological)*, pages 1–38.

Deng, D., Luo, Y., Serizawa, H., Shibahara, M., and Murakawa, H. (2003). Numerical simulation of residual stress and deformation considering phase transformation effects (mechanics, strength & structural design). *Transactions of JWRI*, 32(2):325–333.

Derringer, G. (1980). Simultaneous optimization of several response variables. *Journal of quality technology*, 12(4):214–219.

Dette, H., Bretz, F., Pepelyshev, A., and Pinheiro, J. (2008). Optimal designs for dose-finding studies. *Journal of the American Statistical Association*, 103(483):1225–1237.

Ding, J., Wang, X., Zhou, X.-F., Ren, N.-Q., and Guo, W.-Q. (2010). Cfd optimization of continuous stirred-tank (cstr) reactor for biohydrogen production. *Bioresource technology*, 101(18):7005–7013.

Dror, H. A. and Steinberg, D. M. (2008). Sequential experimental designs for generalized linear models. *Journal of the American Statistical Association*, 103(481):288–298.

Drovandi, C. C., McGree, J. M., and Pettitt, A. N. (2013). Sequential monte carlo for bayesian sequentially designed experiments for discrete data. *Computational Statistics & Data Analysis*, 57(1):320–335.

Elsayed, K. and Lacor, C. (2013). Cfd modeling and multi-objective optimization of cyclone geometry using desirability function, artificial neural networks and genetic algorithms. *Applied Mathematical Modelling*, 37(8):5680–5704.

Fasshauer, G. and McCourt, M. (2015). *Kernel-based approximation methods using Matlab*, volume 19. World Scientific Publishing Co Inc.

Fedorov, V. V. and Müller, W. G. (1997). Another view on optimal design for estimating the point of extremum in quadratic regression. *Metrika*, 46(1):147–157.

Fenton, V. M. and Gallant, A. R. (1996). Qualitative and asymptotic performance of snp density estimators. *Journal of Econometrics*, 74(1):77–118.

Ferreira, J. A., de Oliveira, P., and da Silva, P. (2012). Analytics and numerics of drug release tracking. *Journal of Computational and Applied Mathematics*, 236(15):3572–3583.

Gallant, A. R. and Nychka, D. W. (1987). Semi-nonparametric maximum like-

lihood estimation. *Econometrica: Journal of the Econometric Society*, pages 363–390.

Givens, G. H. and Hoeting, J. A. (2012). *Computational statistics*, volume 710. John Wiley & Sons.

Gontard, N., Guilbert, S., and CUQ, J.-L. (1992). Edible wheat gluten films: influence of the main process variables on film properties using response surface methodology. *Journal of food science*, 57(1):190–195.

Gotwalt, C. M., Jones, B. A., and Steinberg, D. M. (2009). Fast computation of designs robust to parameter uncertainty for nonlinear settings. *Technometrics*, 51(1):88–95.

Greene, W. H. (1994). Accounting for excess zeros and sample selection in poisson and negative binomial regression models.

Groh, C. M., Hubbard, M. E., Jones, P. F., Loadman, P. M., Periasamy, N., Sleeman, B. D., Smye, S. W., Twelves, C. J., and Phillips, R. M. (2014). Mathematical and computational models of drug transport in tumours. *Journal of The Royal Society Interface*, 11(94):20131173.

Hall, D. B. (2000). Zero-inflated poisson and binomial regression with random effects: a case study. *Biometrics*, 56(4):1030–1039.

Hamada, M., Martz, H., Reese, C., and Wilson, A. (2001). Finding near-optimal bayesian experimental designs via genetic algorithms. *The American Statistician*, 55(3):175–181.

Hamada, M. and Nelder, J. A. (1997). Generalized linear models for quality-improvement experiments. *Journal of Quality Technology*, 29(3):292.

Harrington, E. (1965). The desirability function. *Industrial quality control*, 21(10):494–498.

Hasan, M. T. and Sneddon, G. (2009). Zero-inflated poisson regression for longitudinal data. *Communications in Statistics—Simulation and Computation®*, 38(3):638–653.

Herley, P., Greer, A., and Jones, W. (2001). Hillock formation on copper at room temperature by cleaning in ammonia vapor. *Applied Physics Letters*, 79(17):2725–2727.

Huan, X. and Marzouk, Y. M. (2013). Simulation-based optimal bayesian experimental design for nonlinear systems. *Journal of Computational Physics*, 232(1):288–317.

Humphrey, D. G. and Wilson, J. R. (2000). A revised simplex search procedure for stochastic simulation response surface optimization. *INFORMS Journal on Computing*, 12(4):272–283.

Jakkaraju, R. and Greer, A. (2002). Texture and hillocking in sputter-deposited copper thin films. *Journal of Materials Science: Materials in Electronics*, 13(5):285–294.

Jeong, I.-J. and Kim, K.-J. (2009). An interactive desirability function method to multiresponse optimization. *European Journal of Operational Research*, 195(2):412–426.

Johnson, R. T. and Montgomery, D. C. (2009). Choice of second-order response surface designs for logistic and poisson regression models. *International Journal of Experimental Design and Process Optimisation*, 1(1):2–23.

Kanda, J. and Shah, H. (1997). Engineering role in failure cost evaluation for buildings. *Structural Safety*, 19(1):79–90.

Kang, T.-K. and Chou, W.-Y. (2004). Avoiding cu hillocks during the plasma process. *Journal of the Electrochemical Society*, 151(6):G391–G395.

Khuri, A. I., Mukherjee, B., Sinha, B. K., and Ghosh, M. (2006). Design issues for generalized linear models: A review. *Statistical Science*, pages 376–399.

King, G. and Zeng, L. (2001). Logistic regression in rare events data. *Political analysis*, 9(2):137–163.

Kleijnen, J. P. (2014). Simulation-optimization via kriging and bootstrapping: a survey. *Journal of Simulation*, 8(4):241–250.

Korsakissok, I., Mathieu, A., and Didier, D. (2013). Atmospheric dispersion and ground deposition induced by the fukushima nuclear power plant accident: A local-scale simulation and sensitivity study. *Atmospheric environment*, 70:267–279.

Lagrange, S., Brongersma, S., Judelewicz, M., Saerens, A., Vervoort, I., Richard, E., Palmans, R., and Maex, K. (2000). Self-annealing characterization of electroplated copper films. *Microelectronic Engineering*, 50(1):449–457.

Lambert, D. (1992). Zero-inflated poisson regression, with an application to defects in manufacturing. *Technometrics*, 34(1):1–14.

Law, A. M. and McComas, M. G. (2001). Expert fit: how the expertfit distribution-fitting software can make your simulation models more valid. In *Proceedings of the 33nd conference on Winter simulation*, pages 256–261. IEEE Computer Society.

Lewi, J., Butera, R., and Paninski, L. (2009). Sequential optimal design of neurophysiology experiments. *Neural Computation*, 21(3):619–687.

Li, G., Tan, R., Ng, S. H., and Chua, D. (2015). Hurdle model with random effects for the study of copper hillocks growth in integrated circuits manufacturing. In *Industrial Engineering and Engineering Management (IEEM), 2015 IEEE International Conference on*, pages 376–380. IEEE.

Liepe, J., Filippi, S., Komorowski, M., and Stumpf, M. P. (2013). Maximizing the information content of experiments in systems biology. *PLoS computational biology*, 9(1):e1002888.

Lindley, D. V. (1956). On a measure of the information provided by an experiment. *The Annals of Mathematical Statistics*, pages 986–1005.

Lindley, D. V., Lindley, D. V., and Lindley, D. V. (1972). *Bayesian statistics: A review*. SIAM.

Liyana-Pathirana, C. and Shahidi, F. (2005). Optimization of extraction of phenolic compounds from wheat using response surface methodology. *Food chemistry*, 93(1):47–56.

Long, Q., Scavino, M., Tempone, R., and Wang, S. (2013). Fast estimation of expected information gains for bayesian experimental designs based on laplace approximations. *Computer Methods in Applied Mechanics and Engineering*, 259:24–39.

Lu, S., Fred Ramirez, W., and Anseth, K. S. (1998). Modeling and optimization of drug release from laminated polymer matrix devices. *AIChE journal*, 44(7):1689–1696.

MacKay, D. J. (2003). *Information theory, inference and learning algorithms*. Cambridge university press.

Mandal, N. K. and Heiligers, B. (1992). Minimax designs for estimating the optimum point in a quadratic response surface. *Journal of Statistical Planning and Inference*, 31(2):235–244.

Marler, R. T. and Arora, J. S. (2010). The weighted sum method for multi-objective optimization: new insights. *Structural and multidisciplinary optimization*, 41(6):853–862.

McCulloch, C. E. (1994). Maximum likelihood variance components estimation for binary data. *Journal of the American Statistical Association*, 89(425):330–335.

McGree, J., Drovandi, C. C., and Pettitt, A. N. (2012). A sequential monte carlo

approach to the sequential design for discriminating between rival continuous data models.

Miettinen, K. (2012). *Nonlinear multiobjective optimization*, volume 12. Springer Science & Business Media.

Millette, D., Barker, J. F., Comeau, Y., Butler, B. J., Frind, E. O., Clement, B., and Samson, R. (1995). Substrate interaction during aerobic biodegradation of creosote-related compounds: a factorial batch experiment. *Environmental science & technology*, 29(8):1944–1952.

Min, Y. and Agresti, A. (2005). Random effect models for repeated measures of zero-inflated count data. *Statistical Modelling*, 5(1):1–19.

Mitchell, M. (1998). *An introduction to genetic algorithms*. MIT press.

Moghimbeigi, A., Eshraghian, M. R., Mohammad, K., and Mcardle, B. (2008). Multilevel zero-inflated negative binomial regression modeling for over-dispersed count data with extra zeros. *Journal of Applied Statistics*, 35(10):1193–1202.

Mullahy, J. (1986). Specification and testing of some modified count data models. *Journal of econometrics*, 33(3):341–365.

Müller, P. (2005). Simulation based optimal design. *Handbook of Statistics*, 25:509–518.

Ng, S. H. and Chick, S. E. (2004). Design of follow-up experiments for improving model discrimination and parameter estimation. *Naval Research Logistics (NRL)*, 51(8):1129–1148.

O'Leary, D. P. (2009). *Scientific computing with case studies*. SIAM.

Pant, S., Limbert, G., Curzen, N. P., and Bressloff, N. W. (2011). Multiobjective design optimisation of coronary stents. *Biomaterials*, 32(31):7755–7773.

Papadrakakis, M. and Lagaros, N. D. (2002). Reliability-based structural optimization using neural networks and monte carlo simulation. *Computer methods in applied mechanics and engineering*, 191(32):3491–3507.

Park, K. S. and Kim, K.-J. (2005). Optimizing multi-response surface problems: how to use multi-objective optimization techniques. *IIE Transactions*, 37(6):523–532.

Peterson, J. J., Cahya, S., and Castillo, E. (2002). A general approach to confidence regions for optimal factor levels of response surfaces. *Biometrics*, 58(2):422–431.

Piegorsch, W. W. (1990). Maximum likelihood estimation for the negative binomial dispersion parameter. *Biometrics*, pages 863–867.

Pinheiro, J. C. and Bates, D. M. (1995). Approximations to the log-likelihood function in the nonlinear mixed-effects model. *Journal of computational and Graphical Statistics*, 4(1):12–35.

Pronzato, L. and Walter, E. (1993). Experimental design for estimating the optimum point in a response surface. *Acta Applicandae Mathematica*, 33(1):45–68.

Puttlitz, A. F., Ryan, J. G., and Sullivan, T. (1989). Semiconductor interlevel shorts caused by hillock formation in al-cu metallization. *Components, Hybrids, and Manufacturing Technology, IEEE Transactions on*, 12(4):619–626.

Ristow, A., Begović, M., and Rohatgi, A. (2005). Modeling the effects of uncertainty and reliability on the cost of energy from pv systems. Georgia Institute of Technology.

Robinson, T. J., Wulff, S. S., Montgomery, D. C., and Khuri, A. I. (2006). Robust parameter design using generalized linear mixed models. *Journal of Quality Technology*, 38(1):65.

Ruiz, J., Álvarez-Díaz, P., Arbib, Z., Garrido-Pérez, C., Barragán, J., and Perales, J. (2013). Performance of a flat panel reactor in the continuous cul-

ture of microalgae in urban wastewater: prediction from a batch experiment. *Bioresource technology*, 127:456–463.

Russell, K. G., Woods, D. C., Lewis, S., and Eccleston, J. (2009). D-optimal designs for poisson regression models. *Statistica Sinica*, pages 721–730.

Ryan, E. G., Drovandi, C. C., Thompson, M. H., and Pettitt, A. N. (2014). Towards bayesian experimental design for nonlinear models that require a large number of sampling times. *Computational Statistics & Data Analysis*, 70:45–60.

Ryan, K. J. (2003). Estimating expected information gains for experimental designs with application to the random fatigue-limit model. *Journal of Computational and Graphical Statistics*, 12(3):585–603.

Saleh, M. and Pan, R. (2016). Constructing efficient experimental designs for generalized linear models. *Communications in Statistics-Simulation and Computation*, 45(8):2827–2845.

Santner, T. J., Williams, B. J., and Notz, W. I. (2013). *The design and analysis of computer experiments*. Springer Science & Business Media.

Schiesser, W. E. (2012). *Partial differential equation analysis in biomedical engineering: case studies with MATLAB*. Cambridge University Press.

Schilling, S. and Bock, R. D. (2005). High-dimensional maximum marginal likelihood item factor analysis by adaptive quadrature. *psychometrika*, 70(3):533–555.

Shang, Y., Tsung, F., and Zou, C. (2013). Statistical process control for multistage processes with binary outputs. *IIE transactions*, 45(9):1008–1023.

Shannon, C. E. (1948). A mathematical theory of communication. *The Bell System Technical Journal*, 27(3):379–423.

Solonen, A., Haario, H., and Laine, M. (2012). Simulation-based optimal design using a response variance criterion. *Journal of Computational and Graphical Statistics*, 21(1):234–252.

Soltani, M. and Soltani, J. (2016). Determination of optimal combination of applied water and nitrogen for potato yield using response surface methodology (rsm). *BIOSCIENCE BIOTECHNOLOGY RESEARCH COMMUNICATIONS*, 9(1):46–54.

Stapper, C. H. (1985). The effects of wafer to wafer defect density variations on integrated circuit defect and fault distributions. *IBM Journal of Research and Development*, 29(1):87–97.

Stevens, B. and Branam, R. (2015). 3-dimensional aerospike nozzle design. In *APS Division of Fluid Dynamics Meeting Abstracts*.

Stone, M. (1959). Application of a measure of information to the design and comparison of regression experiments. *The Annals of Mathematical Statistics*, pages 55–70.

Tan, M. H. Y. (2015). Stochastic polynomial interpolation for uncertainty quantification with computer experiments. *Technometrics*, 57(4):457–467.

Tooze, J. A., Grunwald, G. K., and Jones, R. H. (2002). Analysis of repeated measures data with clumping at zero. *Statistical methods in medical research*, 11(4):341–355.

Tye, H. (2004). Application of statistical 'design of experiments' methods in drug discovery. *Drug discovery today*, 9(11):485–491.

Verdinelli, I., Polson, N., and Singpurwalla, N. D. (1993). Shannon information and bayesian design for prediction in accelerated life-testing. In *Reliability and Decision Making*, pages 247–256. Springer.

Wallace, S. W. (2000). Decision making under uncertainty: Is sensitivity analysis of any use? *Operations Research*, 48(1):20–25.

Wang, Y., Myers, R. H., Smith, E. P., and Ye, K. (2006). D-optimal designs for poisson regression models. *Journal of statistical planning and inference*, 136(8):2831–2845.

Wasserman, L. (2013). *All of statistics: a concise course in statistical inference*. Springer Science & Business Media.

Weng, T.-W., Melati, D., Melloni, A., and Daniel, L. (2017). Stochastic simulation and robust design optimization of integrated photonic filters. *Nanophotonics*, 6(1):299–308.

Wu, F.-C. (2004). Optimization of correlated multiple quality characteristics using desirability function. *Quality engineering*, 17(1):119–126.

Wurl, R. and Albin, S. (1999). A comparison of multiresponse optimization sensitivity to parameter selection. *Quality Engineering*, 11(3):405–415.

Yalcınkaya, Ö. and Bayhan, G. M. (2009). Modelling and optimization of average travel time for a metro line by simulation and response surface methodology. *European Journal of Operational Research*, 196(1):225–233.

Zhang, D. and Davidian, M. (2001). Linear mixed models with flexible distributions of random effects for longitudinal data. *Biometrics*, 57(3):795–802.

Zhang, H., Jiang, Z., and Guo, C. (2009). Simulation-based optimization of dispatching rules for semiconductor wafer fabrication system scheduling by the response surface methodology. *The International Journal of Advanced Manufacturing Technology*, 41(1-2):110–121.

Zidek, J. V., Sun, W., and Le, N. D. (2000). Designing and integrating composite networks for monitoring multivariate gaussian pollution fields. *Journal of the Royal Statistical Society: Series C (Applied Statistics)*, 49(1):63–79.